JOHANNES GUTENBERG UNIVERSITÄT MAINZ

The bacterial ABC transporter BmrA:

Inhibition – Dimerization – Stability

Dissertation

zur Erlangung des Grades

„Doktor der Naturwissenschaften"

im Promotionsfach Chemie

am Fachbereich Chemie, Pharmazie, Geographie und Geowissenschaften

der Johannes Gutenberg-Universität Mainz

Kristin Oepen

geb. in Worms

Mainz, 2022

D77

Dekanin: [redacted]

1. Berichterstatter: [redacted]

2. Berichterstatter: [redacted]

Tag der mündlichen Prüfung: 11.07.2022

Die vorliegende Dissertation wurde im Zeitraum von September 2017 bis April 2022 im Department Chemie der Johannes Gutenberg-Universität Mainz unter Betreuung von [redacted] angefertigt. Ich versichere, dass ich diese Arbeit selbständig verfasst habe und keine anderen als die angegebenen Quellen und Hilfsmittel verwendet habe.

Table of contents

Summary

ATP-binding cassette (ABC) transporters are involved in the uptake of nutrients and the transport of ions, lipids, peptides, polysaccharides, vitamins and toxins across biological membranes. Consequently, these membrane proteins can be found in all living organisms. Nevertheless, the involvement of ABC transporters in physiological processes can lead, when dysfunctional, to several diseases in humans, such as cystic fibrosis. Also, the overexpression of ABC exporters in cancer cells or pathogenic bacteria can result in the return translocation of any given chemotherapeutics or antimicrobial drugs, resulting in multidrug resistances (MDR).

The bacterial ABC transporter *Bacillus* multidrug resistance ATP (BmrA) is highly homologous to the human P-Glycoprotein, known to cause MDR in cancer cells. For this reason, BmrA can be used as a model protein to investigate MDR causing ABC transporters. The goal of this study was to further analyze dimerization and stability of BmrA as well as investigating the inhibitory traits of myristic acid.

MDR caused by ABC transporters in humans can be a major problem, which is why finding an appropriate inhibitor for these exporters is of great interest in clinical research. As fungi are known to produce pharmaceutically relevant metabolites, e.g., the commonly used antibiotic penicillin, fungal secondary metabolites were screened to identify substances that inhibit the activity of BmrA. Myristic acid was found to inhibit the activity of BmrA, yet, with high inhibitory concentrations, and thus the substance might be given complementarily to the treatment to reduce the drug export out of the cell.

The C-terminal end of the homodimeric ABC transporter BmrA was identified being important for its activity. In particular, interactions of the residues of the anterior part of the C-terminus seem to support dimerization of the BmrA nucleotide-binding domains (NBD) upon ATP-binding. Especially the amino acid F573 seems to be involved in coupling the ATPase activity to substrate transport.

Furthermore, unfolding of BmrA induced by denaturing agents, led to the assumption that the transmembrane domain (TMD) is protected against SDS- and urea-induced denaturation and the observed changes in the Trp fluorescence of the full-length transporter are mainly caused by environmental changes of the W413 in the NBD. Additionally, non-covalent interactions between the TMD and NBD, stabilize the TMD-NBD monomer of BmrA.

Since ABC transporters in general are highly conserved, findings made in this study might be transferred to other transporters of the family.

Zusammenfassung

ATP-bindende Kassette (ABC, englisch: *ATP-binding cassette*)-Transporter sind an der Aufnahme von Nährstoffen und dem Transport von Ionen, Peptiden, Polysacchariden, Vitaminen und Toxinen über biologische Membranen beteiligt. Dementsprechend können diese Membranporteine in allen lebenden Organismen gefunden werden. Durch die Beteiligung der ABC-Transporter an physiologisch relevanten Prozessen kann eine Dysfunktion dieser im Menschen zu Krankheiten führen, wie etwa zur Mukoviszidose. ABC Exporter können *Multidrug*-Resistenz (MDR) verursachen, wenn diese in Krebszellen oder pathogenen Bakterien gehäuft vorkommen, da verabreichte Chemotherapeutika oder Antibiotika wieder aus den Zellen ausgeschleust werden.

Der bakterielle ABC-Transporter BmrA (englisch: *Bacillus multidrug resistance ATP*) ist homolog zu dem humanen P-Glykoprotein, welches MDR in Krebszellen verursachen kann. Aus diesem Grund kann BmrA als Modellprotein verwendet werden, um MDR auslösende ABC-Transporter genauer zu erforschen. Ziel dieser Arbeit war es, die Dimerisierung und Stabilität von BmrA sowie die inhibitorische Wirkung von Myristinsäure zu untersuchen.

Die durch ABC-Transporter verursachte MDR ist problematisch für die menschliche Gesundheit, weshalb die Suche nach einem Inhibitor für diese Exporter von großem Interesse ist. Da Pilze bekannt dafür sind, pharmazeutisch relevante Metabolite, wie z.B. das Antibiotikum Penicillin, zu produzieren, wurden im Rahmen dieser Arbeit pilzliche Sekundärmetabolite auf ihre inhibitorischen Eigenschaften gegenüber der BmrA-Aktivität untersucht. Als eine Substanz mit inhibitorischen Eigenschaften wurde Myristinsäure identifiziert. Um einen inhibitorischen Effekt zu erhalten, sind hohe Konzentrationen notwendig. Deshalb könnte Myristinsäure zusätzlich zur Behandlung verabreicht werden, um ein Ausschleusen der Medikamente aus der Zelle zu reduzieren.

Weiterführende Untersuchungen zur Stabilität des homodimeren ABC-Transporter BmrA zeigten einen wichtigen Einfluss des C-terminalen Endes auf die Transportaktivität auf. Die Aminosäuren am Beginn des C-Terminus scheinen den Dimerisierungsprozess in der Nukleotidbindenden Domäne (NBD) zu unterstützen. Besonders die Aminosäure F573 scheint an der Kopplung von ATPase Aktivität und Transport beteiligt zu sein.

Des Weiteren zeigen Entfaltungsstudien, dass die Transmembrandomäne (TMD) von BmrA gegenüber Entfaltung durch SDS und Harnstoff geschützt ist, und Unterschiede in der gemessenen Trp-Fluoreszenz des Volllängen-Transporters von einer veränderten Umgebung

des W413 in der NBD ausgehen. Zusätzlich wird das BmrA-Monomer, bestehend aus TMD und NBD, durch nicht kovalente (hydrophobe) Interaktionen stabilisiert.

Da ABC-Transporter in allen Domänen des Lebens hoch konserviert sind, können die gewonnen Erkenntnisse auf andere Transporter innerhalb der ABC-Transporter Familie übertragen werden.

1 Introduction

1.1 Biological membranes

The existence of life is closely linked to the existence and function of biological membranes. These membranes mainly consist of lipids and membrane proteins, which form cells and further separate the “inside” from the “outside” [1]. Within a cell, biological membranes can additionally define compartments, i.e., the organelles. In general, membranes build a selective barrier for substances to enter or leave a cell or a compartment [2,3]. The basic structure of a biological membrane is a bilayer of lipids. A lipid structure consists in general of a hydrophobic tail and a hydrophilic head group [4]. In eukaryotic lipid bilayers, three major classes of lipids can be found: (i) phospholipids, (ii) sphingolipids and (iii) sterols (Figure 1). Phospholipids can consist of a phosphate, a glycerol, and two bound fatty acid chains. Sphingolipids have a long-chain amino alcohol (sphingoid) backbone and an amide-bound fatty acyl chain. The head group of phospholipids and sphingolipids can for example be inositol, glycerol, ethanolamine, choline or serine. Sterols consist of a hydroxyl group (head), a four-ring steroid structure and a short hydrocarbon side chain [2,4,5]. The lipid composition of membranes varies between different organisms as well as within an organism [3,6–8].

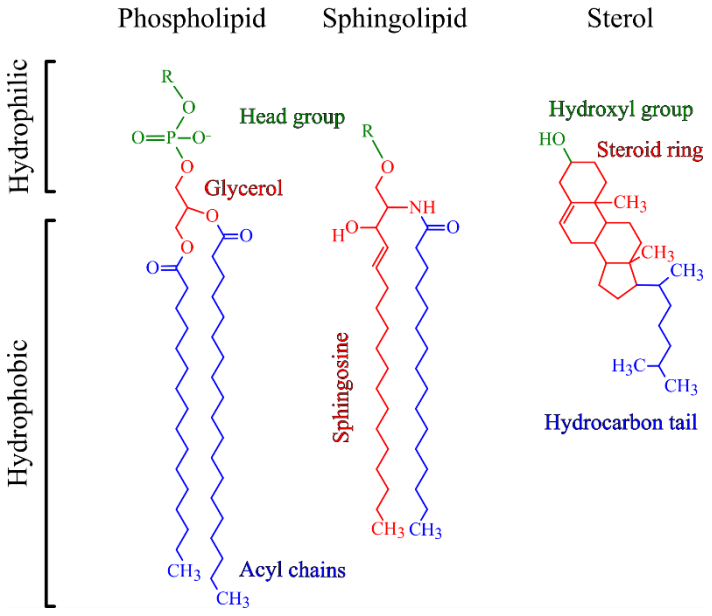

Figure 1: Lipid structures found in eukaryotic cells. Basic structures of a phospholipid, a sphingolipid and the mammalian sterol, cholesterol. These lipids have in general a hydrophilic head group and a hydrophobic tail. The acyl chains (blue) in phospholipids and sphingolipids can be of diverse length. The head groups can be replaced by a sugar or an alcohol, i.e., inositol, glycerol, ethanolamine, choline or serine (R; green). The backbone in phospholipids is a glycerol, in sphingolipids a sphingosine and in sterols a four-ring steroid (red). Structures were drawn using ChemSketch [9].

While water and small lipophilic molecules are able to diffuse across membranes, larger and charged molecules cannot cross lipid bilayers by simple diffusion [2,10]. Thus, transmembrane gradients can be generated, which enable any living organism to produce energy. Proteins embedded in these biological membranes facilitate the selective transport of molecules and ions [2,11]. Thereby, one can distinguish between three different transport mechanisms. In case of passive transport, charged molecules (ions) can pass through channel proteins along an electrochemical gradient without requiring energy [10]. In contrast, active transport requires energy to transport molecules against a concentration gradient [12]. Here it can be differentiated between primary and secondary active transport: Primary active transporters use the energy gained from ATP hydrolysis to transport substances across the membrane [2,13]. In the secondary active transport, the transport of a molecule is generally coupled to the transport of another substance, so that either both solutes cross the membrane in the same direction (symport) or pass through in opposite directions (antiport) [14].

1.2 Membrane protein structure and folding

Membrane proteins are pharmaceutically relevant, as they are targeted by approx. 60% of all currently available drugs [15,16]. Consequently, membrane proteins are of major interest in research and a better understanding of their structure, function(s) and interaction(s) will help to develop as well as to detect new drugs. Whereas around 30% of the human genome encodes for membrane proteins [17,18], until 2021, solely 2.6% of the solved protein structures were membrane proteins [19]. Membrane proteins, especially the transmembrane (TM) segments, adapt to their special surrounding of the lipid bilayer with its hydrophobic center and the hydrophilic head groups of both sides [20]. The *in vitro* analysis of hydrophobic membrane proteins is challenging, since suitable solubilizing agents are needed to solubilize the protein out of the surrounding membranes and to maintain the native structure. Therefore usually detergents or membrane-like structures (liposomes or nanodiscs) are utilized [21–23].

(Integral) membrane proteins are structurally adapted to their amphiphilic environment by their increased hydrophobic properties [24]. Within the membrane, the proteins mostly adopt a β-barrel or α-helical structure [25–27]. A β-barrel is formed by eight to > 20 strands, while the most stable barrels comprise of entirely antiparallel or mixed parallel and antiparallel β-strands [28]. Some β-barrels are stable on their own, and thus can function as a monomer, whilst others are part of oligomeric structures [29]. β-barrel membrane proteins are involved in ion flux or passive nutrient intake [30]. β-barrel proteins exist exclusively in the outer membrane of Gram-

negative bacteria, chloroplasts and mitochondria and facilitate the diffusion of molecules up to 600 Da [29–32].

Nevertheless, the majority of membrane proteins consist of α-helix bundles and these proteins can adapt manifold functional structures within cellular membranes and function as transporters, receptors, channels or enzymes [33]. The α-helix *per se* is a very compact secondary structure element with 3.6 amino acid residues forming a turn in a right-handed helix. These helices are stabilized by H-bonds between the first amino acids carbonyl group and the NH-group of the fourth subsequent amino acid residue [34]. Due to this conformation, the first and fourth side chain are about on the same side of a helix and, depending on the amino acid residue, hydrophilic or hydrophobic patches on one helix side can be formed. The amino acids found in TM helices are mostly hydrophobic. One membrane-spanning helix typically consists of 20–30 amino acids [35].

In comparison to soluble proteins, the folding pathway of membrane proteins is more complex, regarding the correct insertion into the membrane, the correct structure formation and assembly (Figure 2) [36]. However, the folding of membrane proteins is typically investigated in a simplified environment to gain insights into the underlaying mechanisms. Based on *in vitro* experiments, folding of α-helical membrane proteins is simplified in the two-stage model as two thermodynamically distinct steps [37].

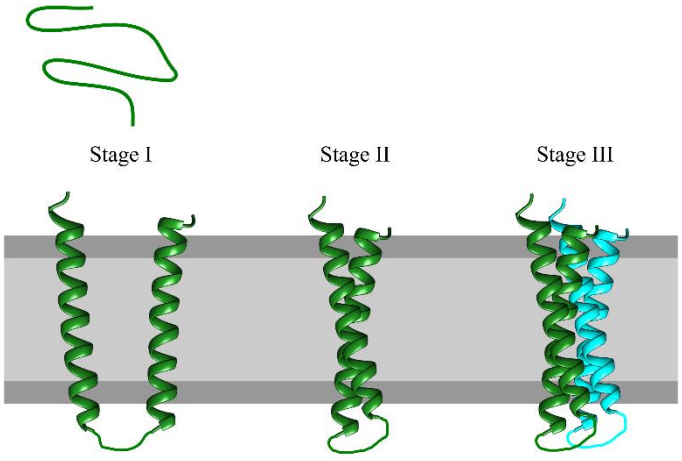

Figure 2: Three-stage model of α-helical membrane protein folding. Stage I shows the inserted polypeptide chain of two connected TM α-helices into the lipid membrane. In stage II, the helices assemble to the tertiary structure. In stage III, the protein oligomerizes with another monomer to its quaternary structure.

In stage I (Figure 2) of this model, the insertion of an individual α-helical TM segments into the membrane is described. As the hydrophobic helices of membrane proteins tend to rather

interact with the lipid bilayer or with each other than with water to minimize the decrease in entropy, the insertion of the α-helices into the bilayer is energetically favored [38,39].

In stage II (Figure 2), the inserted α-helices assemble and fold into a functional tertiary structure. Thus, the TM helices assemble and interact with each other. The interactions between the helices can be diverse, but are mostly stabilized by van der Waals forces. This interaction is also vital for the formation of the native protein structure [40,41]. By increasing helix-helix interactions, the helix-lipid interactions decrease, leading to said native protein structure [42]. Two α-helices can also be stabilized by intertwining of the side chains which maximizes the close packing. This interaction is called the "knobs-into-holes" mechanism [43,44]. A well examined motif for the dimerization of helices is GxxxG (x: can be any amino acid residue) and its surrounding amino acids. Here the small glycine residues facilitate a close contact to the opposite helix which contains a similar motif, whereas the surrounding amino acids strengthen the interaction [40,45,46]. Helix-helix contacts can also be stabilized by hydrogen bonds, ionic and aromatic interactions (π-stacking) [41,47].

Yet, the two-stage model of α-helical membrane protein folding was expanded with a third stage (III) (Figure 2) to include the binding of ligands, the folding of loops outside the membrane, the insertion of peripheral domains and/or the quaternary structure formation [48]. Most membrane proteins oligomerize to be functional. Thus, the single subunits interact non-covalently with each other [49]. The formation of non-covalently linked TM oligomers is constrained by the lipid bilayer [50], and the membrane proteins are stabilized by interactions with the lipid surrounding [51–53]. Sometimes, the tertiary structure of membrane proteins is also stabilized upon oligomerization (quaternary structure) [54]. Larger proteins can assemble from several smaller subunits, which are often connected by linkers. These linkers can vary in length, with shorter linkers enabling functional crosstalk between the domains, whereas longer linkers are more flexible. Here, the subunits do not necessarily functionally interact with each other, but facilitate conformational changes of the protein, which is important for its function [55,56]. These linkers commonly consist of the amino acids Pro, Arg, Phe, Thr, Glu, or Gln [57]. However, individual domains of a multi-domain protein can be isolated and analyzed, while for other proteins the linker is important for the stabilization of the domains [58].

1.3 ABC transporter

ATP-binding cassette (ABC) transporters can be found in all domains of life. In general, ABC transporters consist of two transmembrane domains (TMDs) and two cytoplasmic nucleotide-

binding domains (NBDs). ATP is bound and hydrolyzed at the NBDs and thereby provides the energy to transport substrate through the TMDs across the cell membrane. These four core domains are necessary to build a functional transporter (Figure 3). Furthermore, all four domains can be expressed either on a single polypeptide chain (Figure 3C) or on individual polypeptide chains for the TMDs and NBDs (Figure 3A). Commonly, in bacterial exporters one TMD is fused to a NBD, building so called half-transporters. Here again, two half-transporters have to dimerize to build a functional transporter for which either two identical halves can dimerize to form a homodimer or two different halves generate a heterodimer (Figure 3B) [59–61].

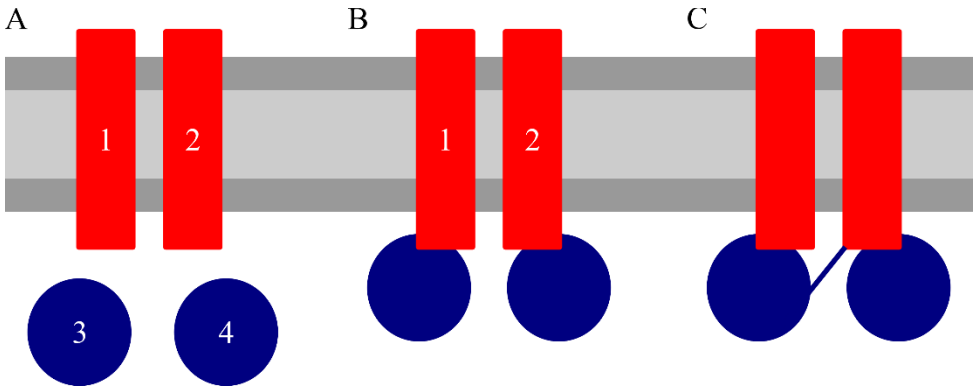

Figure 3: Diverse ABC transporter architectures. The cartoon shows the diversity of the TMD (red) and NBD (blue) assembly in functional ABC transporters. A: Often the TMDs and NBDs of importers are separately expressed and have to assemble to build a functional transporter. Here, 1 and 2 can be the same TMD structure or different, equally applied for the NBD structures 3 and 4. B: A TMD and a NBD are fused together to a half-size transporter and two of these have to dimerize. Either these transporters consist of two equal halves, called a homodimer (1 and 2 are the same half-size transporters) or two different halves (heterodimer, 1 and 2 are two different polypeptide chains). C: All four domains are fused together (TMD-NBD-TMD-NBD) and thereby build a full-size transporter.

Depending on the direction of the transported substrate, ABC transporters can further be divided into subtypes, namely exporter, importer and non-transporter ABC proteins [62,63]. For the import, a so-called substrate-binding protein is necessary, which binds a substrate and passes it on to the extracellular part of the importers TMD [64,65]. In contrast, the substrates for ABC exporters can directly bind to the TMDs, either from the cytoplasm or from the inner leaflet of the membrane. There is also a third subtype in the ABC transporter family, consisting of non-transporter ABC proteins, which lack the TMDs and are mostly involved in cellular processes [66–68].

1.3.1 Human ABC transporter

Remarkably, some human diseases are directly associated with ABC transporters, like cystic fibrosis [69–71], Stargardt disease [72] or Alzheimer's disease [73,74]. The mammalian ABC system is divided into the seven subfamilies ABCA to ABCG, based on sequence similarity and domain order [75–77]. Interestingly, the majority of human ABC transporters are exporters, yet ABCA4 seems to function as an importer [78]. Furthermore, some ABC transporters are ion channels, like ABCC7/CFTR [79], or regulate a potassium channel, such as the sulfonyl urea receptors (ABCC8/SUR1 and ABCC9/SUR2) [80,81]. Due to the lack of the TMDs, ABCE and ABCF only consist of the NBDs and thus do not function as transport proteins [76,82]. Some of these integral membrane proteins are known to transport a diverse range of substrates across biological membranes [83]. Due to their broad substrate range, these transporters are e.g. able to transport chemotherapeutics out of cancer cells, which ultimately leads to multidrug resistance in humans [84,85]. In contrast, bacterial ABC transporter either are able to uptake essential nutrients or extrude toxic substances, which then again are involved in the drug and antibiotic resistance of microbial pathogens [86].

1.3.2 ABC transporter classification

The ABC transporter superfamily is classified into seven types, based on their TMD fold. The diversity in the TMDs as well as the evolutionary similarity between bacterial and eukaryotic transporters led in 2020 to the suggestion of a new ABC transporter classification (Figure 4). This new classification connects the phylogenetic analyses of the TMDs with the results gained from solved high-resolution structures [87]. According to the new classification, types I-III exclusively consist of ABC importers, each type having its individual TMD architecture [64,65]. Type IV ABC transporters are a very diverse group, consisting of mainly exporters as well as some importers yet sharing the same TMD arrangement. Equally diverse are type V ABC transporters, where specific features in the TMD architecture are the amphipathic N-terminal helix as well as the periplasmic gate helices. The TMD folds of type VI transporters consist of six TM helices per monomer, and these do not crossover. The type VII ABC transporters contain in total eight TM helices and two coupling helices per monomer [87].

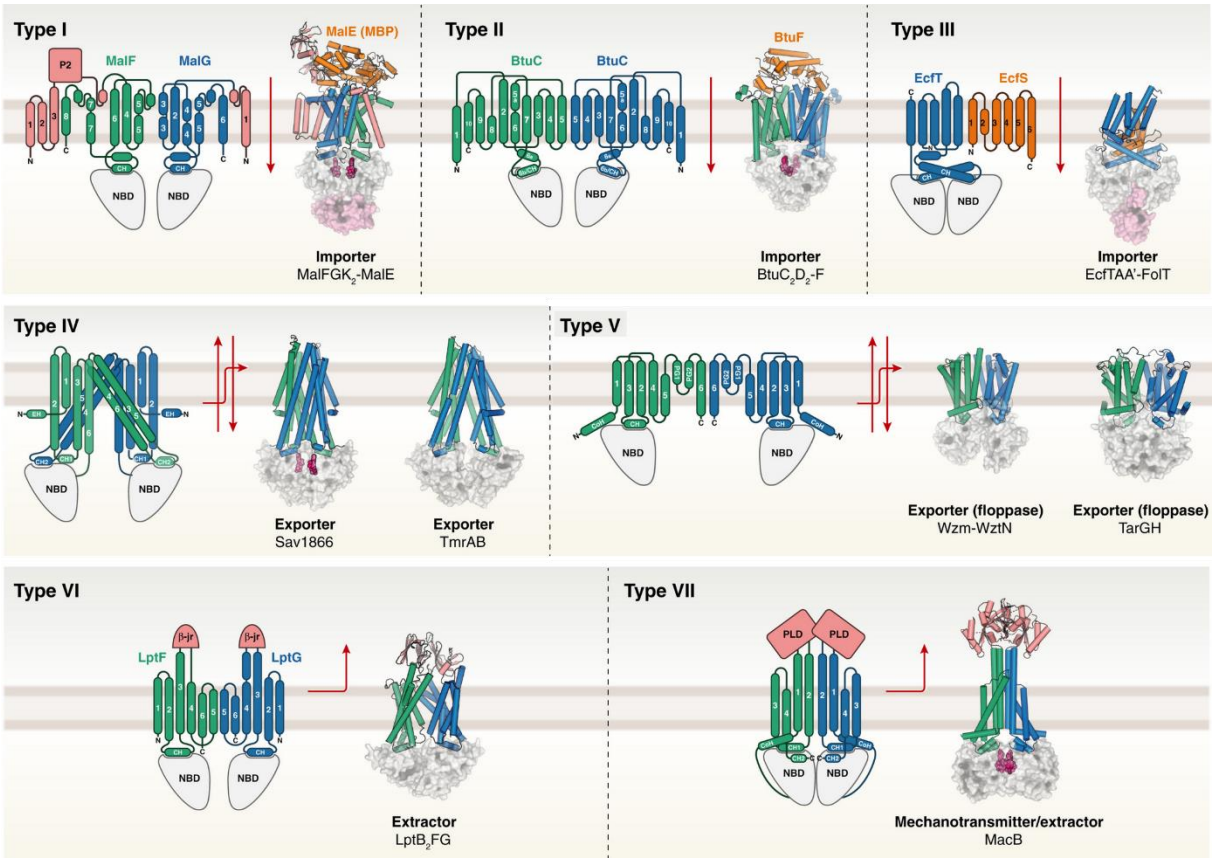

Figure 4: Overview of the different ABC transporter types I-VII. The diversity within ABC transporters is based on the TMD structures. The NBDs are depicted in grey. For the TMDs (green and blue) of the different types a representative formation of each TM helix scaffold is shown. For type I-III importers, the substrate-binding proteins are shown in orange and additional TM helices and auxiliary domains are shown in salmon. Some solved ABC transporter structures show NBD bound nucleotides and Mg^{2+} ions (pink spheres). The red arrows next to each cartoon present the possible transport direction of the members in each type. Pdbs: $MalFGK_2$-MalE: 2R6G; $BtuC_2D_2$-BtuF: 4FI3; EcfTAA'-FolT: 4HUQ; Sav1866: 2HYD; TmrAB: 5MKK; Wzm-WztN: 6OIH; TarGH: 6JBH; $LptB_2FG$: 5X5Y; MacB: 5LJ7. Applied abbreviations: C: C-terminus, N: N-terminus, CH: coupling helix, P2: extracytoplasmic loop, EH: elbow helix, PG: periplasmic gate helix, CoH: connecting helix, b-jr: b-jellyroll-like domain, PLD: periplasmic domain. Figure taken from [87] and modified.

One of the first resolved crystal structures of an ABC transporter was $BtuC_2D_2$ (a Vitamin B_{12} importer) in 2002 [88]. Subsequently, in the last 20 years more and more resolved structures of ABC transporters were added to the protein data bank (pdb), helping to get a better understanding of the interaction between TMD and NBD as well as of the translocation cycle. Hence, in the following the single domains (NBD and TMD) and their individual features will be further described.

1.3.3 Nucleotide-binding domains (NBDs)

The cytoplasmic NBD is a highly conserved domain among ABC transporters [89,90]. The two opposing NBDs dimerize upon the binding of two Mg-ATP molecules, enclosing the nucleotide "sandwich-like" between the NBD-NBD interface and thereby forming the nucleotide binding sites (NBS). These NBSs include the Walker A (also P-loop) and the Walker B motif, as well as the A-, Q- and H-loop (also H-switch) of one NBD monomer and the ABC signature motif (also C-loop or LSGGQ) with the D-loop of the other (opposite) NBD (Figure 5) [86,91–97]. Dimerization of the NBDs is crucial for nucleotide hydrolysis [98–101]. In the ATP-bound state of isolated NBDs and the NBDs of full-length transporters, the structures show a geometrically restricted position for the NBDs. After ATP hydrolysis, the inorganic phosphates are released, and the NBD monomers still remain in proximity [88,102]. In fact, in some ABC transporters (mainly in human ABC transporters) the motifs can be degenerated in one NBS, which results in a catalytically inactive or a very low ATPase active site for these "asymmetric" transporters [103–106].

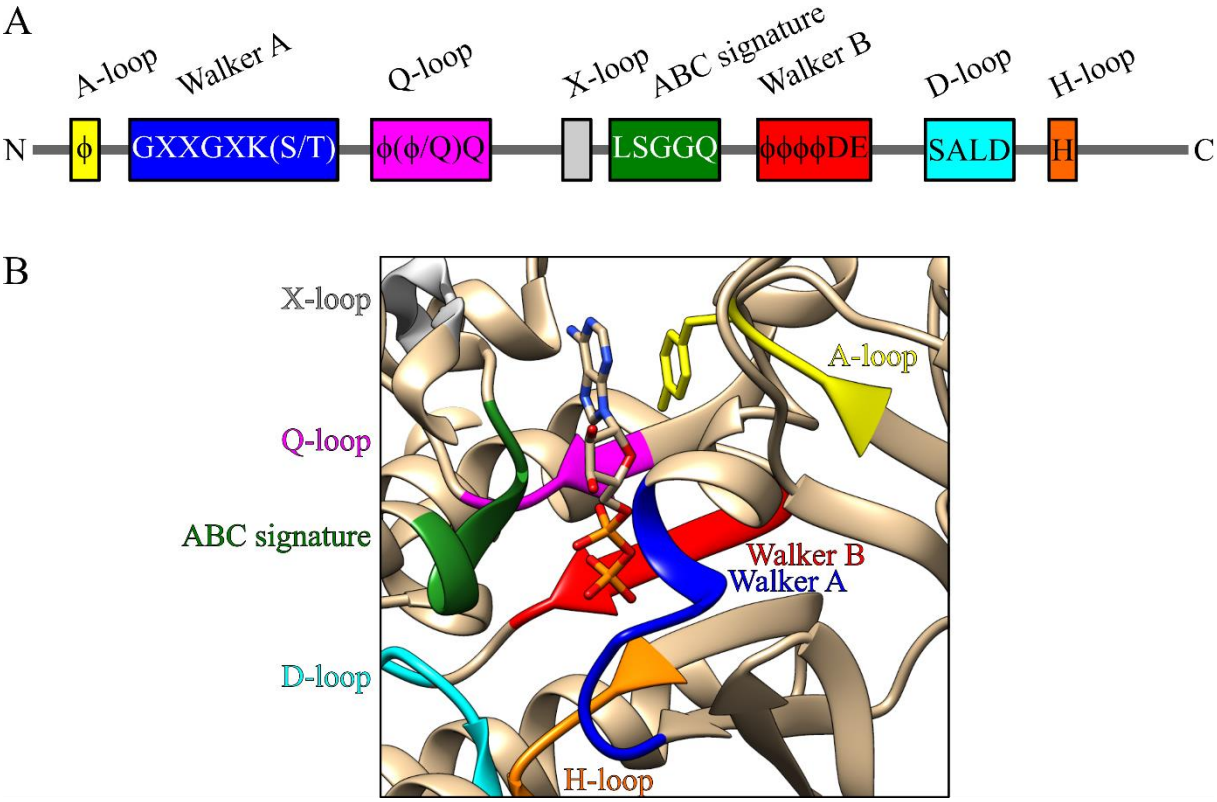

Figure 5: NBD binding motifs and binding of ADP at the NBS of Sav1866 (pdb: 2HYD). A: Arrangement of the motifs found in the NBDs of ABC transporter with the specific sequences. Motifs: A-loop (yellow), Walker A (blue), Q-loop (magenta), X-loop (grey), ABC signature (green), Walker B (red), D-loop (turquoise) and H-loop (orange). B: Bound ADP between the two NBDs of Sav1866. The depicted colors for the motifs are equivalent to the

colors used for the motifs shown in A. Amino acid residues A456-G466 were removed for better visualization. Figure was modified according to [107].

The aromatic side chain residue in the **A-loop** interacts with the adenine ring of the bound Mg-ATP [108,109].

This Mg-ATP is bound by the **Walker A** motif (also phosphate-coordinating P-loop; sequence: GxxGxGK(S/T) – x: can be any amino acid residue). Thus, the conserved lysine within the motif binds the β- and γ-phosphate of the Mg-ATP and additionally, the serine or threonine residue is coordinating the Mg^{2+} ion [110]. Mutations of the lysine impede the transporters ATPase activity or the binding of ATP [60,111].

The eponymous and conserved glutamine of the **Q-loop** (sequence: ϕ(ϕ/Q)Q – ϕ: hydrophobic amino acid residue) senses the γ-phosphate of the nucleotide and is crucial for the connection to the TMD during the catalytic cycle [112–114].

The **ABC signature motif** (sequence: LSGGQ) is crucial for dimerization of the NBDs, since the ATP is sandwiched between the ABC signature motif of one NBD and the Walker A motif of the opposite NBD and is also essential for the hydrolysis of ATP [91,92]. Hence, mutations in the ABC signature motif result in a reduced ATP-binding affinity and a restricted ATP hydrolysis [94,115].

Four hydrophobic amino acid residues an aspartate and a glutamate form the **Walker B** motif (sequence: ϕϕϕϕDE), and the aspartate also recognizes the Mg^{2+} ion of the nucleotide. The conserved glutamate residue in the Walker B motif is needed for the hydrolysis of said ATP by polarizing an attacking water molecule [116–118]. Mutating this glutamate results in a ATPase inactive transporter, which lost the ability to hydrolyze ATP, but is still able to dimerize [119,120].

The NBSs are formed between the **D-loop** (sequence: SALD) of one NBD and the Walker A motif and the H-loop of the opposite NBD and are stabilized by hydrogen bonds as well as electrostatic interactions with said motifs. Due to the location of the D-loop at this interface, it might be crucial for NBD dimerization, the communication between the NBSs and between the NBD and the TMD [121–123].

The conserved histidine residue of the **H-loop** contributes to the catalytic reaction by stabilizing the ATP-binding site with the catalytically active glutamate (of the Walker B motif) and the D-loop [124–126].

The **X-loop** is uniquely found in ABC exporters and is important for transmitting the conformational changes in the NBD (generated by ATP-binding and hydrolysis) to the TMD [95,127–129].

1.3.4 Transmembrane domains (TMDs)

Equally important for the transport of ABC transporters are the TMDs. The substrate-binding site (substrate-binding cavity) is located between two TMD monomers and the TMD dimer thereby forms a translocation pathway for the substrate. The TMDs primarily consist of α-helices. Interestingly, ABC importers contain in a full-transporter between 10 to 20 TM helices, whereas ABC exporters mostly have 12 TM helices [62,130]. In contrast to the highly conserved NBDs, the sequences of the TMDs are less conserved. However, the topologies of TMDs within a transporter type are very similar (Figure 4). Then again, the coupling helices (CH) are structurally conserved and important in the contact between TMDs and NBDs [131]. All types of ABC transporters consist of bilayer-spanning helices. Yet, particularly noticeable are type IV TM helices, which exceed the membrane and intrude into the cytoplasm at roughly 25 Å [95]. Additionally, the 12 TM helices of the type IV transporters MsbA and Sav1866 are intertwined by the TM helices 1, 2, 3 and 6 of one monomer with the TM helices 4’ and 5’ of the opposite monomer [93,95]. During the substrate translocation cycle, the TMDs switch between an inward-facing (IF) and an outward-facing (OF) conformation. Due to the switch, the arrangement of the TM helices changes to TM helices 1, 2, 3’, 4’, 5’ and 6’ [132]. Because of this switch in the conformation of ABC transporters, the path between two TMDs, formed by their TM helices, is for the substrate either open from the cytoplasmic side or from the outside, yet never from both sides. In the IF conformation, the substrate is released for importers, whereas for exporters the substrate is binding. In the OF conformation, the opposite is the case for importers (substrate binding) and exporters (substrate release) [133]. In both, ABC importers and exporters, the helices of both TMDs form the TM path/cavity for the substrate. As a result, substrate-binding amino acid residues were detected in all TM helices [134]. In general, these amino acids expose their residues towards the cavity between the TMDs [135,136]. Some ABC transporters are substrate specific and exclusively transport e.g. sugars, lipids or peptides [136–138]. However, P-glycoprotein (P-gp) for example is called polyspecific [134,139,140], because in said ABC transporter hundreds of compounds of various sizes were found to bind in its binding pocket [140,141]. Nevertheless, it is still unclear whether these diverse molecules bind to distinct or overlapping binding sites [135]. Yet, in the binding pocket

of P-gp, two different compounds can bind simultaneously [142]. In the binding pocket of polyspecific ABC transporters, plenty of hydrophobic residues were commonly found, which results in mostly unspecific hydrophobic interactions with the substrates [143,144].

1.3.5 Translocation cycle of ABC exporter

The translocation cycle of ABC transporters is rather complex and, until now, not fully understood. Due to the broad variety in ABC transporter structures (Figure 4), the translocation cycles can differ between the type I-VII ABC transporters. In general, the interaction between the TMDs and the NBDs, resulting in a structural and conformational change, is necessary for a functional transport mechanism. Until now, based on biochemical and structural data, several models for the substrate transport mechanism of ABC transporters have been proposed. Basically, these models differ in some details of the mechanism, but basic steps are commonly shared in all of these models, like the dimerization of the NBDs induced by ATP as well as the switch in the TMDs between IF and OF (Figure 6) [145]. In the ATP switch model [146–148], the NBDs dimerize upon the binding of ATP [149] and the conformation switches to the OF (Figure 6A). ATP hydrolysis and the subsequent release of ADP and inorganic phosphate results in NBD separation and thereby the transporter switches back into an IF conformation. In contrast, in the constant contact model, the NBDs are permanently associated and, during the steady-state turnover, the NBDs sequentially hydrolyze the ATPs (Figure 6B) [150,151].

In the resting, ground or apo state of an ABC transporter, normally no ATP is bound and the NBDs can be distant (Figure 6A). Subsequently, for exporters, the substrate directly binds to the cavity between the two TMDs. This cavity is accessible from the cytoplasmic side of the membrane. Here, depending on the properties, the substrate can either enter the cavity from the cytosol or the lipid bilayer [134]. After substrate-binding, two ATP molecules bind at the NBD-NBD interface [131,148] and inevitably trigger the dimerization of the NBDs, resulting in "sandwiched" ATPs between the NBSs [120,129,152]. The ATPs are recognized by the Walker A motif of one NBD and the ABC signature motif of the opposite NBD [91,147,153], and this signature motif is subsequent to the X-loop. This loop is non-covalently connected in a ball-and-socket joint [95,154,155] with the short cytoplasmic CH of the TMD [95,122,156,157]. The CH transmits the conformational changes induced by ATP from the NBD to the TMD causing the switch between IF and OF conformation [95,158,159].

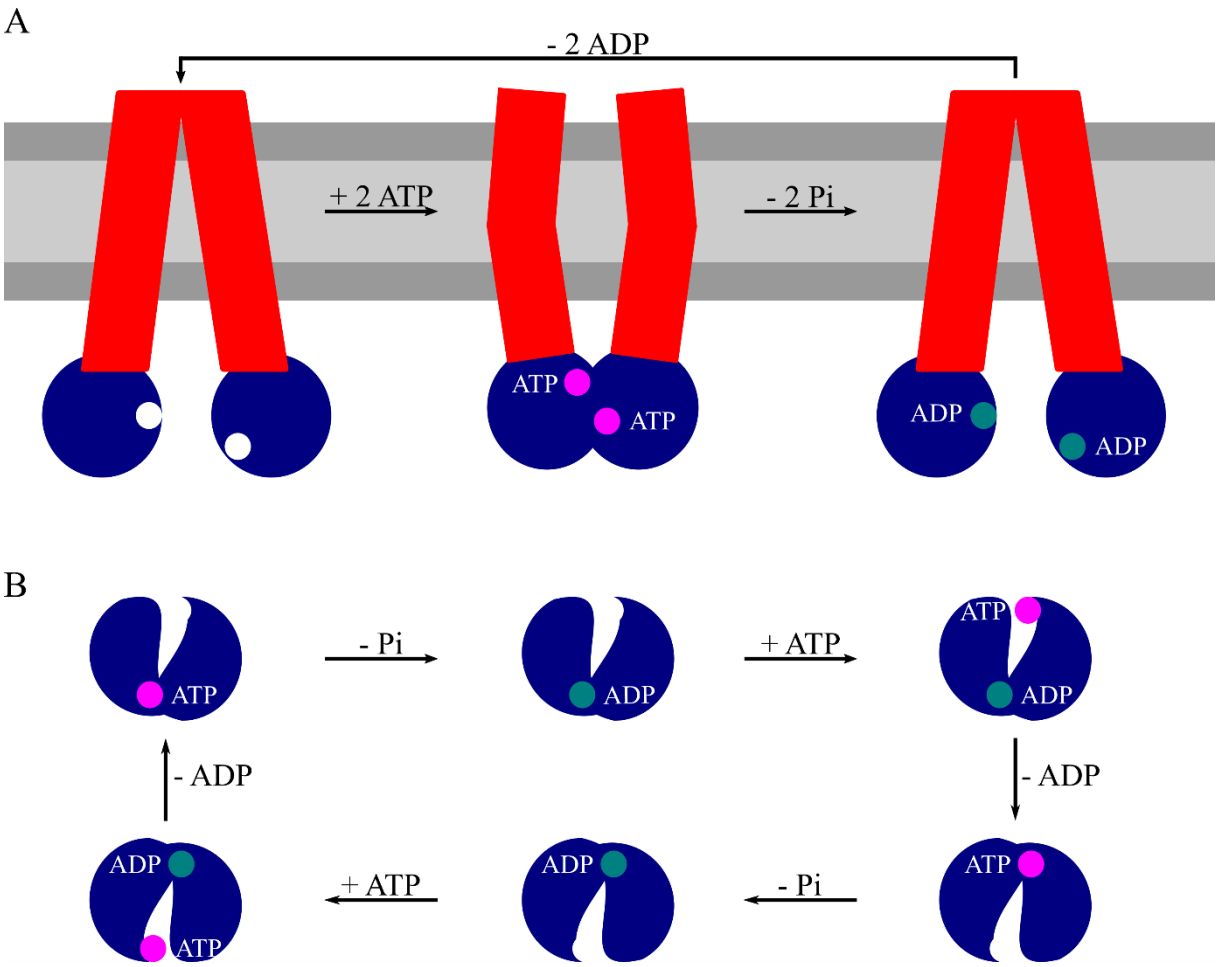

Figure 6: Two models describing the catalytic cycle of ATP binding and hydrolysis in ABC transporter. A: ATP switch model. In the ATP switch model, the NBDs are distant and no ATP is bound (resting state). Then the domains successively bind ATP (magenta circle), which triggers dimerization of the NBDs and results in a conformational switch in the TMDs. ATP is successively hydrolyzed and Pi and ADP (green circle) are released stepwise. Hence, the monomers disengage and the resting state is restored. B: Constant contact model. Here only the NBDs are shown. In this model the NBDs stay continuously in contact, yet a NBS is sequentially accessible or not. If one NBS is closed, the second NBS is open. Thus, the ATP can enter the binding site or the ADP can leave, consequently the hydrolysis of ATP alternates between the two NBSs.

The motifs in the NBDs of ABC transporters are highly conserved, thus it was suggested that the mechanism of ATP hydrolysis might be conserved as well [116]. Analysis of MalK crystal structures demonstrated that the conserved glutamate in the Walker B motif catalyzes ATP hydrolysis with the D-, H- and Q-loop by polarizing the water molecule, which then can attack the nucleotides γ-phosphate. By this, the ATP is hydrolyzed to ADP and inorganic phosphate [116,124,160]. Subsequently, phosphate and ADP are released and the NBDs disengage again. After these steps, the ABC transporter is again in the apo state, ready for the next transport

cycle. Recently solved crystal structures of exporters led to the suggestion that after ATP hydrolysis, the release of the phosphate resets the transporter into the IF conformation [107]. In some studies, the switch from OF to IF after substrate release is induced by the hydrophobicity of the substrate binding cavity leading to its closing, without spending energy provided by ATP hydrolysis [161,162].

As more structures of exporters are solved and captured in different conformations, more is known about the switch between the IF and OF conformation, the hydrolysis of ATP and the transport mechanism in ABC transporter. Since different models of the transport mechanism are proposed for ABC transporters, these previously mentioned steps have to happen at some point during the translocation cycle. Yet until today, there is no universal mechanism identified applicable to all ABC transporters, although the structures and the transport mechanism in some ABC transporters are more thoroughly explored.

1.4 *Bacillus* multidrug resistance ATP

Analysis of the Gram-positive bacterium *Bacillus subtilis* revealed that the genome encodes 78 ABC transporters, of which 38 ought to be importers and 40 to be exporters [163]. When the *B. subtilis* YvcC protein was overexpressed in *E. coli*, the cells were able to transport Hoechst 33342 [164]. Additionally, YvcC was able to transport vast substances, such as ethidium bromide, doxorubicin, 7-aminoactinomycin D or cervimycin C [165,166], and this transporter was shortly later renamed to its current name: *Bacillus* multidrug resistance ATP (BmrA) [165]. This ABC exporter is homodimeric, meaning one NBD and one TMD are part of a single polypeptide chain and two of these half-transporters have to dimerize to be fully functional (Figure 7A) [167,168]. Each half of BmrA is homologous to the bacterial ABC transporters LmrA and MsbA as well as to one half of the eukaryotic P-gp. Due to its TMD similarities, BmrA is a type IV half-transporter of around 65 kDa (per monomer) [87]. Most recently, the structure of BmrA in the OF conformation was solved by single-particle cryo-electron microscopy and X-ray crystallography [144]. Upon substrate recognition at the hydrophobic binding pocket between the TMDs of BmrA and ATP-binding at the NBSs, dimerization of the NBDs is triggered (Figure 7B) [111] and the transporter switches from the IF to the OF conformation [169]. Because of the hydrophobic nature of the substrate-binding pocket, the transporter BmrA changes to its occluded conformation after the substrate release. The substrate-binding pocket is closed to both sides of the membrane and the NBDs are still dimerized. After ATP hydrolysis, the transport cycle can start again [145,161,170]. Thus, the

BmrA transport of substrate depends on the ATPase activity, and solely the inhibition of the ATPase activity by vanadate or mutation of the conserved glutamate (E504) in BmrA inhibit its transport [165]. However, the ATPase activity can be uncoupled from the transport activity, which is the case for the X-loop mutant of BmrA (E474R). This variant is able to hydrolyze ATP, but is not transport active anymore [169].

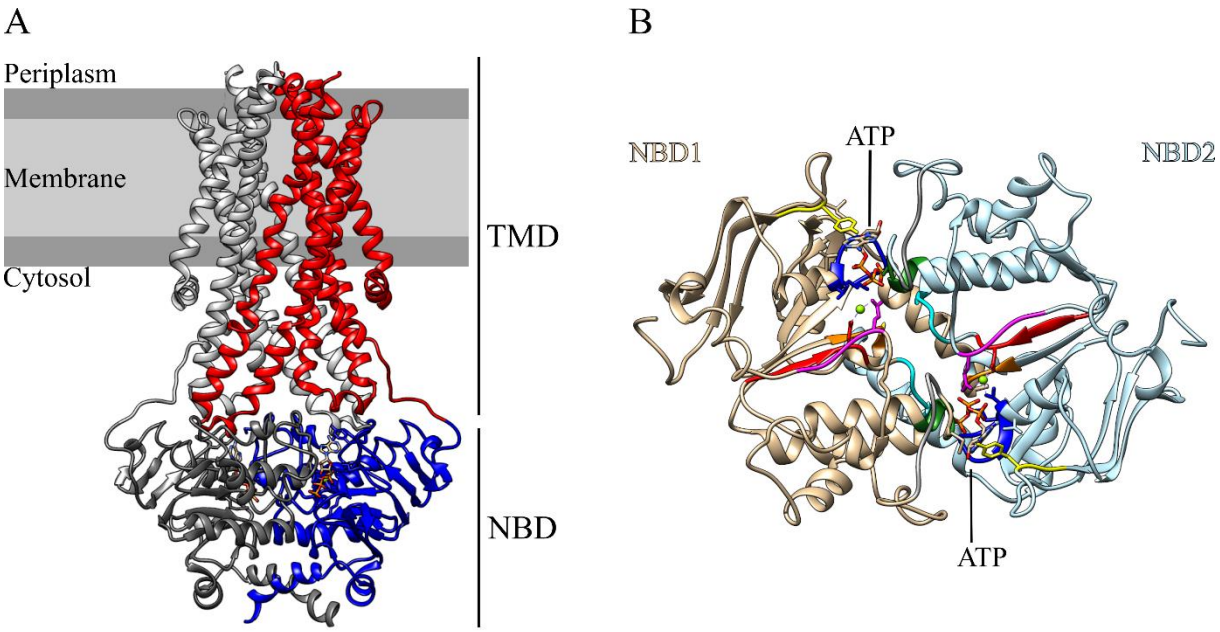

Figure 7: The ABC transporter BmrA (pdb: 6R81). A: The homodimeric BmrA placed within a membrane. One half of the transporter consists of a TMD (light grey/red) fused to a NBD (dark grey/blue). The BmrA structure is depicted in the OF conformation. B: Dimerized NBDs viewed from the membrane, without the TMD. Two ATP (sticks) and Mg^{2+} (green sphere) are sandwiched between the NBDs at the NBSs. The sequence motifs are colored as follows: A-loop (yellow), Walker A (blue), Q-loop (magenta), X-loop (grey), ABC signature (green), Walker B (red), D-loop (turquoise) and H-loop (orange).

1.5 Objectives of the thesis

ABC transporters are involved in many physiological processes within organisms. Their dysfunction in humans can lead to severe diseases, like cystic fibrosis, diabetes or Alzheimer's disease [83,85]. Furthermore, ABC exporters are commonly overexpressed in cancer cells or pathogenic bacteria and thus are responsible for the efflux of anticancer or antimicrobial drugs [67,171]. Often the given drugs do not affect the target sites, and therefore, ABC transporters are involved in or rather directly cause multidrug resistances (MDR) [172].

Not only due to the clinical relevance of P-gp in MDR [173], but also for analyzes of a manageable model protein, in this study the bacterial P-gp homolog BmrA was examined. The two ABC transporters share a high sequence and structure similarity and are able to transport similar substrates [165]. Thus, BmrA can be perfectly used to gain a better understanding of ABC transporters, regarding the following aspects:

I. Identification and characterization of a compound inhibiting the activity of BmrA

MDR, either caused by bacteria or cancer, is affecting the health of humans. Consequently, finding a small compound specifically inhibiting ABC transporters causing MDR is of major interest in clinical research, which is why screening for a possible BmrA inhibitor from fungal secondary metabolites was the basis of this research. The impact of a potential inhibitor was further characterized by performing activity, destabilization and competition assays.

II. Impact of the C-terminal end on the dimerization and activity of ABC transporter

Recently, the C-terminal end of the heterodimeric ABC transporter TmrAB was found to be involved in the dimerization of the NBDs as well as rearrange during the translocation cycle [174]. Thus, the impact of the C-terminal end on BmrA dimerization by performing activity assays of the homodimeric ABC transporter BmrA and C-terminal end variants was examined.

III. Stability of a homodimeric ABC transporter

The architecture of ABC transporters is diverse, since the amino acids of the TMDs and NBDs can be on one continuous polypeptide chain, on four separate polypeptide chains or one TMD and one NBD can be fused on one polypeptide chain. This indicates that the covalent connection between TMD and NBD does not exclusively seem to be crucial for the stability and/or activity of the transporter. Consequently, the impact of the non-covalent interactions at the transmission interface for the stability of BmrA were examined.

2 Materials

2.1 Chemicals

The chemicals used in this work were bought form AppliChem GmbH (Darmstadt, GER), Merck KGaA (Darmstadt, GER), Carl Roth GmbH + Co. KG (Karslruhe, GER), Thermo Fisher Scientific Inc. (Waltham, MA, USA) and VWR International GmbH (Darmstadt, GER).

2.2 Buffers and solutions

The buffers and solutions (Table 1) were prepared with demineralized water. Buffers and solutions were (sterile) filtered or autoclaved, if necessary.

Table 1: Compositions of the buffers and solutions used in this study.

Buffer/solution	Composition
Agarose gel electrophoresis	
6x DNA loading dye	50% glycerol (v/v) 0.2% bromophenol blue (w/v) 0.2% xylencyanol (w/v)
TAE buffer	400 mM Tris 200 mM acetic acid 10 mM EDTA
ATPase assay	
50 mM Hepes-KOH	50 mM Hepes, pH 8.0 5 mM DDM
Protein purification	
50 mM phosphate buffer	50 mM sodium phosphate, pH 8.0 300 mM NaCl 10% glycerol (v/v)
Solubilization buffer	50 mM phosphate buffer, pH 8.0 1% DDM (w/v)
Washing buffer 1	50 mM phosphate buffer, pH 8.0 0.1% DDM (w/v) 10 mM imidazole

Buffer/solution	Composition
Washing buffer 2	50 mM phosphate buffer, pH 8.0 0.1% DDM (w/v) 35 mM imidazole
Washing buffer 3	50 mM phosphate buffer, pH 8.0 0.1% DDM (w/v) 45 mM imidazole
Elution buffer	50 mM phosphate buffer, pH 8.0 0.1% DDM (w/v) 400 mM imidazole
SDS PAGE	
Separation gel buffer	1.5 M Tris, pH 8.8 0.4% SDS (w/v)
Stacking gel buffer	0.5 M Tris, pH 6.8 0.4% SDS (w/v)
5x SDS sample buffer	0.25 M Tris, pH 6.8 10% SDS (w/v) 0.2% bromophenol blue 50% glycerol (v/v) 0.5 M DTT
10x SDS running buffer	0.25 M Tris, pH 8.3 2 M glycine 1% SDS (w/v)
Coomassie staining solution	0.125% Coomassie Brilliant Blue G-250 40% ethanol (v/v) 2% phosphoric acid (v/v)
Coomassie destaining solution	30% ethanol (v/v) 2% phosphoric acid (v/v)
Transport assay	
Buffer A	50 mM Tris-HCl, pH 8.0 5 mM $MgCl_2$ 1 mM DTT 1 mM PMSF

Buffer/solution	Composition
Buffer B	50 mM Tris-HCl, pH 8.0 1.5 mM EDTA 1 mM DTT 1 mM PMSF
Buffer C	20 mM Tris-HCl, pH 8.0 300 mM sucrose 1 mM EDTA
Buffer D	50 mM Hepes-KOH, pH 8.0 2 mM $MgCl_2$ 8.5 mM NaCl 4 mM phosphoenolpyruvate 20 µg/mL pyruvate kinase

2.3 Bacteria

The utilized *E. coli* strains (Table 2) were cultivated and grown in LB medium (Table 3) with added antibiotics (Table 4). The *Bacillus subtilis* strain 168 (AG Unden) was cultivated in LB medium in absence of any antibiotics.

Table 2: Cultivated bacterial strains.

Bacteria	Genotype	Origin
Bacillus subtilis strain 168		AG Unden
E. coli NEB Turbo	F' *proA*$^+$*B*$^+$ *lacI*^{q} Δ*lacZM15* / *fhuA2* Δ*(lac-proAB) glnV galK16 galE15 R(zgb-210::Tn10)*Tet^S *endA1 thi-1* Δ*(hsdS-mcrB)5*	New England Biolabs GmbH (Ipswich, MA, USA)
E. coli BL21(DE3)pLysE	F$^-$ *ompT hsdS*$_B$ ($r_B^-m_B^-$) *gal dcm* (DE3) pLysE (Cam^R)	Merck KGaA (Darmstadt, GER)
E. coli C41(DE3)	F$^-$ *ompT hsdS*$_B$ ($r_B^-m_B^-$) *gal dcm* (DE3)	Merck KGaA (Darmstadt, GER)

Table 3: Media used to cultivate bacteria.

Medium	Composition
LB	1% tryptone (w/v) 0.5% yeast extract (w/v) 1% NaCl (w/v)

Medium	Composition
LB agar	LB 1.5% agar (w/v)
TSB	10% PEG4000 (w/v) 5% DMSO (v/v) 2% 1M $MgCl_2$ (v/v) 1% tryptone (w/v) 0.5% yeast extract (w/v) 0.5% NaCl (w/v)

Table 4: Antibiotic stock solutions.

Antibiotic	Stock solution
Ampicillin	100 mg/mL (50% EtOH (v/v))
Chloramphenicol	30 mg/mL (EtOH)

2.4 Plasmids

In this study the following plasmids containing an ampicillin resistance gene were used (Table **5**).

Table 5: Plasmids.

Plasmid	Origin
pET303-CT/His	Invitrogen (Carlsbad, CA, USA)
pET303-CT/His BmrA wt	this work
pET303-CT/His BmrA-NBD	AG Schneider
pET303-CT/His BmrA-TMD	AG Schneider
pET303-CT/His BmrA ΔCTh	this work
pET303-CT/His BmrA ΔCT	this work
pET303-CT/His BmrA L569A	this work
pET303-CT/His BmrA Y570A	this work
pET303-CT/His BmrA R571A	this work
pET303-CT/His BmrA D572A	this work
pET303-CT/His BmrA F573A	this work
pET303-CT/His BmrA A574V	this work
pET303-CT/His BmrA E575A	this work
pET303-CT/His BmrA Q576A	this work
pET303-CT/His BmrA Q577A	this work
pET303-CT/His BmrA L578A	this work

Plasmid	Origin
pET303-CT/His BmrA K579C	this work
pET303-CT/His BmrA M580C	this work
pET303-CT/His BmrA N581C	this work
pET303-CT/His BmrA A582C	this work
pET303-CT/His BmrA D583C	this work
pET303-CT/His BmrA W104YW164A	this work
pET303-CT/His BmrA W413Y	this work

2.5 Oligonucleotides

The oligonucleotides (Table 6) were synthesized by Sigma-Aldrich (Merck KGaA (Darmstadt, GER)).

Table 6: Utilized oligonucleotides. Highlighted in bold are the mutated bases. Sequences recognized by a restriction enzyme used for cloning are underlined.

Primer	5'-Sequence-3'
BmrA wt fw	GCTACCTCTAGAATGCCAACCAAGAAACAAAAATCTAAAAG
BmrA wt rev	GCTATTCTCGAGCCCGGCTTTGTTTTCTAAG
BmrA ΔCTh	GCTACCCTCGAG**ACCACCAGAACCACC**CAGCTGCTGTTCAG CAAAATC
BmrA ΔCT	GCTACCCTCGAG**ACCACCAGAACCACC**GCCATGGGAAGCC ATTAAC
BmrA L569A fw	GTTAATGGCTTCCCATGGC**GCG**TACCGGGATTTTGCTG
BmrA L569A rev	CAGCAAAATCCCGGTA**CGC**GCCATGGGAAGCCATTAAC
BmrA Y570A fw	GCTTCCCATGGCCTT**GCG**CGGGATTTTGCTGAAC
BmrA Y570A rev	GTTCAGCAAAATCCCG**CGC**AAGGCCATGGGAAGC
BmrA R571A fw	GCTTCCCATGGCCTTTAC**GC**GGATTTTGCTGAACAG
BmrA R571A rev	CTGTTCAGCAAAATCC**GC**GTAAAGGCCATGGGAAGC
BmrA D572A fw	CATGGCCTTTACCGGG**CG**TTTGCTGAACAGCAG
BmrA D572A rev	CTGCTGTTCAGCAAA**CG**CCCGGTAAAGGCCATG
BmrA F573A fw	GGCCTTTACCGGGAT**GCG**GCTGAACAGCAGCTG
BmrA F573A rev	CAGCTGCTGTTCAGC**CGC**ATCCCGGTAAAGGCC
BmrA A574V fw	CTTTACCGGGATTTTG**TG**GAACAGCAGCTGAAAATG
BmrA A574V rev	CATTTTCAGCTGCTGTTC**CA**CAAAATCCCGGTAAAG
BmrA E575A fw	CTTTACCGGGATTTTGCTG**CG**CAGCAGCTGAAAATG
BmrA E575A rev	CATTTTCAGCTGCTG**CG**CAGCAAAATCCCGGTAAAG
BmrA Q576A fw	CGGGATTTTGCTGAA**GC**GCAGCTGAAAATGAATGCG
BmrA Q576A rev	CGCATTCATTTTCAGCTGC**GC**TTCAGCAAAATCCCG
BmrA Q577A fw	GATTTTGCTGAACAG**GC**GCTGAAAATGAATGCG
BmrA Q577A rev	CGCATTCATTTTCAGC**GC**CTGTTCAGCAAAATC

Primer	5'-Sequence-3'
BmrA L578A fw	GATTTTGCTGAACAGCAG**GC**GAAAATGAATGCGGAC
BmrA L578A rev	GTCCGCATTCATTTTC**GC**CTGCTGTTCAGCAAAATC
BmrA K579C fw	GCTGAACAGCAGCTG**TGC**ATGAATGCGGACTTAG
BmrA K579C rev	CTAAGTCCGCATTCAT**GCA**CAGCTGCTGTTCAGC
BmrA M580C fw	GAACAGCAGCTGAAA**TGC**AATGCGGACTTAGAAAAC
BmrA M580C rev	GTTTTCTAAGTCCGCATT**GCA**TTTCAGCTGCTGTTC
BmrA N581C fw	CAGCAGCTGAAAATG**TGC**GCGGACTTAGAAAAC
BmrA N581C rev	GTTTTCTAAGTCCGC**GCA**CATTTTCAGCTGCTG
BmrA A582C fw	CAGCTGAAAATGAAT**TGC**GACTTAGAAAACAAAGCC
BmrA A582C rev	GGCTTTGTTTTCTAAGTC**GCA**ATTCATTTTCAGCTG
BmrA D583C fw	CTGAAAATGAATGCG**TG**CTTAGAAAACAAAGCC
BmrA D583C rev	GGCTTTGTTTTCTAAG**CA**CGCATTCATTTTCAG
BmrA W104Y fw	CTGCGGGAGTTATTAT**AT**AAGAAATTAATTAAG
BmrA W104Y rev	CTTAATTAATTTCTT**AT**ATAATAACTCCCGCAG
BmrA W164A fw	CTTGTTTATTATGAAC**GC**GAAGCTGACACTGCTTG
BmrA W164A rev	CAAGCAGTGTCAGCTTC**GC**GTTCATAATAAACAAG
BmrA W413Y fw	CTCGCTTGAATCGT**AT**AGGGAGCATATCGGG
BmrA W413Y rev	CCCGATATGCTCCCT**AT**ACGATTCAAGCGAG

2.6 Kits

Kits were used for extracting gel/PCR fragments, for plasmid preparation and to determine the protein concentration (Table 7).

Table 7: Kits.

Kit	Manufacturer
NucleoSpin Gel and PCR Clean-up	Macherey-Nagel GmbH & Co. KG (Düren, GER)
NucleoSpin Plasmid Kit	Macherey-Nagel GmbH & Co. KG (Düren, GER)
BCA Protein Assay Kit	Thermo Fisher Scientific Inc. (Waltham, MA, USA)

2.7 Instruments

Instruments used to perform experiments (Table 8).

Table 8: Instruments.

Instrument	Model	Manufacturer
Centrifuge	Avanti J-26XP	Beckman Coulter GmbH (Krefeld, GER)

Instrument	Model	Manufacturer
Centrifuge	Optima™ L-100K Ultracentrifuge	Beckman Coulter GmbH (Krefeld, GER)
	Sprout	Biozym Scientific GmbH (Hessisch Oldendorf, GER)
	5415 R	Eppendorf SE (Hamburg, GER)
	5810 R	Eppendorf SE (Hamburg, GER)
Electrophoresis chamber	Mini-Protean 3 Cell	Bio-Rad Laboratories GmbH (Feldkirchen, GER)
Electrophoresis chamber	Mini-Protean Tetra Cell	Bio-Rad Laboratories GmbH (Feldkirchen, GER)
	PerfectBlue Gelsystem S, M, L	VWR International GmbH (Darmstadt, GER)
Electrophoresis power supply	PowerPac Basic	Bio-Rad Laboratories GmbH (Feldkirchen, GER)
Fluorescence spectrometer	FluoroMax-4	Horiba Instruments Inc. (Edison, USA)
Gel documentation	Quantum-ST4 1100/26MX	VWR International GmbH (Darmstadt, GER)
Gel scanner	ViewPix 700	biostep GmbH (Burkhardtsdorf, GER)
Heating block	Thermomixer comfort	Eppendorf SE (Hamburg, GER)
Horizontal shaker	Polymax 1040	Heidolph Instruments GmbH & Co. KG (Schwabach, GER)
Incubator	B28	Binder GmbH (Tuttlingen, GER)
	Multitron HT	Infors AG (Bottmingen, CHE)
Overhead shaker	CMV-ROM	Labortechnik Fröbel GmbH (Lindau, GER)
pH-meter	pH211 Microprocessor	Hanna Instruments GmbH (Vöhringen, GER)
Photometer	Lambda 35	PerkinElmer GmbH (Waltham, MA, USA)
	Nanodrop 2000C	Thermo Fisher Scientific Inc. (Waltham, MA, USA)
	Ultrospec 10- Cell density meter	Amersham Biosciences (Amersham, GBR)
Plate Reader	Fluostar Omega	BMG Labtech GmbH (Ortenberg, GER)
Rotors	JA 25.50	Beckman Coulter GmbH (Krefeld, GER)
	JLA-8.100	Beckman Coulter GmbH (Krefeld, GER)
	45 Ti	Beckman Coulter GmbH (Krefeld, GER)
	70 Ti	Beckman Coulter GmbH (Krefeld, GER)
	90 Ti	Beckman Coulter GmbH (Krefeld, GER)
Shear homogenizer	Microfluidizer LM20	Microfluidics (Westwood, MA, USA)
Stir and heating plate	MR Hei-Standard	Heidolph Instruments GmbH & Co. KG (Schwabach, GER)
Test tube shaker	Vortex shaker	VWR International GmbH (Darmstadt, GER)
Thermocycler	Tgradient 96	Biometra GmbH (Göttingen, GER)

2.8 Software

Used software and programs (Table 9).

Table 9: Software and programs.

Application	Software	Company
Chemical structure	ACD/ChemSketch, version 2021.1.1	[9]; Advanced Chemistry Development Inc. (Toronto, ON, CAN)
Data analysis	Excel Microsoft 365	Microsoft Corporation (Redmond, WA, USA)
	Origin 2019b	OriginLab Corporation (Northampton, MA, USA)
Figure editing	Adobe Photoshop 2020	Adobe Systems Software Ireland Limited (Dublin, IRL)
	Inkscape, version 1.1.1	GNU General Public License
	PowerPoint Microsoft 365	Microsoft Corporation (Redmond, WA, USA)
Protein structure	UCFS Chimera 1.15	Resource for Biocomputing, Visualization, and Informatics (RBVI; San Francisco, CA, USA)
Reference management	Mendeley 1.19.8	Elsevier Inc. (New York, NY, USA)
SDS PAGE quantification	ImageJ 1.47	[175]; GNU General Public License
Text editing	Word Microsoft 365	Microsoft Corporation (Redmond, WA, USA)

3 Methods

3.1 Molecular biological methods

3.1.1 Polymerase chain reaction

The polymerase chain reaction (PCR) was used to amplify a specific DNA fragment defined by primers or for site-directed mutagenesis (Table 6). For PCRs, the polymerase Phusion (Thermo Fisher Scientific Inc. (Waltham, MA, USA)) was used. The components (Table 10) for amplifying segments of DNA and site-directed mutagenesis were the same. Though, for the temperature program (Table 11), the cycles of denaturation, annealing and extension used for site-directed mutagenesis were 16 instead of 36.

Table 10: PCR reaction components.

Component	Volume [µL]
DNA	1.0
10 µM primer (forward)	1.0
10 µM primer (reverse)	1.0
2 mM dNTPs	1.0
Phusion polymerase	0.5
5x Phusion buffer	10.0
DMSO	1.0
25 mM $MgCl_2$	1.0
Nuclease free H_2O	33.5

Table 11: PCR program.

	Temperature [°C]	Time [min]	Cycle
Initial denaturation	98	1.0	1
Denaturation	98	0.5	36
Annealing	55	1.0	
Extension	72	1.0/kb	
Final extension	72	7.5	1

The amplified DNA segments were mixed with the 6x loading dye (Table 1) and run on a 1% agarose gel in TAE buffer. For separation of the DNA segments on an agarose gel a voltage of 120–150 V was applied. After staining the gel with ethidium bromide, the DNA signals could be detected by UV-light.

To the site-specifically mutated DNA, 1 µL DpnI was added and the sample was incubated for 1 h at 37 °C to digest the original DNA.

3.1.2 Isolation of DNA fragments

The DNA fragments amplified by PCR and separated on an agarose gel were stained by ethidium bromide. The DNA signals were visible under UV-light. Agarose gel pieces containing the desired DNA were extracted with a scalpel. Said DNA fragments were purified using the NucleoSpin Gel and PCR Clean-up kit according to the manufacturer's instructions (Table 7).

3.1.3 Construction of the BmrA wt plasmid

The *B. subtilis* strain 168 gene *bmrA* was amplified via PCR from genomic DNA (chapter 3.1.1). The isolated PCR fragment (chapter 3.1.2) was restriction digested by the restriction enzymes XhoI and XbaI to generate specific sticky ends. The DNA fragment, restriction enzymes and buffers were used and incubated in accordance with the manufacturer's instructions (New England Biolabs GmbH (Ipswich, MA, USA)). The PCR fragment with sticky ends was again run on and extracted from an agarose gel. The same restriction enzymes were used to digest and linearize the pET303-CT/His plasmid (Table 5). The two DNA fragments with complementary ends (plasmid and *bmrA*) were ligated by the T4 DNA ligase (Thermo Fisher Scientific Inc. (Waltham, MA, USA)). For the ligation, 100 ng of the linearized plasmid and a 4fold excess of the insert gene were used and incubated for 2 h at RT following the manufacturer's instructions. The ligated vector pET303-CT/His BmrA wt (Figure 26) was transformed into competent NEB Turbo *E. coli* cells (Table 2).

3.1.4 Plasmid preparation

The amplified or mutated plasmids were purified using the NucleoSpin Plasmid kit following the manufacturer's instructions (Table 7). The DNA concentration was determined via measuring the absorption at 260 nm. The DNA sequence was confirmed by sequencing (Eurofins Genomics GmbH (Ebersberg, GER)).

3.2 Microbiological methods

3.2.1 Preparation of competent *E. coli* cells

Following the one-step procedure developed by Chung *et al.* in 1989, *E. coli* cells were made competent for transformation [176]. A culture of 50 mL LB medium was inoculated either 40:1 with an overnight preculture of a single colony or directly with a single NEB Turbo *E. coli* colony. The culture was incubated at 37 °C and 200 rpm in an incubator until the optical density determined at 600 nm (OD_{600}) was ≥ 0.5. Then, the bacteria were pelleted by centrifugation (3220 x g, 10 min, 4 °C). After discarding the supernatant, the pellet was resuspended in 5 mL ice-cold TSB medium (Table 3). Aliquots of 100 µL cell suspension were frozen in liquid nitrogen and stored at –80 °C.

3.2.2 Transformation in competent *E. coli* cells

Transformation of plasmids in chemically competent *E. coli* cells was used to amplify plasmids or for heterologous protein expression. Therefore, 1 µL of plasmid DNA was added to the competent cells under sterile conditions. After 20 min incubation on ice, the cells were exposed to heat (43 °C, 1.5 min) and 500 mL LB medium was added. After incubating the *E. coli* cells for 1 h (37 °C and 200 rpm) in an incubator, 200 µL of the suspension was plated on LB medium agar plates with the appropriate antibiotics to sort out untransformed cells.

3.2.3 Heterologous expression of BmrA proteins

For heterologous protein expression, a single colony of transformed BL21(DE3)pLysE or C41(DE3) *E. coli* cells (Table 2) was used to inoculate an overnight culture (50 mL LB medium), which was used the next morning to inoculate a 2 L LB medium culture, containing 100 µg/mL ampicillin and 30 µg/mL chloramphenicol (when the BL21(DE3)pLysE strain was used). The cells were cultivated at 37 °C with constant agitation (150 rpm). When the culture reached an OD_{600} of ~0.8, protein expression was induced via addition of IPTG to a final concentration of 0.5 mM or 0.7 mM (when the C41(DE3) strain was utilized). The bacterial cells were harvested after 3–4 hours via centrifugation (3050 x g, 10 min at 4 °C). The cell pellets then were stored at –20°C until further use.

3.3 Biochemical methods

3.3.1 Purification of BmrA

The cell pellets containing the overexpressed proteins were resuspended in 50 mM phosphate buffer (Table 1) and lysed using a microfluidizer (18000 PSI). After centrifuging the cell lysate at 12075 x g (10 min at 4 °C), the supernatant was centrifuged again at 165000 x g for 1 h at 4 °C to isolate the BmrA containing membranes. The membranes were solubilized in solubilization buffer (Table 1) to extract membrane-incorporated proteins. After 1 h of incubation under constant agitation, insolubilized proteins were removed by centrifugation (165000 x g, 20 min) and the equilibrated Protino® Ni-NTA agarose (2 mL resin/L *E. coli* culture; Macherey-Nagel GmbH & Co. KG (Düren, GER)) was mixed with the solubilized proteins and incubated for 1 h. The proteins contain a His_6-tag attached to the C-terminus, which binds to the Ni-NTA. After transferring the Ni-NTA agarose with bound protein to a polyethylene filter column (Thermo Fisher Scientific Inc. (Waltham, MA, USA)), the column matrix was washed with 25 mL washing buffer 1 (Table 1), 50 mL washing buffer 2 (Table 1) and 35 mL washing buffer 3 (Table 1). Then the protein was eluted with 5 mL elution buffer (Table 1).

Purification of the soluble isolated NBD of BmrA differed from the purification of the full-length membrane proteins. Yet, the cell lysis and the initial centrifugation of the cell lysate were identical. The supernatant, obtained after the centrifugation of broken cells expressing the soluble NBD, was directly incubated with the equilibrated Ni-NTA resin. After a 1 h incubation, the matrix was washed with 50 mL of 50 mM phosphate buffer (Table 1) followed by 50 mL 50 mM phosphate buffer (Table 1) with 10 mM imidazole and 25 mL 50 mM phosphate buffer (Table 1) with 40 mM imidazole. The protein was eluted with 5 mL 50 mM phosphate buffer (Table 1) containing 400 mM imidazole.

To exchange the buffer of a protein to a required assay buffer, a PD-10 desalting column (Macherey-Nagel GmbH & Co. KG (Düren, GER)) was utilized. Using the Lambert-Beer law (equation 1) the concentration of the purified protein was determined.

$$E_{280} = \varepsilon \cdot c \cdot d \tag{1}$$

To determine the concentration (c in mol/L), the equation 1, consisting of the proteins extinction at λ = 280 nm (E_{280}), the respective extinction coefficient (ε) in $M^{-1}cm^{-1}$ (Table 12), calculated with ExPASy ProtParam [177] and the length of solution the light passes through (in cm), had to be rearranged.

Table 12: Extinction coefficients and molecular weights of BmrA and BmrA variants.

Protein	Extinction coefficient [$M^{-1}cm^{-1}$]	Molecular weight [Da]
BmrA wt	38850	65584.27
BmrA NBD	15930	29730.69
BmrA TMD	22920	37067.91
BmrA ΔCTh	38850	64727.24
BmrA ΔCT	37360	63462.83
BmrA L569A	38850	65542.19
BmrA Y570A	37360	65492.17
BmrA R571A	38850	65499.16
BmrA D572A	38850	65540.26
BmrA F573A	38850	65508.17
BmrA A574V	38850	65612.33
BmrA E575A	38850	65526.24
BmrA Q576A	38850	65527.22
BmrA Q577A	38850	65527.22
BmrA L578A	38850	65542.19
BmrA K579C	38975	65559.24
BmrA M580C	38975	65556.22
BmrA N581C	38975	65573.31
BmrA A582C	38975	65616.33
BmrA D583C	38975	65572.32
BmrA W104YW164A	29340	65446.10
BmrA W413Y	34840	65561.23

3.3.2 SDS Polyacrylamide gel electrophoresis

SDS Polyacrylamide gel electrophoresis (PAGE) was used to separate proteins by their molecular mass [178]. In this study, 10% discontinuous SDS PAGE gels were used (Table 13).

Table 13: Separation and stacking gel compositions.

	Separation gel	Stacking gel
H_2O	5.0 mL	6.0 mL
Acrylamide (40%)	2.5 mL	1.5 mL
Separation gel buffer	2.5 mL	-
Stacking gel buffer	-	2.5 mL
APS (10%)	100 µL	100 µL
TEMED	40 µL	40 µL

Protein samples were mixed with 5x SDS sample buffer (Table 1). To visualize Cys-crosslinked proteins, DTT was omitted from the 5x SDS sample buffer (Table 1). The electrophoresis was performed for 45 min at 200 V in SDS running buffer. The SDS PAGE gels were stained for 1 h with Coomassie staining solution and then incubated for at least 1 h in Coomassie destaining solution to visualize the proteins separated in the gels.

3.3.3 SDS-induced unfolding

To unfold full-length BmrA wt, $BmrA_{W104YW164A}$, $BmrA_{W413Y}$ as well as the isolated NBD and TMD, 2 µM of each purified protein in assay buffer (50 mM sodium phosphate (Table 1) with 5 mM DDM) was exposed to increasing concentrations of SDS. As mixed DDM/SDS micelles form upon the addition of SDS, the SDS mole fraction (χ_{SDS}) was used to describe the detergent concentration in the mixed micelles. The χ_{SDS} was determined as in equation 2, describing the ratio of the detergents (SDS+DDM) to SDS and ranging from $\chi_{SDS} = 0$ to $\chi_{SDS} = 0.95$ (Table **16**). In the equation c_{SDS} refers to the SDS concentration and c_{DDM} to the concentration of DDM.

$$\chi_{SDS} = \frac{c_{SDS}}{(c_{SDS+}c_{DDM})} \quad (2)$$

The samples containing the proteins in DDM and varying concentrations of SDS were incubated for 1 h at 25 °C and then Trp fluorescence spectra were recorded (chapter 3.4.2).

3.3.4 Urea-induced unfolding

BmrA wt, $BmrA_{W104YW164A}$, $BmrA_{W413Y}$ as well as the isolated NBD and TMD were exposed to increasing concentrations of urea. Thus, a urea stock solution in 50 mM sodium phosphate (Table 1) with 5 mM DDM was prepared and its concentration determined by equation 3 using the refractive index of the assay buffer ($n_{D,\,buffer}$) as well as refractive index of the urea stock solution (urea dissolved in the buffer, $n_{D,\,urea}$).

$$\text{urea [M]} = 0.1527 \times (n_{D,\,urea}-n_{D,\,buffer}) + 0.001216 \times (n_{D,\,urea}-n_{D,\,buffer})^2 \quad (3)$$

The purified proteins at 2 µM final concentration were each exposed to increasing urea concentrations (ranging from 0 to 6.5 M urea in 0.5 M steps), and the samples were incubated at 25 °C for 1 h. After the incubation, the Trp fluorescence spectra were recorded (chapter 3.4.2).

3.3.5 Destabilization of BmrA in DDM micelles

Purified BmrA (2 µM) in 50 mM phosphate buffer with 5 mM DDM was mixed with increasing amounts myristic acid (concentrations: 0 mM, 0.1 mM, 0.2 mM, 0.3 mM, 0.4 mM, 0.5 mM, 0.75 mM, 1.0 mM). The samples were incubated at room temperature for 1 h and the Trp fluorescence spectra were recorded (chapter 3.4.2). As a control, samples were incubated with SDS and prepared as described in chapter 3.3.3 with concentrations of 0 mM, 0.21 mM, 0.43 mM, 0.68 mM, 0.95 mM and 1.25 mM SDS.

3.3.6 Preparation of inverted *E. coli* membrane vesicles

For the preparation of inverted *E. coli* membrane vesicles [164] C41(DE3) cells (Table 2) with overexpressed BmrA were used. The buffers needed for the preparation are listed in Table **1**, DTT and PMSF was added before use and all steps were performed on ice. A cell pellet of a 2 L expression culture was resuspended in buffer A and lysed using a microfluidizer (18000 PSI). After the lysis, EDTA (pH 8, 10 mM final concentration) was added to the cells and the debris and unbroken cells were removed by centrifugation (10000 x g, 30 min, 4 °C). The cell membranes with overexpressed proteins were gained after centrifuging the supernatant at 140000 x g for 1 h at 4 °C. The supernatant was discarded, the pellet was resuspended in 20 ml buffer B and subsequently centrifuged again for 1 h at 140000 x g and 4 °C. The pellet containing the membrane vesicles was resuspended in 4 ml buffer C. Small aliquots were frozen in liquid nitrogen and stored at –80 °C. The protein concentration was determined with a BCA assay (Table 7), following the manufacturer´s instructions.

3.3.7 Stability of BmrA in inverted vesicles

Inverted vesicles (250 µg/mL) with overexpressed BmrA wt were incubated with either 0.1 mM or 1.0 mM myristic acid for 1 h at room temperature under constant agitation. As a control, 0.5% (v/v) methanol was added to the inverted vesicles. As a second control, vesicles were incubated with 1 mM SDS. After incubation, the samples were centrifuged at 140000 x g for 1 h at 25 °C. Samples were taken before incubation with the substances and after centrifugation (from the supernatant as well as the pellet). A total of 10 µL of each sample was analyzed on a 10% SDS PAGE gel (chapter 3.3.2).

3.3.8 BS^3-crosslink

Purified BmrA wt, isolated TMD and NBD in 50 mM phosphate buffer (Table 1) containing 5 mM DDM were crosslinked using the BS^3-crosslinker (Thermo Fisher Scientific Inc. (Rockford, IL, USA)). The BS^3-crosslinker was dissolved in 20 mM sodium phosphate buffer at a concentration of 12.5 mM. The protein concentration was 0.25 mg/mL of purified BmrA wt, isolated TMD, isolated NBD or mixed TMD+NBD. A 50fold molar excess of the crosslinker was utilized and the samples were incubated for 30 min at 25 °C and 400 rpm agitation in a heating block. The reaction was quenched by adding Tris-HCl (pH 8.0) with a final concentration of 50 mM Tris and incubating the samples for 15 min at room temperature. The samples were mixed with 5x SDS sample buffer (Table 1) and analyzed via SDS PAGE (chapter 3.3.2).

3.4 Biophysical methods

3.4.1 ATPase activity of purified BmrA

The ATPase activity of 0.2 µM BmrA wt protein or BmrA variants was measured in DDM micelles at 25 °C in 50 mM Hepes-KOH (Table 1) with 3.5 mM ATP, 10 mM $MgCl_2$, 0.28 mM NADH, 2 mM phosphoenolpyruvate, by adding 2 µL of pyruvate kinase (PK, 600–1000 U/mL)/lactate dehydrogenase (LDH, 900–1400 U/mL) mix (Sigma-Aldrich, Merck KGaA (Darmstadt, GER)) to the 200 µL test volume (Table 14).

Table 14: Components used for the ATPase activity assay.

Component	Final concentration	Volume added
BmrA	0.2 µM	
ATP	3.5 mM	
$MgCl_2$	10 mM	
NADH	0.28 mM	
Phosphoenolpyruvate	2 mM	
PK/LDH mix		2 µL
50 mM Hepes-KOH, 5 mM DDM		ad. 200 µL

The changes in absorption, originating from the consumption of NADH, were measured at a wavelength of 340 nm and a slit width of 4 nm using a Lambda 35 UV/Vis spectrophotometer. The NADH decrease was measured for 180 s and converted into the BmrA activity in min^{-1}.

$$ATPase\ activity = -\frac{\Delta A_{340}}{\Delta t} \cdot \frac{1}{l \cdot \varepsilon_{NADH}} \quad (4)$$

Equation 4 consists of the slope ($\frac{\Delta A_{340}}{\Delta t}$) of the NADH decrease, the optical pathlength (l in cm) and the extinction coefficient of NADH (ε_{NADH} = 6220 $M^{-1}cm^{-1}$).

3.4.1.1 ATPase activity of BmrA wt in presence of myristic acid

To determine the inhibitory effect of myristic acid in chapter 4.1 on the ATPase activity (chapter 3.4.1) of BmrA wt, commercially available myristic acid (Sigma-Aldrich, Merck KGaA (Darmstadt, GER), M3128) with a high purity (≥ 99%) was used to perform the experiments. For the experiment, myristic acid (dissolved in methanol) or DMPC (solved in chloroform) was pipetted at the specified amounts into the reaction tubes. Subsequently, the solvent was removed by a constant stream of nitrogen, and these reaction tubes were further stored for at least 30 min under vacuum. The dried fatty acid was dissolved in 50 mM Hepes-KOH (Table 1) and the solution was vortexed and further incubated for at least 1 h under constant agitation (500 rpm). Thereafter, the protein was added, and the solution incubated for another 10 min at 25 °C. After adding the other compounds to the solution (Table 14), the decrease in absorbance was immediately monitored. The BmrA wt ATPase activity was set as 100% and the data points measured at different myristic acid and DMPC concentrations were normalized to this level with respect to the error propagation.

3.4.2 Tryptophan fluorescence spectroscopy

The Trp residues occurring naturally in proteins can be used to study protein structural changes. Local changes in the polarity in the environment of a Trp can be detected by fluorescence spectroscopy. Thus, a Trp fluorescence emission spectrum can change in intensity plus the intensity maximum can shift. A Trp exposed to a hydrophobic environment leads to a shift in the maximum intensity to smaller wavelengths (blue-shift) as well as an increase in the Trp fluorescence emission intensity [179].

In this study, the Trp fluorescence intensity was used to study the stability of BmrA towards denaturing agents (SDS and urea) and the fatty acid myristic acid.

Trp fluorescence emission spectra of the samples (chapter 3.3.3, 3.3.4, 3.3.5) were recorded at 25 °C from 290 nm to 450 nm (slit width 3 nm) and excitation at 280 nm (slit width 3 nm). The measurements were performed using a FluoroMax-4 fluorometer.

For the data analysis of the fluorescence emission spectra gained for the samples of the proteins in presence of SDS (chapter 3.3.3), the fluorescence intensities at a fixed wavelength were determined for each SDS mole fraction.

For the analysis of the urea-induced unfolded protein samples (chapter 3.3.4), the maximum fluorescence intensities of the emission spectra for each concentration were determined.

For the destabilization experiment described in chapter 3.3.5, the average emission wavelength (<λ>), which represents changes in shape and position of the spectrum, was used to characterize the entire measured Trp fluorescence emission spectrum. The <λ> was calculated as described in the following equation 5.

$$< \lambda >= \frac{(\Sigma_i \lambda_i \cdot I_i)}{\Sigma_i I_i} \quad (5)$$

Here λ is the wavelength in nm and I is the fluorescence intensity.

3.4.3 Hoechst 33342 transport activity of BmrA in inverted membrane vesicles

The transport activity of BmrA, which was overexpressed in inverted *E. coli* membrane vesicles (chapter 3.3.6), was determined in the Hoechst 33342 transport activity assay. In this assay, the hydrophobic dye 2'-[4-ethoxyphenyl]-5-[4-methyl-1-piperazinyl]-2,5'-bis-1H-benzimidazole (Hoechst 33342) was used as a substrate for BmrA. For each sample, 50 µg protein of inverted membrane vesicles was used in a total volume of 200 µL. The samples were diluted in buffer D (Table **1**) and kept at 25 °C for 10 min. The fluorescence emission was measured for 10 min in total at 457 nm using a FluoroMax-4 fluorometer upon excitation at 355 nm, with excitation and emission slit widths of 2 nm and 3 nm, respectively. First, the fluorescence was monitored for approx. 50 s and then the measurement was stopped. Subsequently, 2 µM Hoechst 33342 was added, the sample mixed, and the fluorescence was measured again for approx. 50 s. Then, ATP was added (final concentration of 2 mM) and the sample was quickly mixed afterwards. The fluorescence was further monitored for overall ~500 s. Data points were collected every 0.5 s and the initial slope of the measured fluorescence intensity after ATP addition was determined.

The expression level of BmrA wt and the different variants (experiments performed in chapter 4.2) was determined based on the signal intensity of the overexpressed BmrA and the variants obtained by SDS PAGE analysis. The relative expression level was quantified using ImageJ [175] and the determined transport activities were normalized to the respective

expression level assuming a linear correlation. The transport activity determined for BmrA wt was set as 100% and the different variants were normalized to this transport activity with error propagation.

3.4.3.1 Transport activity of BmrA wt in presence of myristic acid

Myristic acid (dissolved in methanol) of various concentrations (3 µM, 7 µM, 10 µM, 20 µM, 30 µM, 40 µM, 50 µM, 75 µM, 100 µM, 200 µM, 300 µM, 400 µM, 500 µM, 750 µM, 1000 µM) was added to the inverted vesicles with overexpressed BmrA wt (50 µg protein) and the samples were incubated for more than 10 min. The maximal concentration of methanol in this reaction mixture was 0.5% (v/v). The transport activity of BmrA wt in the presence of myristic acid was followed by fluorescence spectroscopy (chapter 3.4.3). The slope of the measured fluorescence intensity (after addition of ATP) was determined by fitting a linear regression line with a large coefficient of determination. To evaluate the inhibitory effect of myristic acid, the absolute value of the slope of the sample containing inverted membrane vesicles with overexpressed BmrA wt plus methanol (0.5% (v/v)) was set as 100% transport activity and the data points obtained at different myristic acid concentrations were normalized to this, considering error propagation. All presented data are based on at least three independent inverted vesicle preparations, and the mean with corresponding SEM was calculated.

3.4.3.2 Competition assay

For the Hoechst 33342 vs. myristic acid competition assay, the inverted membrane vesicles containing 50 µg protein were incubated with 0.2 mM myristic acid for at least 10 min at 25 °C. The fluorescence signal was measured as described (chapter 3.4.3; exception: slit width of 3 nm). When the measurement was started, the fluorescence was monitored for 50 s. Then, varying concentrations of Hoechst 33342 were added (0.03 µM, 0.06 µM, 0.12 µM, 0.24 µM, 0.3 µM, 0.4 µM, 0.5 µM, 0.6 µM, 1.0 µM, 1.2 µM) and the measurement and data evaluation continued as described before (chapter 3.4.3).

4 Results and Discussion

4.1 Myristic acid inhibits the activity of the bacterial ABC transporter BmrA

A version of this chapter has been originally published in the International Journal of Molecular Science in 2021:

Oepen, K.; Özbek, H.; Schüffler, A.; Liermann, J.C.; Thines, E.; Schneider, D. Myristic Acid Inhibits the Activity of the Bacterial ABC Transporter BmrA. Int. J. Mol. Sci. 2021, 22, 13565. https://doi.org/ 10.3390/ijms222413565

This chapter contains the unchanged text of the introduction, results, discussion, conclusions and implications. The numbering of figures is continuous in this dissertation, as well as the references. Materials and methods used to perform the experiments can be found in chapter 2 and 3. Methods used by co-authors can be found in the appendix 11.2. The author contributions are listed in Table 15 and the authors affiliations in chapter 10. The original publication is added in chapter 11.3 [180].

Table 15: Author contributions Myristic acid inhibits the activity of the bacterial ABC transporter BmrA.

Study conception	Complete study	KO, AS, DS
Writing	Original draft	KO, DS
	Review and editing	KO, DS
Project administration, Funding acquisition, Resources	Complete study	ET, DS
Supervision	Complete study	AS, ET, DS
Methodology	Screening	HÖ, AS
	NMR	JCL

Figures (numbers refer to the original publication)	**Methodology, Investigation, Formal analysis**	**Data visualization**
Figure 1A-C	KO	KO
Figure 2	KO	KO
Figure 3A, B	KO	KO
Figure 4	KO	KO
Figure 5	KO	KO

4.1.1 Introduction

Membrane integral transport proteins mediate and control the translocation of essential compounds across biological membranes, involving the uptake and efflux of sugars, inorganic ions, nucleotides or drugs [133]. Primary active transporters use the energy gained via ATP hydrolysis for transport [133,181], and such transport ATPases are typically represented by ion pumps and ATP-binding cassette (ABC) transporters [181]. ABC transporters can be found in all kingdoms of life and they either import or export substrates against a concentration gradient. While, in bacteria, ABC importers and exporters can be found, eukaryotes mainly have exporters [133,182]. Structurally, all ABC transporters consist of two nucleotide binding domains (NBDs) and two transmembrane domains (TMDs). The TMDs consist of α-helix bundles that mediate the actual TM flux of the substrates, whereas ATP is hydrolyzed in the NBDs [138,160,182]. In contrast to the NBD, the sequences of the TMDs are typically less conserved and the TM topology can vary. The four domains of an ABC transporter can be part of a single polypeptide chain, or the transporter assembles form two to four individual subunits [102,138]. One TMD and one NBD can be fused to form a so-called half-transporter, which can either form a homodimeric (identical half-transporters) or assemble as a heterodimeric (different half-transporters) full-transporter [91,133,182,183].

Many ABC transporters appear to be involved in bacterial multidrug resistances [184]. For example, in cervimycin C resistant *Bacillus subtilis* colonies the *bmrA* gene, encoding an ABC half-transporter, was strongly overexpressed, which led to the assumption that BmrA (*Bacillus* multidrug-resistance ATP) is able to effectively transport this antibiotic out of the cell [165,166]. Besides cervimycin C, BmrA can transport a broad range of substrates, which include Hoechst 33342, doxorubicin as well as 7-aminoactinomycin D [165].

BmrA, a homodimeric ABC transporter with a molecular mass of 64.9 kDa, is homologous to the bacterial ABC transporters LmrA and MsbA [102,168] as well as to the human P-glycoprotein [165,182]. In recent years, BmrA became a paradigm for studying ABC transporters, mostly due to the vast number of seemingly unrelated substrates as well as its homology to the human P-glycoprotein [165,168,185].

As BmrA is involved in excretion of certain antibiotics out of bacterial cells, we aimed at identifying small molecules which inhibit the BmrA transport activity and thus might be used to modulate the BmrA transport activity. Screening of extract libraries isolated from fungi revealed that the C14 fatty acid myristic acid has an inhibitory effect on the BmrA ATPase as well as the transport activity. Thus, BmrA “sleeps with the enemy”, as a natural membrane

constituent inhibits its activity, a finding with physiological consequences as to the activity and regulation of ABC transporter activities in biological membranes.

4.1.2 Results

4.1.2.1 Myristic acid inhibits the ATPase activity of the ABC transporter BmrA.

In total, 448 fungal extracts were tested for an inhibitory effect on the BmrA ATPase activity and 22 were found to be active. One of the most promising candidates, the mycelial extract of strain IBWF 030-11, was selected for further characterization. To identify the natural product responsible for the inhibitory effects, the fungus was cultivated in 20 L scale and the active principle was isolated. Based on NMR analysis, the isolated substance was identified as the C14 fatty acid myristic acid (Figure 8A), 0.25 mg of which was isolated per L axenic fungus culture.

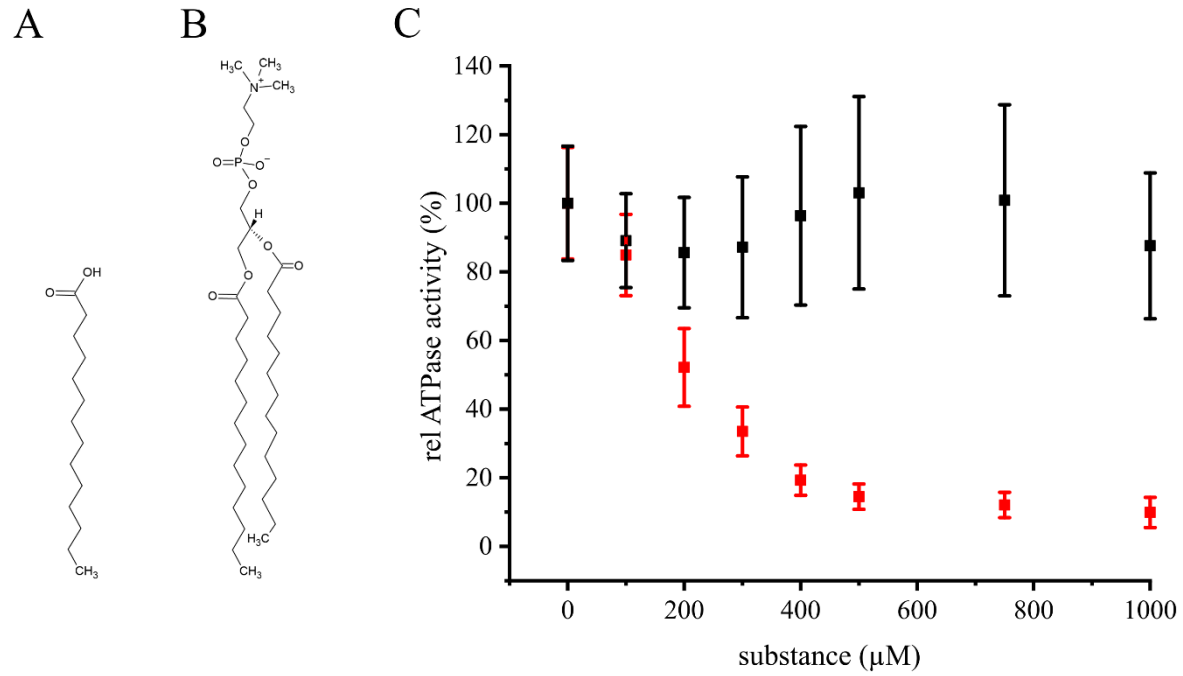

Figure 8: Inhibition of the BmrA ATPase activity by myristic acid. (A) Structure of the fatty acid myristic acid ($C_{14}H_{28}O_2$). (B) Structure of 1,2-dimyristoyl-sn-glycero-3-phosphocholine (DMPC), a membrane phospholipid containing two myristic acids as fatty acids. The structures were created using ChemSketch [9]. (C): Myristic acid ($n \geq 6$, ± SEM; red) inhibits the *in vitro* ATPase activity of detergent solubilized BmrA, whereas the lipid 1,2-dimyristoyl-sn-glycero-3-phosphocholin (DMPC, n = 12, ± SEM; black) does not.

To quantitatively evaluate the inhibitory potential of myristic acid, we next examined the *in vitro* ATPase activity of BmrA at increasing myristic acid concentrations (Figure 8C, red).

The BmrA ATPase activity was determined in buffer containing myristic acid concentrations ranging from 0 to 1000 µM to calculate the IC_{50} value, i.e., the substance concentration required to inhibit 50% of the protein´s ATPase activity. The ATPase activity of BmrA in pure 5 mM DDM was 1.0 ± 0.16 µmol/min per mg protein, a value comparable to values previously determined under slightly different experimental conditions [111,167]. As expected in the presence of an inhibitor, the ATPase activity constantly decreased with increasing myristic acid concentrations, until at ~500 µM myristic acid the activity levelled off to about 12%. Based on this analysis, the turning point, i.e., the IC_{50}, is at approximately 200 µM myristic acid. Furthermore, these results additionally indicate that myristic acid is not a BmrA substrate that stimulates the ATPase activity, as has been observed with other ABC transporter substrates [186–188].

Nevertheless, the concentration for free myristic acid within the membrane is low *in vivo*, as myristic acid typically is part of diacylglycerol lipids. This now raised the question whether the ATPase activity of BmrA is also affected by myristic acid-containing phospholipids. Thus, we next tested the *in vitro* ATPase activity of isolated BmrA in presence of increasing concentrations of 1,2-dimyristoyl-sn-glycero-3-phosphocholine (DMPC, Figure 8B, C, black). DMPC is a glycerophospholipid, containing two myristic acids as fatty acids attached to the glycerol backbone. As the determined ATPase activity of BmrA is not significantly affected by DMPC, the inhibitory effects observed before can clearly be linked to the isolated myristic acid.

4.1.2.2 The stability of BmrA in micelles is not affected by myristic acid

Myristic acid has detergent properties and can form micelles in solution [189]. As harsh detergents can unfold (membrane) proteins [190], at least to some extent, the question arose whether myristic acid does not inhibit the BmrA ATPase activity via binding but via denaturation of the protein structure, resulting in a diminished protein activity.

As changes in a local tryptophan environment, e.g., caused by protein denaturation, result in a different fluorescence emission spectrum, the stability of purified BmrA in DDM micelles can be determined by fluorescence spectroscopy. A well-established approach to unfold membrane proteins is to solubilize the protein in a mild detergent, such as DDM, and to subsequently titrate in increasing amounts of a harsh detergent, typically SDS [191,192]. Addition of SDS results in formation of mixed DDM/SDS micelles, which eventually unfold α-helical membrane proteins. It is noteworthy that, while the mixed micelles can indeed unfold soluble regions or domains of membrane proteins, the membrane integral protein parts typically retain their helical

structure, and the term “unfolding” here in fact describes the separation of previously interacting individual TM α-helices [193].

When the purified protein was exposed to increasing SDS concentrations, the average emission wavelength (<λ>) decreased (Figure 9, black). At a low SDS mole fraction of χ_{SDS} = 0.04 the <λ> slightly increased, a behavior also observed with other TM proteins [194], whereas higher SDS concentrations led to a dramatic decrease in the average emission wavelength. In contrast, while addition of low myristic acid concentration also resulted in a slight increase in the <λ>, further increasing the myristic acid concentration resulted in a slightly decrease, albeit the <λ> myristic acid never changed to an extent as observed with SDS. This indicates that myristic acid does not substantially destabilize the protein, in contrast to SDS.

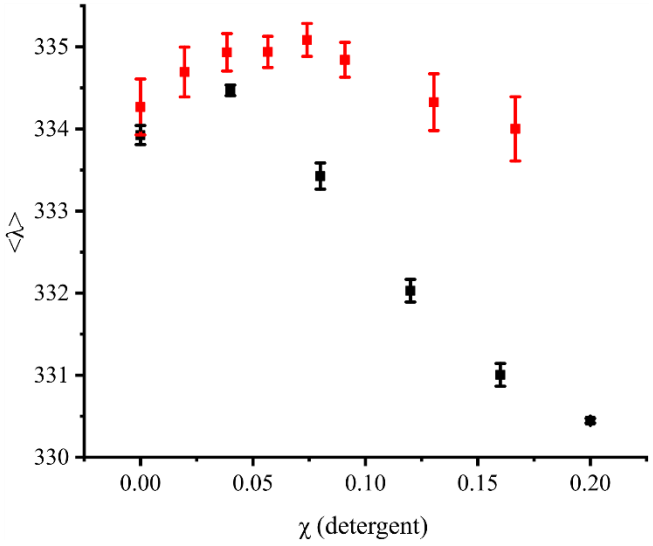

Figure 9: Myristic acid does not destabilize the BmrA structure as SDS. Increasing amounts of myristic acid (n = 9, ± SEM; red) or SDS (n = 7, ± SEM; black) were titrated to BmrA solubilized in DDM micelles. While addition of SDS leads to a larger decrease in the average emission wavelength (<λ>), this was not observed when myristic acid was added.

4.1.2.3 Myristic acid inhibits the BmrA-mediated transport of Hoechst 33342 in inverted membrane vesicles.

Hoechst 33342 is a substrate commonly used when the BmrA activity is studied in inverted membrane vesicles. Upon spontaneous membrane partitioning, the dye´s fluorescence increases. When the dye is actively transported out of the lipid membrane by BmrA and expelled to the liquid surrounding, the fluorescence decreases again. Importantly, the transport of Hoechst 33342 depends on the BmrA ATPase activity [165].

At first, the initial fluorescence of the inverted membrane vesicles was monitored in absence of Hoechst 33342 (Figure 10A). Subsequently, upon addition (Figure 10A, 1) and membrane incorporation of Hoechst 33342, the fluorescence increased tremendously due to membrane partitioning of the dye [195]. After addition of ATP the fluorescence intensity decreased again due to the removal of Hoechst 33342 from the membrane. The decrease in the fluorescence intensity thus directly correlates with the BmrA transport activity [195]. When the BmrA-mediated Hoechst 33342 transport was measured in inverted membrane vesicles pre-incubated with myristic acid, the initial fluorescence intensities were similar. Upon ATP addition (Figure 10A, 2), the fluorescence intensity first decreased, as observed in absence of myristic acid, yet remained on a higher fluorescence level. This implies that more Hoechst 33342 molecules remained incorporated within the lipid bilayer, and thus, less Hoechst 33342 molecules were transported by the ABC transporter (Figure 10A; red). For comparison, the absolute value of the slope was used to quantify the transport activity. The BmrA wild type transport activity was set as 100% and the generated values at increasing myristic acid concentrations were normalized to the wild type (Figure 10B).

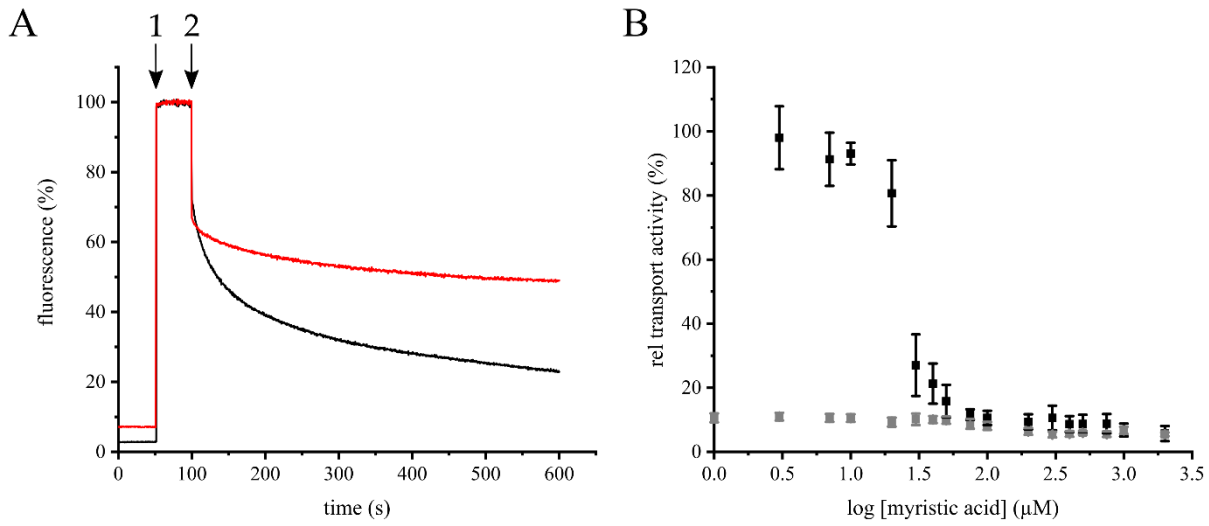

Figure 10: Myristic acid inhibits Hoechst 33342 transport in inverted C41(DE3) *E. coli* membrane vesicles. (A) Kinetics of Hoechst 33342 transport followed in absence (black) or presence of 1000 µM myristic acid (red), 1: addition of Hoechst 33342, 2: addition of ATP. (B) 3–1000 µM myristic acid was added to inverted membrane vesicles prepared from BmrA expression cells (black) or *E. coli* C41(DE3) cells transformed with an empty vector (grey) and Hoechst 33342 transport was quantified (n = 3, ± SEM).

To test a (potential) inhibition of the BmrA transport activity, myristic acid was added to inverted membrane vesicles at increasing concentrations (3–1000 µM) and the Hoechst 33342 transport was quantified (Figure 10B) The BmrA transport activity was essentially not affected

up to myristic acid concentrations of 10 µM. However, at 20–50 µM myristic acid, the transport activity of BmrA massively decreased, and at around 100 µM myristic acid a plateau was reached. Based on a Boltzmann fit, an IC_{50} value of about 25 µM myristic acid was determined for the Hoechst transport using inverted vesicles. As expected, the inverted vesicles prepared from *E. coli* C41(DE3) cells transformed with an empty vector did not show activity at any given myristic acid concentration.

Yet, myristic acid might not inhibit the BmrA transport activity but in fact is a substrate that simply competes with Hoechst 33342 for transport. To test this assumption, inverted vesicles were first exposed to 0.2 mM myristic acid, and the Hoechst 33342 transport was measured as before, but at different Hoechst 33342 concentrations. Upon addition of ATP, the absolute value of the slope of the fluorescence decrease was determined at each Hoechst 33342 concentration (Figure 11). When Hoechst 33342 and myristic acid compete for transport, addition of small amounts of Hoechst 33342 should not result in a measurable transport activity, and only at rather high Hoechst 33342 concentrations is an activity is expected to be observed. As can be seen in Figure 11, the absolute value of the slope increased linearly with increasing Hoechst 33342 concentrations for the control (no myristic acid). In contrast, the activity of the inverted vesicles containing a constant myristic acid concentration but increasing Hoechst 33342 concentrations increased linearly up to a concentration of ~0.6 µM Hoechst 33342. At higher Hoechst 33342 concentrations, the initial slope remained more or less constant. If Hoechst 33342 and myristic acid were both substrates competing for binding and translocation, an initial significantly slowed down Hoechst 33342 transport would be expected at the (high) constant myristic acid concentration. However, this was not observed. Instead, the transport activity leveled off at a rather low Hoechst concentration. Consequently, the data indicate that there is no simple competitive or non- or uncompetitive inhibition of BmrA by myristic acid. The BmrA activity is inhibited by myristic acid via a rather complex mechanism. Noteworthy, the fluorescence intensities (without ATP added) of the control and the myristic acid-incubated inverted vesicles were more or less equal for each Hoechst 33342 concentration. The increasing amounts of Hoechst 33342 lead to a linearly increasing slope (data not shown).

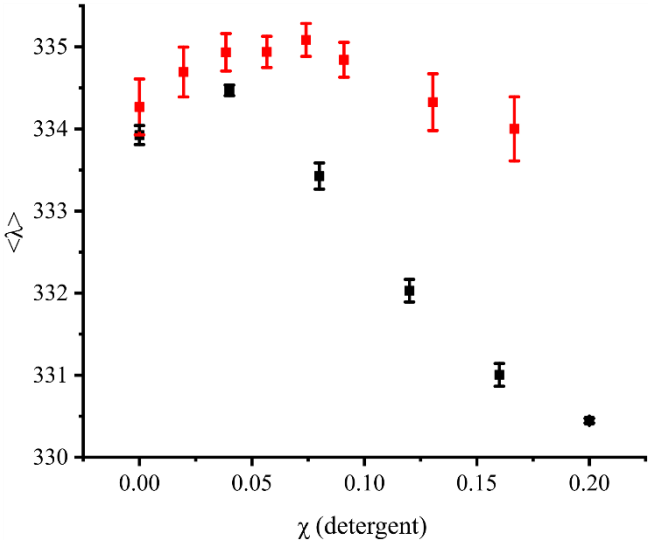

Figure 11: BmrA-mediated Hoechst 33342 transport at a constant myristic acid concentration. 0.2 mM myristic acid (red) or methanol (control; black) were added to the inverted membrane vesicles and Hoechst 33342 transport was tested at increasing Hoechst 33342 concentrations (n = 3, ± SEM).

4.1.2.4 Myristic acid does not solubilize overexpressed BmrA in inverted vesicles

Due to the detergent properties of myristic acid, it was possible that the fatty acid solubilized the overexpressed protein in the inverted vesicles, resulting in the observed decreased BmrA transport activity. To finally exclude this, vesicles were incubated with the detergent SDS or myristic acid for 1 h. Subsequently, solubilized protein was separated from membranes via ultracentrifugation, and solubilized proteins were analyzed via SDS PAGE. As can be seen in Figure 12, while BmrA was properly solubilized by SDS, neither at low nor at high myristic acid concentrations BmrA was extracted from the membranes. Thus, the inverted vesicles remained intact at the here analyzed myristic acid concentrations.

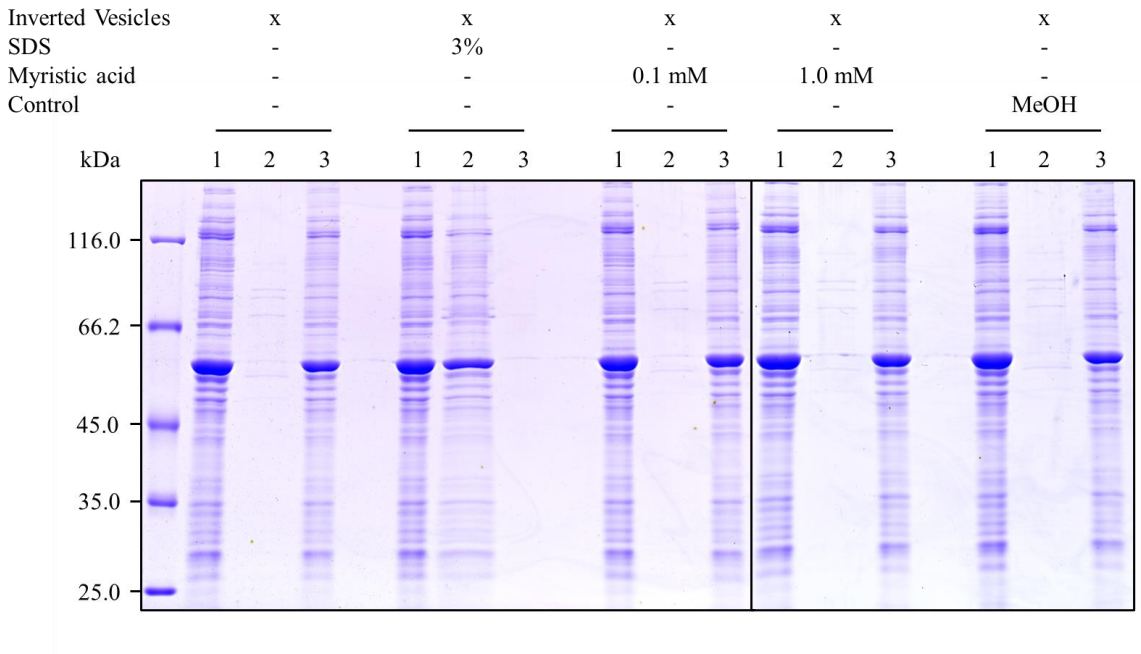

Figure 12: Stability assay of inverted vesicles with overexpressed BmrA. Inverted vesicles were exposed to either SDS (3% (w/v)), myristic acid (0.1 mM or 1.0 mM dissolved in methanol) or methanol (0.5% (v/v)). Intact membranes were found in the pellet, whereas solubilized membrane proteins were found in the supernatant (solely when SDS was added). 1: BmrA and membrane proteins in inverted vesicles not influenced by any substances. 2: Supernatant after ultracentrifugation containing solubilized BmrA (and other membrane proteins). 3: Pellet after ultracentrifugation comprising of inverted vesicles with overexpressed BmrA. This experiment was performed three times with three different inverted membrane vesicle preparations, which all showed the same results.

4.1.3 Discussion

In the present study, we identified myristic acid as a potential inhibitor of the BmrA ATPase and transport activity. This saturated C14 fatty acid (Figure 8A) is widely distributed in plant and animal fat and can naturally be found in high concentrations in coconut oil as well as in butter fat. Furthermore, myristic acid is utilized in the food industry as multifunctional food additive and flavor excipient [196]. In *Bacillus subtilis*, around 3.6% of all lipids are myristic acid [197]. Yet, myristic acid inhibits the BmrA activity exclusively as a free acid, but not when part of phospholipids (Figure 8C; black). Thus, while 3–4% of all lipids in *Bacillus subtilis* are myristic acid, most of these will be part of di- or even triacylglycerols and thus the concentration of the inhibiting species, i.e., the free acid, will be low.

As we have shown here, myristic acid does neither inhibit the BmrA activity indirectly, via destabilizing membranes and extracting the protein from membranes (Figure 12), nor via detergent-induced denaturation of the protein (Figure 9). Thus, myristic acid appears to directly

inhibit the BmrA ATPase and transport activities (Figure 8C, Figure 10B), albeit the inhibitory mechanism appears to be complex.

It is well known that, e.g., the detergent Triton X-100 stimulates the ATPase activity of the ABC transporter P-glycoprotein [198], and based on this and other observations, it has been concluded that detergents can serve as P-glycoprotein substrates [199]. In many cases, addition of substrate even increases the ATPase activity of ABC transporters, which was, however, not observed here. ABC transporter substrates have rather diverse structures [165], and also fatty acids are transported by ABC transporters [200]. This has been shown for some ABC transporters, such as MsbA or LmrA [201,202]. When the lipid A ABC transporter MsbA was heterologously expressed in *L. lactis* cells, it has been observed that myristic acid might be transported due to no change in the determined IC_{50} value [202]. Yet, based on the results presented here (Figure 11), myristic acid appears not to simply compete with Hoechst 33342 for the substrate binding site and transport.

But why is the determined IC_{50} value so much higher when the ATPase activity was monitored than when the transport activity was monitored? Although we cannot ultimately answer this question, these two measurements can only be compared to some extent. While we have a well-defined protein and detergent concentration when the isolated protein was analyzed, this was not the case in the inverted vesicles. Furthermore, in inverted vesicles we might have other components that interact with myristic acid. Yet, this would probably reduce, and not increase, the inhibitory activity of myristic acid. In bacterial membranes, most membrane lipids are not part of bulk lipids, but are (more or less tightly) bound to membrane proteins (reviewed [203]). Thus, the concentration of myristic acid added to the lipid phase is probably much higher at any given total myristic acid concentration, compared to the situation in micelles. In the latter, the myristic acid will incorporate into free micelles as well as into BmrA-containing micelles to form mixed micelles. Thus, myristic acid likely is highly diluted in the micellar system, which results in a rather high IC_{50} value for the determined ATPase activity. Finally, it is also possible that myristic acid induces a conformational change or decoupling of the NBD and TMD in the lipid environment, as e.g., observed with the mutant BmrA E474R [169].

4.1.4 Conclusions and Implications

At first, inhibition of an ABC transporter activity by a naturally occurring fatty acid appears to be unexpected, albeit the physiological concentration of myristic acid in *Bacillus subtilis* membranes is probably not sufficiently high to compromise the BmrA transport activity.

However, it might even be beneficial to inhibit a basal ATPase activity, by which ATP might be wasted in cells, *in vivo* using naturally occurring membrane incorporated substances, such as myristic acid.

The initial idea of this project was to identify potential modulators of the BmrA activity. Based on the presented results myristic acid might qualify as a drug excipient, as co-application with ABC transporter substrates might reduce the risk of drug export out of a cell. Furthermore, as mentioned in the discussion, myristic acid is used as a multifunctional food additive and flavor excipient [196]. Thus, this food additive has the potential to interfere with (human) ABC transporters, an aspect which, to the best of our knowledge, has never been discussed thus far and which we will explore in future experiments.

4.2 The C-terminus is crucial for homodimerization and activity of the ABC transporter BmrA

4.2.1 Introduction

The family of ABC transporters is conserved in all kingdoms of life [67,204]. These transporters either import (mainly in bacteria and plants) or export a broad variety of substrates [62,65]. Structurally, ABC transporters consist of four core domains: two TMDs and two cytosolic NBDs, albeit the exact molecular architecture of these transporters is extremely diverse (Figure 3) [62,131,182]. In fact, a transporter can consist of a single polypeptide chain that contains all four domains, or, if one TMD and one NBD are part of one polypeptide chain, two different of these half-transporters either heterodimerize, such as the ABC transporter TAP1/TAP2 [59] or two identical half-transporters homodimerize (e.g. Sav1866) to form an active transporter [95]. Finally, when each of the four domains are individual proteins, these have to oligomerize to form a functional ABC exporter [182,205].

ABC exporters mostly consist of twelve TM helices [62,130] and the substrate-binding cavity is located between these helices. The structurally diverse substrates enter this cavity either from the cytosolic side of the membrane or the membrane [206,207] and during a translocation cycle the transporter undergoes major conformational changes (chapter 1.3.5), finally resulting in transmembrane transport of a substrate against a concentration gradient [95,146,161,182,208]. Transport requires ATP hydrolysis by the NBDs, which are located at the cytosolic side. The sequences and topologies of NBDs of different ABC transporters are highly similar and motifs involved in ATP recognition, binding and hydrolysis are conserved [90,131,209]. These motifs within the NBDs are located in two different subdomains of the NBD, an α-helical domain with the ABC signature motif and the X-loop, and a RecA-like subdomain with the Walker A and Walker B motifs, Q-, D- and H-loop. Basically, ATP is bound between the Walker A of one NBD and the ABC signature motif of the opposing NBD (Figure 5, Figure 7B) [86,97]. Consequently the ATP-binding sites are created by both NBDs and thus ATP-binding triggers dimerization of the two opposing NBDs [91,94,100,108,111,210]. This in turn causes a conformational change of the exporter from an IF conformation via an occluded to an OF conformation. Furthermore, the CHs at the cytoplasmic side of the protein are relevant for the NBD-TMD communication [93,95,157]. After the transporter switches to an OF conformation, the TMDs cavity is open to the periplasmic side of the membrane and the substrate is released. Substrate release and ATP hydrolysis set the transporter back into the IF conformation and the transporter is ready for the next translocation cycle (chapter 1.3.5) [105].

Isolated NBDs tend not to dimerize in absence of ATP [211], yet, in full- or half-transporters the TMDs facilitate NBD dimerization upon ATP binding. Sometimes, NBDs of transporters contain additional domains, and e.g. the ABC importer MalK has an extra C-terminal regulatory domain (of 136 residues) to stabilize the dimer also in absence of ATP [212,213]. Furthermore, the NBDs of the tetrameric ABC transporter $ModB_2C_2$ are suggested to be in constant contact, mediated by the C-terminal ends, which are α-helices that interact to a certain amount and thereby connect the NBDs [214]. Likewise, the homodimers Atm1 [215] and HlyB [124] appear to have interacting helices at their NBDs C-terminus, which were postulated to stabilize the dimer. Since many ABC exporters have C-terminal α-helices, this structure might contribute to the dimer stability in general [216]. Yet, the exact role of these short C-terminal helices in the translocation cycle is essentially still enigmatic, albeit the C-terminal helices are important for and rearrange during the translocation cycle of the heterodimeric ABC exporter TmrAB [174].

Could this also be the case for the homodimeric ABC transporter BmrA (1.4)? Recently, the structure of the BmrA exporter in the OF conformation was solved by X-ray and cryo EM (Figure 7) [144] and in these structures, BmrA shows overlapping, mostly α-helices at the C-terminal end of the NBDs.

4.2.2 Results

The structure of BmrA has recently been solved in the OF conformation [144]. In line with previous observations, that many ABC exporters have α-helices at the C-terminal end which might contribute to the dimer stability [216], in BmrA a short α-helix is present at the very C-terminus of the protein as well, and the two C-terminal helices of two interacting monomers arrange in an anti-parallel fashion to each other (Figure 7, Figure 13). Yet, based on the recently solved structures of the BmrA (pdb: 6R81, pdb: 6R72, pdb: 7OW8, pdb: 7BG4), these C-terminal ends are not always entirely α-helical, plus the helix is not continuous but can be interrupted by a small unstructured region (M580/N581), which separates two rather short helical segments. Therefore, in the present study we analyzed (i) whether the BmrA C-terminal helices are crucial for the BmrA activity and (ii) whether the C-termini of adjacent BmrA half-transporters interact.

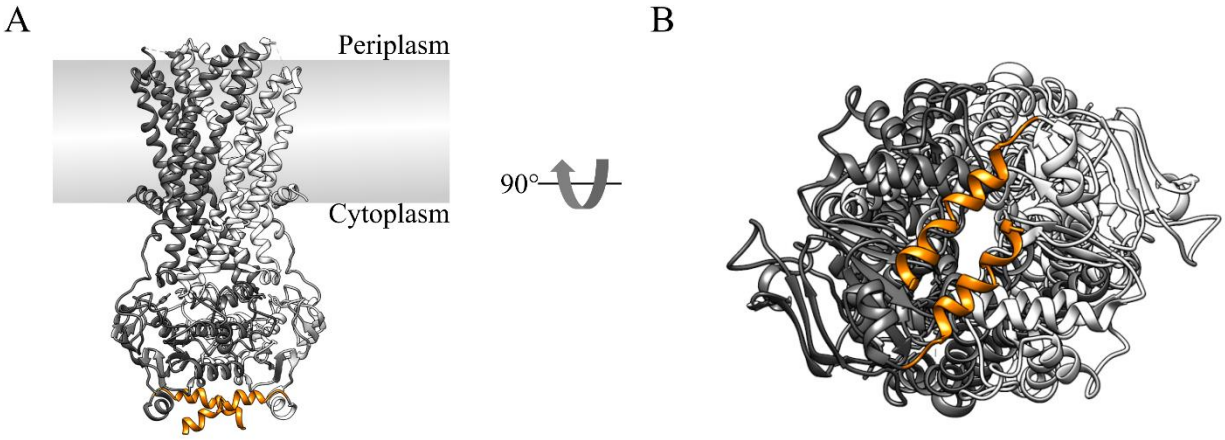

Figure 13: The ABC transporter BmrA in the OF conformation (pdb: 6R81). A: BmrA dimer (half-transporters: white and dark grey) with the α-helices at the C-terminal ends (orange) of the NBDs depicted within a lipid bilayer (grey). B: View on the C-termini from the cytosolic side after a 90 ° rotation of the BmrA dimer.

4.2.2.1 The C-terminus is crucial for the BmrA activity

To analyze the putative role of the C-terminal helix on the BmrA activity in greater detail, the C-terminal α-helix of BmrA was either completely (residues L569-G589, ΔCT, Figure 13, Figure 14A) or solely half of the residues of the very C-terminal end (residues K579-G589, ΔCTh, ”h” for half, Figure 14A) were removed.

While the ATPase activity of BmrA ΔCTh was not significantly reduced compared to the wt (Figure 14B), indicating a dispensable function of this region, the ATPase activity was essentially completely abolished when the entire C-terminus was removed.

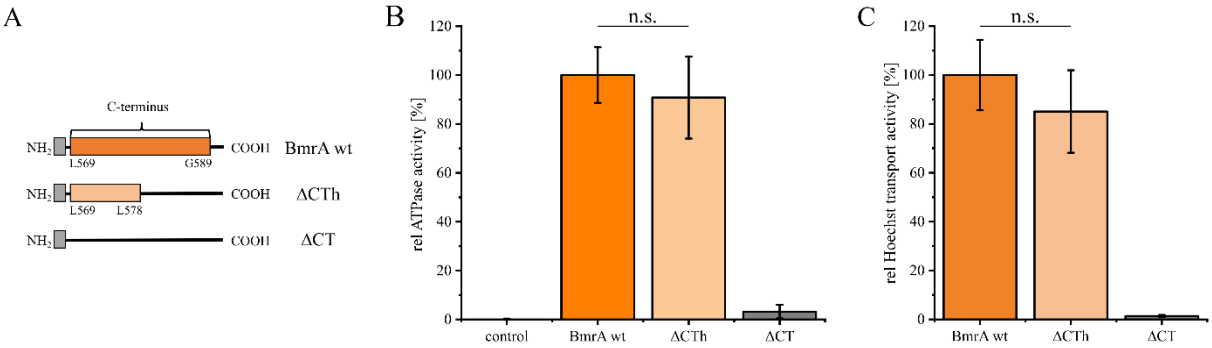

Figure 14: BmrA lost its ATPase and Hoechst 33342 transport activity when the C-terminal end was removed completely. A: Sketch of the C-terminal end showing the ΔCTh and the ΔCT compared to BmrA wt. B: Relative ATPase activity of BmrA wt and the variants in DDM micelles ($n \geq 11$, ± SEM, two-sample t-test). C: Relative Hoechst 33342 transport activity assay of inverted membrane vesicles containing overexpressed BmrA wt or variants ($n \geq 9$, ± SEM, two-sample t-test).

Next, we aimed to quantify the substrate transport activity of the BmrA variants and used inverted membrane vesicles to determine transport of the hydrophobic dye Hoechst 33342 across the membrane. Similar to the above presented observations, ΔCTh showed a slightly, yet not significantly reduced transport activity compared to BmrA wt, whereas the transport activity of ΔCT was essentially completely abolished (Figure 14C).

Thus, we concluded that the C-terminal residues L569 to L578 are crucial for the BmrA wt ATPase activity, whereas the amino acids at the very C-terminal end appear to have neither an impact on the ATPase nor on the transport activity of BmrA.

4.2.2.2 Ala scanning of essential C-terminal residues

Based on the results presented above, we next elucidated which of the amino acids of the essential C-terminal helix fragment (residues L569 to L578) were most critical for the ATPase and transport activity of BmrA. For this purpose, the individual amino acids of the C-terminus were replaced by Ala (or Val, when an Ala was naturally present), and the ATPase as well as the Hoechst 33342 transport activities of these BmrA variants were tested (Figure 15). While the variants D572A-E575A displayed an ATPase activity (Figure 15A), which was > 70% of the wt activity, the activity of most of the other variants was < 50% of the wt activity. The ATPase activity of the variants L569A and Y570A was most severely affected and reduced to 15% and 3% of the wt activity, respectively. Thus, based on these analyses, the core of this helical fragment (residues D572-E575) did most likely not establish crucial contacts, whereas the bordering residues L569-Y571 and Q576-L578 appeared to be more crucial for the BmrA ATPase activity.

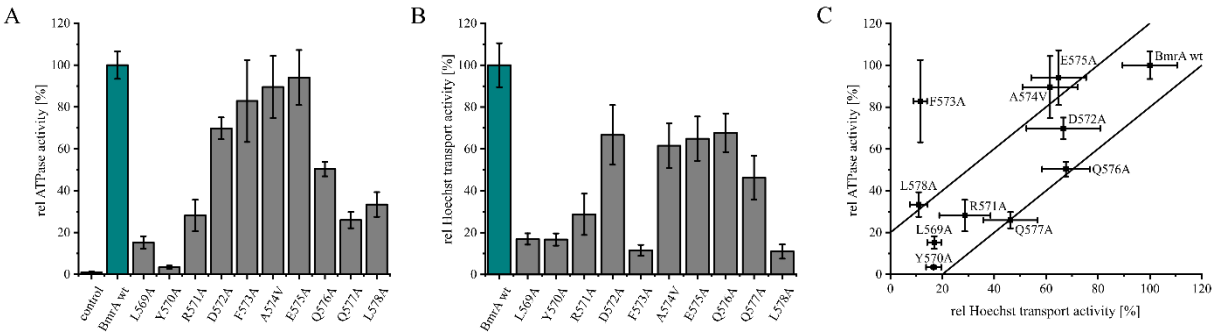

Figure 15: ATPase activity and Hoechst 33342 transport activity of BmrA wt and the C-terminal Ala (Val) variants L569A-L578A. A: Relative ATPase activity of BmrA wt and the Ala (Val) variants in DDM micelles (n ≥ 6, ± SEM). B: Relative Hoechst transport activity of BmrA wt and the Ala variants overexpressed in inverted membrane vesicles (n ≥ 7, ± SEM). C: Relative ATPase activity versus the relative transport activity with a 20% error range.

Whether the determined ATPase and the relative Hoechst transport activity correlate, was next analyzed using inverted membrane vesicles (Figure 15B). The transport activity of four variants (L569A, Y570A, F573A and L578A) was less than 20% compared to the BmrA wt activity, whereas the activity of the variants D572A and A574V-Q577A was reduced "only" to about 70% of the wt activity. While for most variants, the respective ATPase and Hoechst transport activities were decreased to a similar extent (Figure 15C), one variant showed a strikingly different pattern: BmrA F573A had an almost wt-like ATPase activity, albeit its relative transport activity was drastically reduced. Thus, the decrease in the transport activity of most variants was due to the decrease in the ATPase activity, whereas for the F573A variant solely the transport activity was affected.

4.2.2.3 Cys scanning mutagenesis and Cys crosslinking of the C-terminus

Recently, a direct interaction of the C-terminal helices of two adjacent ABC half-transporters has been observed and it has been proposed that this interaction prevents transmembrane substrate transport [174]. Based on the available BmrA structures, the C-terminal helices of two protomers seem to form an antiparallel helix dimer, and the two helices cross at residue N581 where the distance between the C_α residues is about 7 Å in the OF conformation (Figure 16).

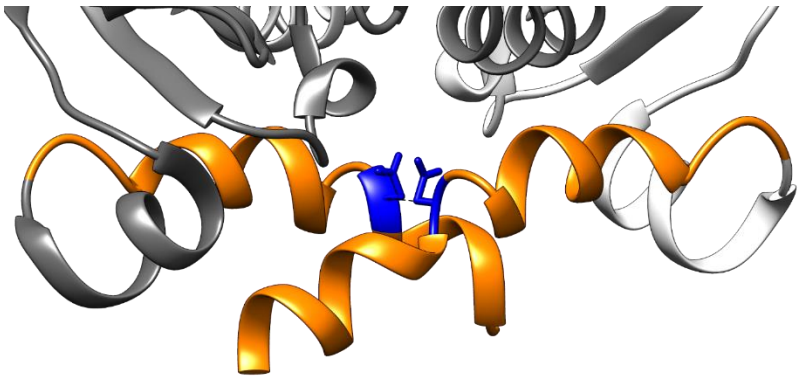

Figure 16: Antiparallel C-terminal helix dimer of BmrA in the OF conformation (pdb: 6R81). The C-terminal helices (orange) of two BmrA monomers (grey and white) are in closes distance and cross at the amino acid N581 (blue). The distance of the C_α of opposing N581 is about 7 Å.

Thus, we aimed at crosslinking the two C-terminal helices of interacting BmrA half-transporters via introducing a Cys residue at position N581 to analyze the potential impact of enforced dimerization on the BmrA activity. Furthermore, we individually replaced the neighboring residues K579 to D583 by Cys to check whether here disulfide bridges and covalent linkage of

two neighboring NBDs also form in absence of ATP. Subsequently, the ATPase activity of these variants was tested under reducing as well as oxidizing conditions, where disulfide bridges might form (Figure 17A). If a mutation had no severe impact on the BmrA activity under reducing conditions, but affected the activity under oxidizing conditions, the impact of covalent linkage could be studied. The ATPase activity of BmrA wt under oxidizing conditions was at approx. 0.5 ± 0.16 µmol/min per mg protein and under reducing conditions slightly decreased to around 0.4 ± 0.15 µmol/min per mg protein, demonstrating, that the reducing agent does not significantly influence the activity in this assay *per se*.

However, for the variants the ATPase activity was somewhat reduced under reducing conditions (Figure 17A, black) compared to the BmrA wt, indicating that the respective mutations directly affected, but not abolished, the BmrA activity to some extent (Figure 14B).

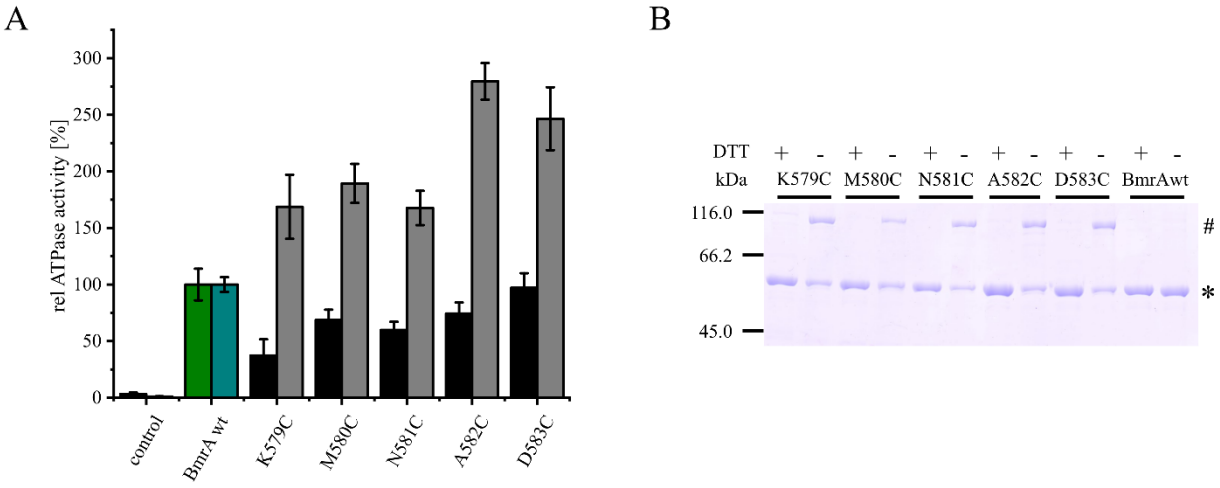

Figure 17: Relative ATPase activity and crosslinking of BmrA wt and the Cys variants under different oxidation states. A: BmrA wt and the Cys variants in DDM micelles were tested in a pyruvate kinase/lactate dehydrogenase-coupled assay under reducing (black) and oxidizing (grey) conditions to identify the ATPase activity ($n \geq 6$; ± SEM). B: SDS PAGE analysis of the purified proteins under reduced (+) and oxidized (-) conditions shows the monomers (*, between 45.0 and 66.2 kDa of the marker signal) and the crosslinked dimer signals (#, around 116.0 kDa marker signal).

Strikingly, under oxidizing conditions (Figure 17A, grey), i.e. when formation of disulfide bridges was promoted, the ATPase activity of the analyzed variants was up to 3fold higher than measured for the wt, indicating that disulfide-bond formation significantly enhanced the ATPase activity. In fact, all variants formed stably crosslinked dimers, as observed via SDS PAGE analysis (Figure 17B), and thus covalent linkage of BmrA NBDs and facilitated dimer formation clearly increased the ATPase activity of the protein. Furthermore, while in the structure the C-terminal helices cross at residue N581, the capability of all analyzed Cys

variants to crosslink indicates a certain flexibility of this part, since no preferred interacting residue could be determined.

Next the impact of enforced NBD dimerization on the Hoechst 33342 transport activity was studied (Figure 18A). When compared to the wt, the overall transport activity of the variants was decreased under reducing conditions, in line with the results of the ATPase assay. Similarly, all variants were equally or less transport active determined under oxidized conditions compared to the respective wt. In line with the ATPase activity measurements, the BmrA variants M580C-D583C displayed an increased transport activity under oxidizing conditions when compared to reducing conditions (Figure 17A), while BmrA K579C was significantly more active under reducing than under oxidizing conditions.

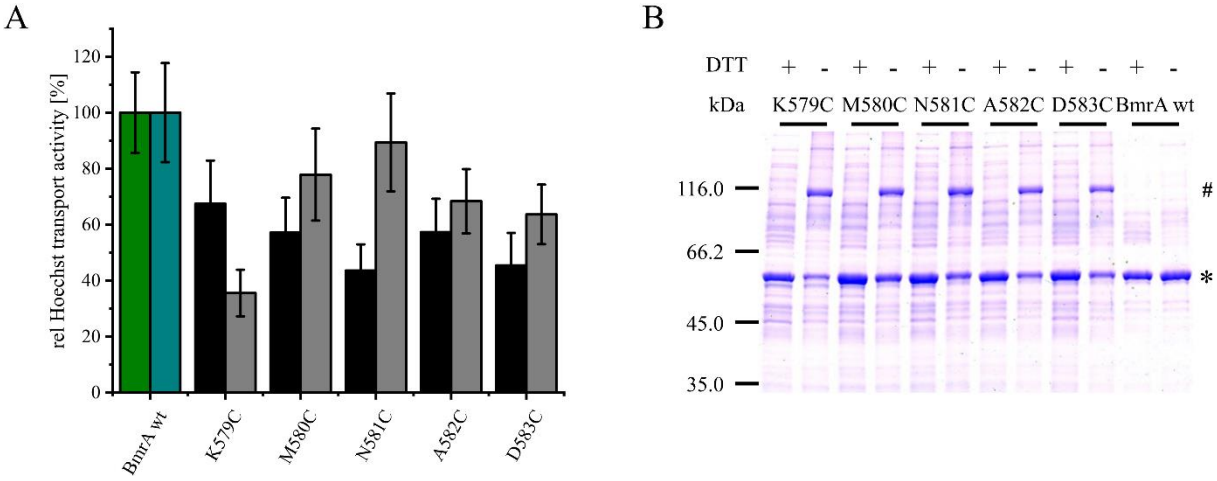

Figure 18: Relative Hoechst 33342 transport activity and crosslinking of BmrA wt and the Cys variants under reducing and oxidizing conditions. A: The relative Hoechst 33342 transport activity was determined in inverted membrane vesicles with overexpressed BmrA wt or Cys variants under reducing (black) or oxidized (grey) conditions ($n \geq 6$, ± SEM). B: The inverted vesicles with overexpressed protein were analyzed via SDS PAGE under reducing (+) and oxidizing (-) conditions. The monomers (*) and dimers (#) showed a slightly brighter signal.

To verify dimer formation, the inverted membrane vesicles with overexpressed BmrA wt and the Cys variants were analyzed via SDS PAGE (Figure 18B). In line with the analyses of the isolated proteins, all proteins were detected as monomers as well as crosslinked dimers under oxidizing conditions.

As the ATPase activity of ABC transporters is linked to the transport activity [169], next we compared the determined *in vitro* ATPase activity to the transport activity of the different Cys variants (Figure 19). The ATPase activities of the five BmrA Cys variants K579C to D583C

were dramatically increased under oxidizing conditions, whereas simultaneously, the transport activity was marginally reduced compared to BmrA wt. This might suggest that crosslinking the very C-terminal end facilitated the basal ATP hydrolysis activity but did not inevitably lead to an altered transport activity.

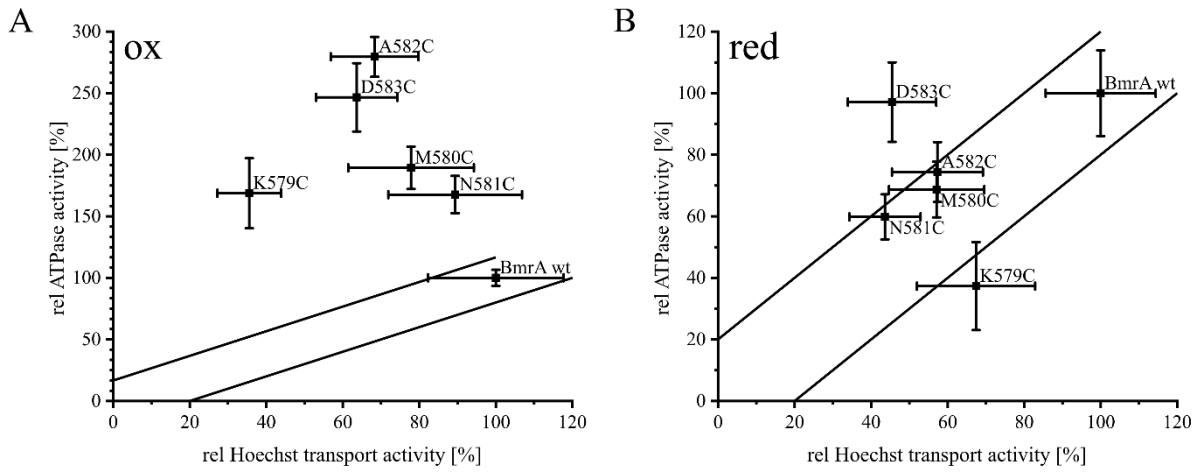

Figure 19: Comparison of relative ATPase and Hoechst 33342 transport activities. ATPase vs. transport activity of BmrA wt and the C-terminal end Cys variants under oxidized (A) and reduced (B) conditions. The markings show a 20% limit.

Yet, under reducing conditions, BmrA D583C showed a wt-like ATPase activity, although the relative transport activity was reduced to ~50% compared to BmrA wt. This suggests that the Cys might have impeded the substrate transport or the mutation resulted in uncoupling of ATPase and transport activity.

4.2.3 Discussion

ABC exporter-mediated transmembrane substrate transport involves major conformational changes of the transporter structure, from an IF to an OF conformation and backwards. Here, not only interactions between TMDs and NBDs are crucial, but additionally interactions between the NBDs are essential to finally form stable dimers leading to a proper ATP hydrolysis and substrate transport. Based on the structure of dimeric ABC exporters, their NBDs are already in close proximity [102]. Yet, ATP binding is necessary for proper NBD dimerization [160], whereas ATP hydrolysis is needed for the dissociation of the NBDs to reset the translocation cycle [170,217]. Based on the recently published BmrA structures in an OF conformation [144], it is apparent that the C-terminal ends do overlap to some extent (Figure

13, Figure 16). Consequently, we investigated in this study a putative involvement of the C-terminal helix in dimerization and activity of BmrA.

The C-terminal helix of BmrA wt can be subdivided into two shorter α-helical fragments (Figure 13). When the entire helix (ΔCT) was deleted, the BmrA ATPase as well as transport activity was completely abolished, indicating a critical role of this helix (Figure 14). Yet, when solely the very C-terminal helix fragment was deleted (ΔCTh), the activity was essentially unaltered, and thus this helical region apparently did not establish crucial interactions within or between half-transporters (Figure 14).

Since ΔCT showed only a poor ATPase activity, we concluded that some or all amino acids from L569 to L578 of the C-terminal end are crucial for the activity of BmrA. By mutating single amino acids of this part to Ala/Val we wanted to detect essential residues in this particular C-terminal part of BmrA. Based on our mutational analyses, especially the residues L569-R571 and Q576-L578 were crucial for the BmrA ATPase activity, whereas replacement of the core residues of this fragment (D572-E575) did not affect the BmrA activity as dramatically (Figure 15). Due to their position, the residues L569-R571 are in proximity to the Walker A motif of the same monomer (Figure 20). The Walker A motif mediates ATP binding and triggers NBD dimerization [111], and therefore it is reasonable to assume that mutating an amino acid residue of L569-R571 to Ala affected the dimerization of BmrA and thereby resulted in the decreased ATPase activity. A decreased ATPase activity could also be determined for the residues Q576-L578; these amino acids are in close distance (C_α < 10 Å) to residues of the H-loop of the same monomer. This loop recognizes and adjusts ATP and is consequently needed for proper dimerization and ATPase activity of an ABC transporter. E.g. mutations of the eponymous H in the H-loop cause a drastically decreased ATPase activity and no transport activity of HisP, MalK and HlyB [124,218,219]. Simultaneously, the amino acid residues Q576 and Q577 are close to the D-helix of the opposite NBD. For example, this helix, found in TAP1, is crucially involved in dimerization of the transporter [123]. Thus, interactions between the C-terminal amino acid residues Q576 to L578 and the H-loop as well as with the D-helix of the opposite NBD might be important for the dimerization process of BmrA and thereby for the ATPase activity, which is supported by our results.

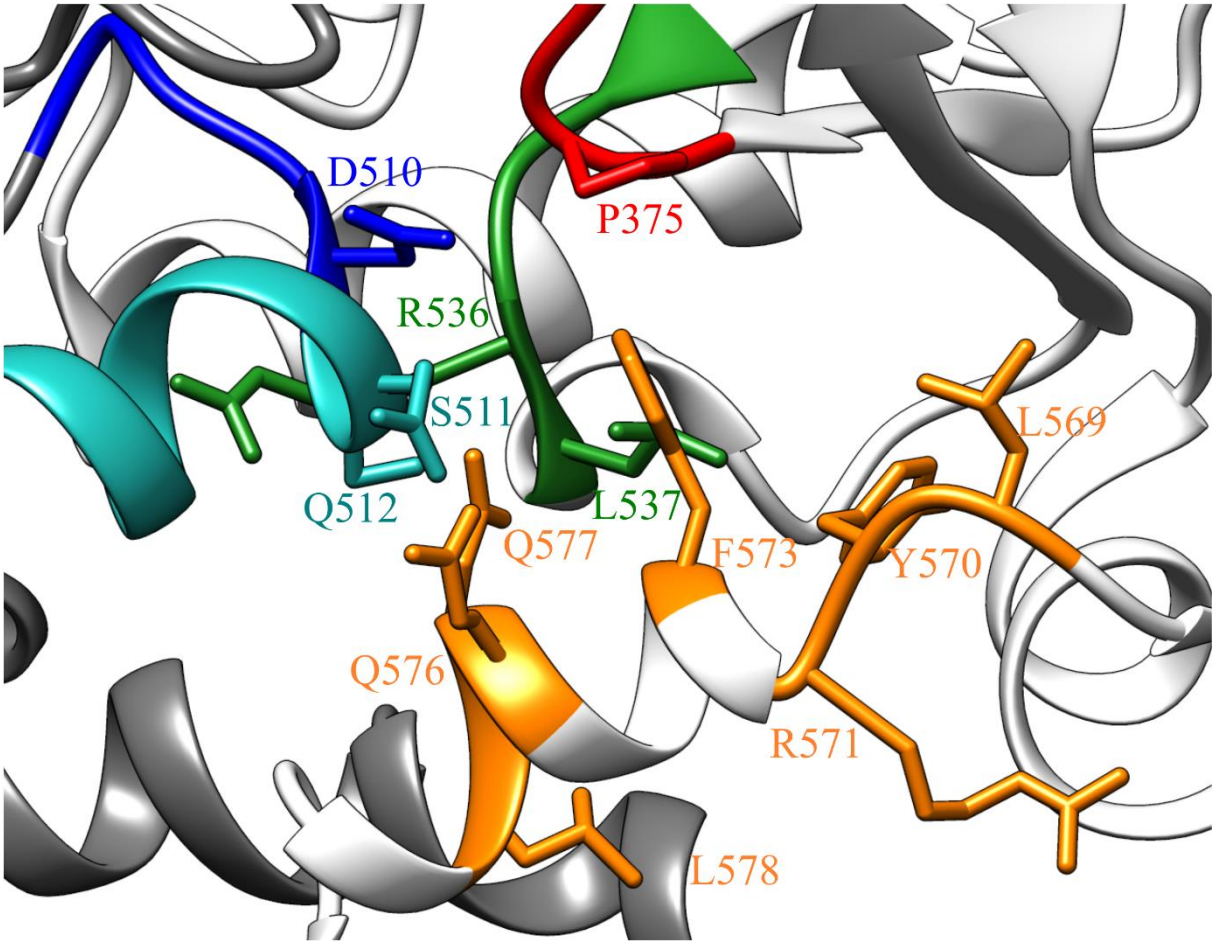

Figure 20: Structure of BmrA with possible interaction partners of crucial residues at the C-terminal end. BmrA monomers (grey and white) with orange marked amino acid residues of the C-terminal end, the Walker A motif (red) and the H-loop (green) of the same monomer as the marked C-terminus, the D-loop (blue) with the D-helix (turquoise) of the opposite monomer.

While for most variants, the respective ATPase and Hoechst transport activities were similarly decreased (Figure 15C), due to the ATP-coupled transport [169]. Different results were obtained for F573A. This variant was wt-like ATPase active, yet the relative transport activity was drastically reduced, indicating that the replacement of F573 to Ala affected solely the transport activity of the ABC transporter. As mentioned before, during the translocation cycle, the ABC exporter structure rearranges from an IF to an OF conformation [107]. Regarding the proposed structure of BmrA (Figure 20), the amino acid F573 of the C-terminal end could have a central position between the Walker A motif and the H-loop of the same monomer as well as with the D-loop of the opposing monomer. For HlyB it was postulated that some amino acids at the C-terminal end communicate with the D-loop of the opposite NBD [124]. This interaction seems to be important for the monomer-monomer stabilization during the translocation

cycle [123]. Additionally, the D-loop with the opposite Walker A motif is important in ABC transporters for the hydrolysis of ATP [122,220] but is also essential for both the NBD-NBD and the NBD-TMD communication [221]. This central location of F573 might be important for transmitting the information about ATP-binding at the Walker A motif and the H-loop to the D-loop and thereby organizing a stable dimerization process of the ABC transporter, necessary for the substrate transport.

The impact of enforced NBD dimerization via covalent Cys crosslinking on the BmrA activity was examined by replacing the residues K579-D583 individually by Cys. Upon exchange of a single amino acid of the C-terminal end by Cys, adjacent NBD dimer were expected to covalently crosslink under oxidized conditions and form disulfide bridges when two Cys residues are in close contact. Our assumption was, that in the α-helices only opposite Cys would be able to crosslink. Unexpectedly, for all oxidized Cys variants, formation of stable dimers was observed in the SDS PAGE analyses (Figure 17B, Figure 18B). Thus, the very C-terminal end of BmrA must be highly flexible and is possibly not completely α-helical at all times. Similar results were obtained for the isolated ADP-bound BmrA-NBD monomer in NMR studies [222]. In fact, when comparing the recently published structures of BmrA wt (pdb: 6R81, pdb: 6R72, pdb: 7OW8, pdb: 7BG4), the very C-terminal region indeed appears to be rather flexible and has varying α-helix content.

Interestingly, if the C-terminus lacked exactly the amino acids K579 to D583, which was the case for ΔCTh, then for this variant, no significant decrease in the ATPase and transport activity was determined (Figure 14). Due to these results, it appears that this very C-terminal end does not form crucial contacts necessary for the activity of BmrA. However, replacing a single amino acid by Cys (K579C-D583C) resulted in a slightly reduced activity under reducing conditions (Figure 17A, Figure 18A). Possibly, on account of an altered interaction of the C-terminus with the protein, the position of the previous C-terminal part (L569-L578) changed, which resulted in the reduced activity leading to the assumption that this last C-terminal part (K579-D583) is not completely free. These observations were supported by the formation of disulfide bridges under oxidizing conditions. Due to the crosslinking of the introduced Cys, the NBDs are steadily in proximity, which resulted in an increased ATPase activity (Figure 17A). Thus, if this crosslinking had no further consequences, an increase in transport activity would be expected, yet was not the case (Figure 18A). Hence, the amino acid residues of the very C-terminal end were repeatedly in spatial proximity, but without the enforced dimerization these interactions did not stabilize the dimer and by this the activity.

In summary the C-terminal end of BmrA is of importance for the ABC transporter to be fully active. Especially the proximity of the residues L569-R571 to the Walker A motif and the interactions of Q576-L578 with the H-loop of the same NBD and the D-helix of the opposite NBD seem to be important for dimerization and thereby the ATPase activity of BmrA wt. In particular, the proximity of the amino acid F573 to the Walker A motif and H-loop of the same monomer and to the D-loop of the opposite monomer seems to be necessary for NBD-TMD interactions and by this for the transport being coupled to the ATPase activity.

4.3 The TMD of BmrA stabilizes the NBD, studied by unfolding an ABC transporter *in vitro*

4.3.1 Introduction

Approx. 20–30% of all genes in any genome encode for membrane proteins [18]. Missense mutations in human membrane proteins often result in malfunction, yet also in destabilization, misfolding or improper intracellular trafficking [223–226]. Clearly, proper folding and assembly of membrane proteins is imperative for their function (chapter 1.2) [36,39,227,228]. Yet, mostly due to experimental difficulties, folding and stability of membrane proteins is far less studied and understood as in case of soluble proteins. Thus, increased research efforts in this field are urgently needed.

In the last years, *in vitro* folding and stability of these exceedingly hydrophobic proteins were analyzed in diverse studies [25,229,230], typically with focus on "simple" monomeric or smaller oligomeric proteins [231–233], such as bacteriorhodopsin [234,235], diacylglycerol kinase [236,237], EmrE [238,239] or KcsA [240,241].

The thermodynamic stability as well as the folding pathway of soluble proteins are typically studied via unfolding (and refolding) of proteins by chaotropic agents, such as guanidinium hydrochloride or urea. The chaotropic denaturant urea can either directly bind to the protein to dismantle the tertiary structure or indirectly affect the protein structure by the altered solvent environment. Nevertheless, when using urea as a denaturant, solely the soluble domains of an α-helical membrane protein can be examined, while the hydrophobic membrane integral parts are typically covered by the lipid bilayer or membrane mimicking detergents and thereby are inaccessible for urea [242–245]. Yet, membrane proteins might be unfolded *in vitro* by the anionic detergent SDS [237,246]. When a membrane protein is dissolved in a mild, non-ionic detergent, upon addition of SDS mixed micelles form with the detergent used to solubilize a membrane protein. At increasing SDS concentrations, the SDS content in the mixed micelles increases, eventually resulting in membrane protein destabilization and/or unfolding. However, while SDS weakens helix-helix-contacts of a membrane protein, the α-helix content of a TMD typically is preserved [193,237,242], meaning, associated α-helices might monomerize upon the addition of SDS [247,248]. Thus, SDS denaturation of α-helical membrane proteins in fact probes the second stage of the two-stage model of α-helical membrane protein folding (Figure 2), i.e., lateral association of TM helices and the formation of well-structured TM helix bundles.

Usually, most membrane proteins are oligomeric [49] and due to their monomer location within a biological membrane, their orientations are limited by the lipid bilayer, hence the subunits

can interact without covalent linkages [50]. Yet, while some membrane proteins not only have a membrane integrated part with small, soluble loop regions, others have additional larger soluble domains. As these domains are crucial for establishing interactions with subsequent (signaling) proteins, which are of direct functional importance, signal transmission from the transmembrane to the soluble domains, or *vice versa*, requires functional interactions and establishing contacts that allow signal transmission. Consequently, covalently linking of a soluble interaction partner, i.e. expression of polypeptides containing a TM as well as soluble domains, is advantageous [50]. Nevertheless, TM and soluble domains are not always linked, and e.g., in case of the tetrameric Vitamin B12 transport protein $BtuC_2D_2$ of *E. coli*, four subunits consisting of two TM and two cytosolic monomers have to assemble to build a functional transporter (Figure 3) [249]. Mostly, such protein-protein interfaces are stabilized by hydrophobic interactions or salt bridges [54,250]. $BtuC_2D_2$ is a member of the ABC transporter family, which actively transports chemically diverse substances across cellular membranes by using energy gained via ATP hydrolysis [83,84,86]. The vast substrate diversity in some ABC transporter can facilitate the resistance against antibiotics in some bacterial cells [209,251] and resistance to chemotherapeutic agents in cancer cells [172]. Nevertheless, ABC transporters can be found in all kingdoms of life and either are able to import or to export substrates [251]. In general, for the transmembrane substrate transport, the energy released in a soluble NBD is used in a TMD, and thus these domains have to be functionally linked. All ABC transporters consist of four core domains, two TMDs and two NBDs [131,182]. Either these four domains are altogether part of a single polypeptide chain, or one TMD and one NBD are fused together as a half-transporter, and two identical or different half-transporter homo- or heterodimerize, respectively, to form a full-transporter (Figure 3). Yet, in ABC importers, also the four domains can be separate proteins, which have to assemble to build a functional transporter [182], as mentioned before. Basically, during the substrate transport, ABC transporter switch between an IF and an OF conformation, which involves major conformational changes (chapter 1.3.5). Consequently, a tight interaction of the domains in the full-transporter is crucial. In general, conformational changes in ABC transporters occur when (i) the binding of ATP between the NBDs triggers the dimerization of said domains and (ii) the dimerization process is forwarded to the TMDs to initiate the structural switch. The motifs in the NBDs involved in the recognition, binding and hydrolysis of ATP are highly conserved among ABC transporters (chapter 1.3.3) [90,131]. Two ATP bind between a Walker A motif of one NBD and an ABC signature motif of the opposite NBD (Figure 5B, Figure 7B) [86,97], and thereby dimerization with an opposing NBD is triggered [91,100,108,210]. Among ABC transporters,

CH are conserved structural elements of the TMDs (chapter 1.3.4) [131]. These short helices are located at the cytoplasmic side of the transporters TMDs and interact in a "ball-and-socket" joint [154] with the NBDs and thereby establish an important non-covalent connection between the NBD and TMD plus enable the NBD-TMD communication during the translocation cycle [88,93,95,154].

In the present study, we used the ABC transporter BmrA of the Gram-positive bacterium *Bacillus subtilis* as a model to study the interaction and stabilization of the NBD and TMD (Figure 7, Figure 21). As all type IV ABC transporter, BmrA contains two CHs per monomer (Figure 4) [107]. Structurally, CH1 is located between TM2 and TM3 and CH2 between TM4 and TM5. Notably, CH1 of one half-transporter is in proximity to both NBDs of the transporter, whereas CH2 is coupling with the NBD of the opposite half-transporter. Therefore, TM4 and TM5 are arranged diagonally, to make it possible for CH2 to interact with the opposing NBD [93,95]. Both CHs seem to interact with the X-loop of the NBD, this conserved motif is exclusively found in ABC exporters and seems to crosslink the CHs. Thus, this loop establishes crucial interactions between both TMDs and each NBD and transfers conformational changes mediated by ATP (binding and hydrolysis at the ABC signature motif) in the NBDs to the CHs of the TMDs [95]. We aimed at analyzing whether the linkage between the TMD and the NBD influences the stability of the single domains, as well as the non-covalent interactions between the CHs and the NBDs. Thus, we investigated the destabilization of BmrA induced by urea and SDS by monitoring the intrinsic Trp fluorescence emission signal. Our results indicate that the NBD is more prone to denaturing agents than the TMD. Additionally, the isolated NBDs were more vulnerable to urea- and SDS-denaturation than the NBDs as part of a full-length transporter. Crucially, the NBDs were mostly stabilized by hydrophobic interactions at the TMD-NBD interface.

4.3.2 Results

An established method used to study the (un)folding of proteins is monitoring changes in a protein's intrinsic fluorescence emission. Via recording fluorescence emission spectra, the polarity of the direct environment of a Trp can be monitored [252]. In this study, the impact of increasing amounts of SDS or urea on BmrA wt, $BmrA_{W413Y}$, $BmrA_{W104YW164A}$, TMD, NBD and NBD+TMD, were examined via recording Trp emission spectra.

4.3.2.1 SDS-induced unfolding of full-length BmrA wt and variants

The anionic detergent SDS is able to form mixed micelles with the mild detergent DDM, eventually resulting in tertiary structure destabilization, albeit the α-helical structure of membrane proteins typically is maintained [193]. Due to its amphiphilic character, SDS interacts with charged amino acids as well as establishes hydrophobic interactions with aliphatic and/or aromatic amino acids [253]. To analyze the stability of BmrA wt, the intrinsic Trp fluorescence emission characteristics were determined. The naturally occurring Trp can be used as a sensor for a protein's stability, since changes of the polarity in a Trp environment alter its fluorescence emission spectrum [252]. Three Trp residues naturally occur in the BmrA wt monomer (Figure 21). Two Trp residues are located in the TM segment of the protein. More precisely, W104 is localized in the TMD at the cytoplasmic side of the membrane, whereas W164 is part of a short unstructured loop of a polypeptide chain linking TM3 and TM4 at the extracellular side (extracellular loop 2), close to the head groups of the lipid bilayer. One Trp (W413) is located within an unstructured part in the C-terminal cytosolic NBD and consequently, it is exposed to a more hydrophilic environment.

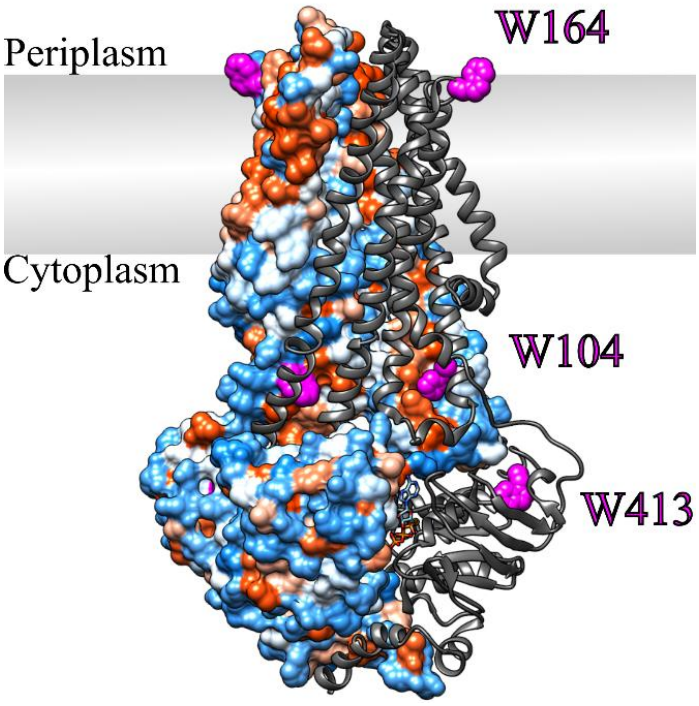

Figure 21: BmrA wt dimer with labelled Trp residues (pdb: 6R81). The Trp residues (magenta) W104, W164 and W413 within the BmrA wt dimer are shown. One monomer is colored in dark grey, and the opposite shows the hydrophobicity within the monomer (blue: polar, orange: hydrophobic, white: neutral residues).

We first analyzed the influence of increasing SDS mole fractions on the Trp fluorescence emission using the full-length BmrA wt protein. We also generated and analyzed a BmrA variant, which only contained a single Trp (W413) in the NBD to specifically analyze the impact of SDS on the NBD in the context of the full-length protein. In this variant, the two residues W104 and W164 of the TMD were replaced by Tyr and Ala and in the following referred to as $BmrA_{W104YW164A}$. The amino acid residue exchange was based on ATPase and Hoechst transport activity analysis (Figure 27) to gain a single active Trp variant of BmrA. Furthermore, another variant was generated, possessing solely the Trp residues of the TMD and lacking the Trp (W413) of the NBD, which was replaced by a Tyr ($BmrA_{W413Y}$). These two BmrA variants were unfolded by increasing SDS mole fractions (Figure 22).

The Trp fluorescence intensity at 322 nm for BmrA wt reduces between the native and the highest SDS mole fraction ($\chi_{SDS} = 0.95$) approx. 45% (Figure 22, black). At low SDS concentrations, the intensities did not change, until at $\chi_{SDS} = 0.08$ the intensity diminished drastically by approx. 16% and from $\chi_{SDS} = 0.16$ the Trp fluorescence intensities gradually decreased until the lowest value was reached at $\chi_{SDS} = 0.95$.

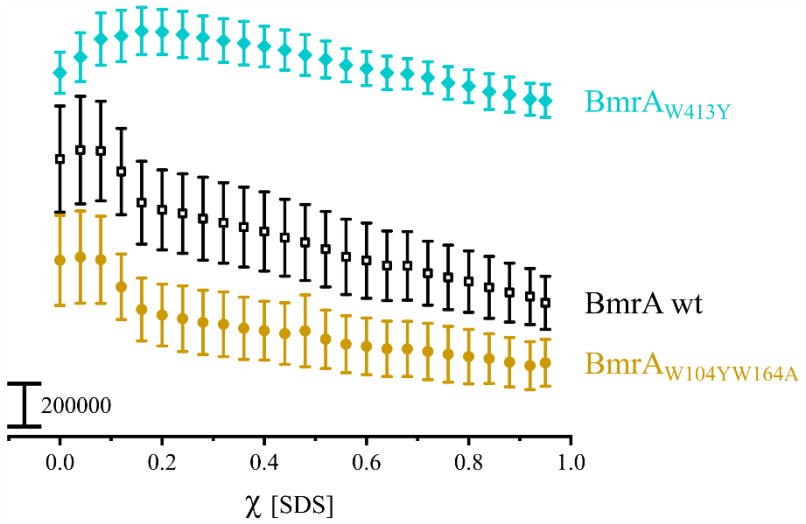

Figure 22: SDS-induced unfolding of BmrA wt and Trp variants. The fluorescence intensities of BmrA wt (black), $BmrA_{W413Y}$ (turquoise) and $BmrA_{W104YW164A}$ (ocher) at increasing χ_{SDS} were determined at a fixed wavelength (BmrA wt: 322 nm; $BmrA_{W413Y}$: 320 nm; $BmrA_{W104YW164A}$: 318 nm). Data points represent the means of three independent purifications with standard derivation (SD), without any given unit.

The changes in BmrA wt and the $BmrA_{W104YW164A}$ fluorescence emission characteristics were nearly identical. For $BmrA_{W104YW164A}$ (Figure 22, ocher), i.e. the variant which allowed monitoring exclusively structural changes occurring in the NBD, the fluorescence intensities at

increasing SDS concentrations were at the same level until at χ_{SDS} = 0.16 the intensity decreased around 23%, and with further increasing SDS concentrations constantly further decreased. The overall reduction in the fluorescence intensity between χ_{SDS} = 0 and χ_{SDS} = 0.95 was approx. 47%.

The determined fluorescence intensities at increasing SDS concentrations for $BmrA_{W413Y}$ (Figure 22, turquoise) differed from BmrA wt, as here the Trp intensities initially increased until at χ_{SDS} = 0.16 a maximum was reached. Thereafter, the fluorescence intensities linearly decreased with increasing SDS concentrations. Interestingly, at around χ_{SDS} = 0.2 the course of BmrA wt and $BmrA_{W413Y}$ appears to run parallel. The fluorescence intensity at χ_{SDS} = 0.95 was slightly decreased (approx. 15%) compared to the native state (without SDS).

The differences in the graphs of the maximum fluorescence intensities for $BmrA_{W104YW164A}$ and $BmrA_{W413Y}$ suggest that the Trp environment of the soluble part and the membrane integral domains as part of the full-length BmrA were differently affected by SDS. Simultaneously, the high degree of similarity of the graphs for BmrA wt and $BmrA_{W104YW164A}$ indicates that the changes in the Trp environment of BmrA mostly originated from W413, which is located in the NBD of BmrA.

4.3.2.2 SDS-induced unfolding of isolated BmrA domains

The graphs of the Trp fluorescence intensity changes at increasing SDS mole fractions seemed to be similar for BmrA wt and the full-length variant $BmrA_{W104YW164A}$ (Figure 22). Thus, we next examined the impact of increasing χ_{SDS} on the isolated NBD, the isolated TMD and upon mixing the isolated domains (NBD+TMD) by recording the Trp emission spectra (Figure 23). For BmrA wt, each isolated domain and the mixed NBD+TMD (measured and calculated) spectra were recorded. The spectra of the native state (χ_{SDS} = 0) and the SDS unfolded proteins at the maximal mole fraction of χ_{SDS} = 0.95 of BmrA wt (black), the mixed NBD+TMD (green) and the calculated NBD+TMD (grey, dotted line) are shown in Figure 23A.

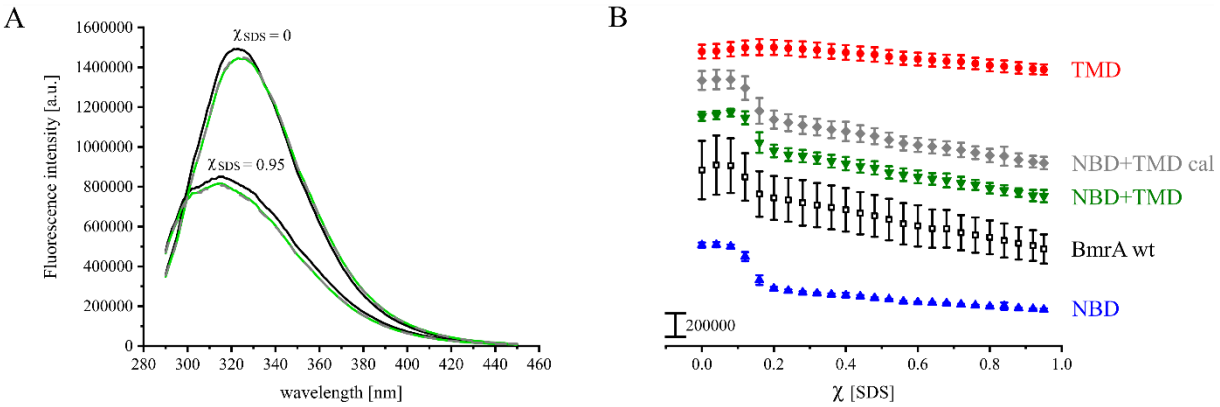

Figure 23: SDS-induced unfolding of BmrA wt, TMD and NBD variations. The emission spectra present the native proteins ($\chi_{SDS} = 0$) and the proteins with the highest SDS mole fraction ($\chi_{SDS} = 0.95$). A: BmrA wt full-length measured (black), NBD+TMD measured (green), NBD+TMD calculated (grey, dotted line). The mean values of the recorded spectra were determined and shown (without SD). B: The fluorescence intensities of BmrA wt (black, same as in Figure 22), NBD (blue), TMD (red), NBD+TMD measured (green), NBD+TMD calculated (grey) at increasing χ_{SDS} were determined at a fixed wavelength (BmrA wt: 322 nm; NBD: 324 nm; TMD: 328 nm; NBD+TMD measured: 323 nm; NBD+TMD calculated (cal): 323 nm). Data points represent the means of three independent purifications with SD, without any given unit.

Unfolding the full-length BmrA wt with increasing χ_{SDS} (Figure 23A, black) led to a decrease in the maximum fluorescence intensity, and the wavelength of the maximum fluorescence intensity shifted to shorter wavelengths. Similar results, but at varying extent, were obtained for each isolated domain of BmrA, NBD and TMD. Yet, the decrease in the Trp fluorescence intensity for the TMD was not as distinct as for BmrA wt and the isolated NBD. Noteworthy, the isolated NBD, as a soluble protein, would not necessarily require detergent, but to allow mixed micelle formation and thus a direct comparison a of the results, DDM was present in the buffer.

The Trp fluorescence intensities of the isolated NBD (Figure 23B, blue) decreased by approx. 40% at SDS mole fractions higher than $\chi_{SDS} = 0.08$. The overall decrease in the fluorescence intensity was around two thirds compared to the intensity measured for the native NBD. For the isolated TMD (Figure 23B, red), the fluorescence intensity increased around 6% until at $\chi_{SDS} = 0.16$ a maximum was reached. Thereafter, the intensities decreased and the overall change in the fluorescence intensity between $\chi_{SDS} = 0$ and $\chi_{SDS} = 0.95$ was approx. 25%. The difference between the graphs of the maximum fluorescence intensities for NBD and TMD indicates that the Trp residues, and by this the stability of the soluble part and the membrane

integral part of BmrA, were differently affected by SDS, which complements the observations made with the full-length proteins.

Interestingly, mixing the isolated NBD with the isolated TMD and unfolding the mixture via increasing the mole fraction SDS, similar emission spectra were obtained (Figure 23A, green) as with the full-length BmrA wt protein (Figure 23A, black). Additionally, we summed up the spectra recorded with the isolated NBD and the isolated TMD (respectively for $\chi_{SDS} = 0$ and $\chi_{SDS} = 0.95$), which resulted in the calculated TMD+NBD spectrum (Figure 23A, grey). No differences were observed between the spectra of the full-length BmrA wt (Figure 23A, black), the mixed TMD+NBD (Figure 23A, green) and the calculated TMD+NBD (Figure 23A, grey). Furthermore, evaluation of the maximum fluorescence intensities at increasing χ_{SDS} lead to a comparable graph for full-length BmrA wt (Figure 23B, black), the mixed NBD+TMD (Figure 23B, green) and the calculated NBD+TMD (Figure 23B, grey). For the calculated NBD+TMD (Figure 23B, grey), the maximum fluorescence intensity values of the isolated NBD (Figure 23B, blue) were added to the values of the isolated TMD (Figure 23B, red). These observations suggest, that the Trp fluorescence emission measured with the full-length BmrA wt protein was the sum of the isolated domains NBD and TMD, and thus the covalent link and/or association of the two domains did not affect the Trp fluorescence characteristics. Consequently, the covalent link between the TMD and NBD might not be inevitably crucial for the stability of BmrA.

4.3.2.3 BS^3-crosslink of the proteins

Since BmrA forms dimers *in vivo*, we analyzed the effect of homodimerization on the stability of the protein. Therefore, we crosslinked the purified full-length BmrA wt in micelles with BS^3. Furthermore, we examined whether the isolated TMD and the isolated NBD could assemble as a functional BmrA. SDS PAGE analysis of the proteins BmrA wt, TMD, NBD and the mixed NBD+TMD resulted in mostly successful crosslink of dimers, when the proteins contained the TMD (Figure 24).

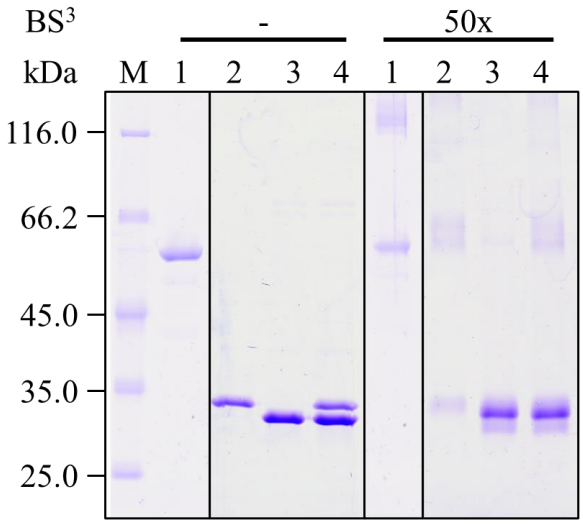

Figure 24: BmrA wt and variants without and with BS^3-crosslinker. The isolated proteins BmrA wt (1), TMD (2), NBD (3) and NBD+TMD (4) on a Coomassie brilliant blue stained 10% SDS PAGE gel. The proteins were separated on the gel without BS^3-crosslinker (-) and with a 50fold excess of BS^3-crosslinker (50x).

As expected, without the crosslinker, only a monomer signal, or rather two for the mixed NBD+TMD, were detected. Upon BS^3-crosslinking of the proteins, the monomer signals became indistinct and a second signal at higher molecular weights appeared. For the full-length ABC transporter BmrA wt the monomer signals were at around 60 kDa. The signal remained at that height but fainted for the BS^3-crosslinked wt BmrA. The second signal was at around 120 kDa and was less well defined and diffuse. Similar observations were made for the isolated TMD, except, due to the different molecular weights, the monomer signal of the TMD (~37 kDa; Table 12) was detected just below the 35 kDa marker signal and the BS^3-crosslinked signal was diffuse below the marker signal at 66.2 kDa. The isolated NBD (~30 kDa, Table 12) was detected at around 30 kDa. After crosslinking with BS^3, the signal became a little more expanded, but still with a very distinct signal at this height. However, a signal of a BS^3-crosslinked NBD dimer was not detectable. When mixing the isolated NBD with the isolated TMD, two signals were detected, one for each domain at the heights described before for the isolated domains (Figure 24, lane 2 and 3). When BS^3-crosslinked, these proteins showed a similar signal at the monomer height as it was the case for the isolated NBD and a similar lane as for the crosslinked TMD (expanded signal close to 66.2 kDa). Seemingly, the isolated TMD crosslinked, but likely no assembled full-length-like BmrA protein comprising of two isolated NBDs and TMDs each could be detected by using this method under the here applied conditions.

The analysis of the BS^3-crosslinking indicated that the proteins containing a membrane integral part, such as the full-length protein BmrA wt and the isolated TMD, were able to form dimers. The NBD on the other hand, appeared to be mainly monomeric and seemed not to interact with another NBD or the TMD, although the isolated NBDs are in principle able to crosslink upon BS^3-crosslinker addition (personal communication by [redacted]).

4.3.2.4 Urea-induced unfolding of BmrA

Compared to SDS, proteins are differently denatured by the chaotropic agent urea. Yet, the exact denaturing mechanism is not yet fully understood, however the hydrophilic urea denatures preferably the hydrophilic protein parts [227,245,254]. Since the surface of soluble proteins is to a greater extent exposed to water, we expected larger differences in the cytosolic part of the full-length protein ($BmrA_{W104YW164A}$) and in the isolated soluble protein (NBD) upon the addition of increasing concentrations of urea. Thus, increasing urea concentrations inevitably lead for soluble proteins or more hydrophilic parts of a membrane integral protein, to an increased amount of denatured/partly unfolded protein.

Again, we monitored the fluorescence emission spectra, this time at increasing urea concentrations (Figure 25). The normalized emission spectra of the native BmrA wt and the native isolated NBD were comparable (Figure 25A). Though, the maximum fluorescence intensity of the spectrum of the native $BmrA_{W104YW164A}$, was slightly shifted (approx. 5 nm) to smaller wavelengths. At concentrations of 6.5 M urea, the maxima of the emission spectra of BmrA wt, $BmrA_{W104YW164A}$ and isolated NBD decreased in the fluorescence intensity. Noteworthy, here the wavelengths of the maximum intensities of BmrA wt and the isolated NBD shifted to higher wavelengths (Figure 25A, dotted black and blue graphs), whereas the wavelength of the maximum intensity of $BmrA_{W104YW164A}$ shifted to an even smaller wavelength (Figure 25A, dashed ocher graph).

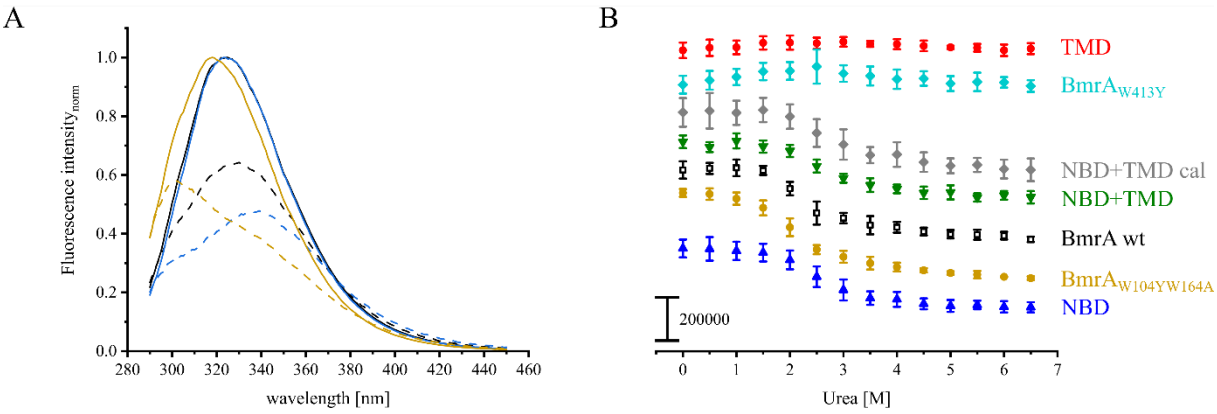

Figure 25: Urea denaturation of BmrA wt and variants. A: Normalized fluorescence emission spectra of BmrA wt (black), NBD (blue) and BmrA$_{W104YW164A}$ (ocher) of the native protein (line) and the protein exposed to 6.5 M urea (dotted line). The relative emission spectra show the mean values (without SD). B: The wavelengths of the maximum fluorescence intensities of each protein at the different urea concentrations are given for full-length BmrA wt (black), TMD (red), BmrA$_{W413Y}$ (turquoise), calculated NBD+TMD (grey, cal), NBD+TMD (green), BmrA$_{W104YW164A}$ (ocher) and NBD (blue). Data points represent the means of three independent purifications with SD, without any given unit.

The wavelengths of the maximum intensities for the ABC transporter BmrA wt shifted at increasing urea concentrations to higher wavelengths (Figure 25A, black). Here the maximum fluorescence intensity was at a wavelength of around 323 nm and shifted to ~329 nm when the protein was exposed to 6.5 M urea. The overall decrease in the max. florescence intensity measured for BmrA wt was at around 42% between native protein and exposed to 6.5 M urea (Figure 25B, black). In contrast, for the full-length variant BmrA$_{W413Y}$, no change in the maximum fluorescence intensities at increasing urea concentrations was observed (Figure 25B, turquoise).

In the full-length variant BmrA$_{W104YW164A}$ changes in the environment of W413 upon increasing concentrations of urea can be exclusively followed. Compared to BmrA wt, the wavelength of the maximum fluorescence intensity of the native BmrA$_{W104YW164A}$, was shifted to approx. 318 nm (Figure 25A, ocher). Until an urea concentration of 1 M, the max. fluorescence intensity of BmrA$_{W104YW164A}$ decreased only slightly (Figure 25B, ocher). Yet, at a concentration of 6.5 M urea, the wavelength of the fluorescence intensity maximum shifted to smaller wavelength to around 301 nm, indicating a more hydrophobic Trp environment. The overall decrease in the maximum fluorescence intensity was of approx. 54%. For the isolated NBD, slightly different results were obtained (Figure 25A, B, blue), albeit here also the environment of the W413 was monitored. Due to a better comparability between BmrA$_{W104YW164A}$ and the

isolated NBD, DDM was present in the experimental buffer to allow DDM micelle formation. The wavelength of the maximum fluorescence intensity of the native isolated NBD was at around 324 nm (Figure 25A, blue). The maximum fluorescence intensity wavelength of isolated NBD exposed to 6.5 M urea was at ~337 nm. At the same time, the max. fluorescence intensity at increasing urea concentrations decreased of around 67% (native protein compared to protein exposed to 6.5 M urea). The shift to higher wavelengths indicates that the W413 of the isolated NBD was in a more hydrophilic environment when exposed to increasing concentrations of urea. The differences in the wavelengths, determined for the maximum fluorescence intensities at increasing urea concentrations, observed for the isolated NBD (Figure 25, blue) vs. the full-length $BmrA_{W104YW164A}$ variant (Figure 25, ocher), imply that the W413 environment changed differently when the NBD was isolated (more hydrophilic) or part of the full-length protein (more hydrophobic).

Expectedly, the isolated TMD (Figure 25B, red), exposed to increasing concentrations of urea, showed neither a decrease in the maximum fluorescence intensity nor a shift in the wavelengths at said fluorescence intensities. This is reasonable, since the Trp residues, as part of the TMD, are surrounded by hydrophobic detergent micelles and are thereby protected from the urea.

As expected, the curve for the mixture of the isolated NBD and TMD (Figure 25B, green) as well as the curve calculated for the NBD+TMD from the individual spectra (Figure 25B, grey), showed a decrease of the max. fluorescence intensities comparable to the BmrA wt (Figure 25B, black). Also, the overall decrease in the intensities between native and exposed to 6.5 M urea was of around 25% for the measured NBD+TMD and 24% for the calculated NBD+TMD.

4.3.3 Discussion

In this study, we monitored changes in the structure of wt BmrA as well as of variants and isolated domains via Trp fluorescence changes. The ABC transporter BmrA wt has three Trp residues per monomer, two in the TMD plus one in the NBD, and two of these Trp residues are located at the cytoplasmic side and one at the periplasmic side of the protein (Figure 21). To examine the stability of BmrA, we analyzed the changes in the Trp surrounding of the full-length protein and its variants $BmrA_{W104YW164A}$ and $BmrA_{W413Y}$ as well as of the isolated NBD and TMD in this study. Therefore, BmrA wt and its variants were exposed to increasing amounts of SDS or urea. The fluorescence intensity maxima detected for BmrA wt and its variants indicated that the Trp residues are mainly located in a hydrophobic environment [255]. In general, the fluorescence intensities for most proteins decreased at increasing concentrations

of denaturing agents. Additionally, the wavelength of the fluorescence intensity maxima for BmrA wt shifted to shorter wavelengths when incubated with SDS (Figure 23A), or, when incubated with urea, slightly shifted to longer wavelength (Figure 25A). This indicated that the environment of one, two or all three Trp residues in the monomer was altered in hydrophobicity. Usually, shifts to shorter wavelength point to a more hydrophobic surrounding, whereas shifts to longer wavelength suggest an exposure to a more hydrophilic setting. As the fluorescence spectra for BmrA wt reflected environmental changes of all individual Trp residues, interpreting this given data is rather complicated.

Nevertheless, we analyzed the full-length wt BmrA as well as we consequently examined full-length BmrA variants either containing the Trp residues located in the TMD ($BmrA_{W413Y}$) or the Trp in the NBD ($BmrA_{W104YW164A}$) and in each isolated domain (TMD and NBD) at increasing amounts of SDS or urea. Here, due to the Trp location within the protein, the environments were differently affected by the denaturing agents.

At increasing SDS mole fractions a similar course in the fluorescence intensity decrease was detected for BmrA wt (Figure 22, black) and for the full-length variant $BmrA_{W104YW164A}$ (Figure 22, ocher), indicating that changes observed with the full-length wt protein resulted most likely from the W413 in the NBD. Also, the Trp of the isolated NBD was similarly altered in its course when exposed to increasing χ_{SDS} (Figure 23B). But, as the overall change in fluorescence intensity between native protein and protein with the highest SDS mole fraction was more pronounced for the isolated NBD (~66%) than for the full-length $BmrA_{W104YW164A}$ (47%), the Trp environment of $BmrA_{W104YW164A}$ likely was not as altered as in case of the isolated domain. The anionic detergent SDS forms mixed micelles with the DDM in the protein solution, but furthermore was most likely to solve the tertiary structure and thereby partially destabilized the environment around the W413 in the NBD. However, the graphs obtained with the $BmrA_{W104YW164A}$ full-length protein and the isolated NBD differ, although in both cases solely the Trp environment of the NBD was observed. This suggests that the W413 environment of the $BmrA_{W104YW164A}$ variant might be protected and stabilized by the TMD and/or non-covalent interactions at the NBD-TMD interface between the NBDs and the CHs of the TMDs. The results obtained for the W413 environment of $BmrA_{W104YW164A}$ and the isolated NBD at increasing urea concentrations complement our SDS titration results. While for the isolated NBD the wavelength of the maximum intensities shifted to higher wavelengths (Figure 25A, blue), the opposite was found for $BmrA_{W104YW164A}$; here, the wavelengths shifted to shorter values (Figure 25A, ocher). The red-shift of the maximum fluorescence intensity wavelengths of the isolated NBD corresponds to an exposure of W413 into a more hydrophilic surrounding.

Here, urea can bind directly to the NBD and hence unfold the protein and thereby stabilize the unfolded state. The blue-shifted W413 spectrum monitored with the $BmrA_{W104YW164A}$ protein indicates exposure of W413 to a more hydrophobic environment. This again leads to the assumption that the NBD, as part of the full-length protein, was less vulnerable against urea-denaturation and was stabilized by the non-covalent interactions of the CHs with the NBDs and/or the proximity to the membrane mimicking hydrophobic DDM prevents the NBD from the hydrophilic urea.

The environment of the Trp residues in the full-length $BmrA_{W413Y}$ or in the isolated TMD were most probably not affected by SDS and urea, implied by monitoring the environment of these Trp residues, because here the detected fluorescence intensities for $BmrA_{W413Y}$ (Figure 22, Figure 25B, turquoise) and TMD (Figure 23B, Figure 25B, red) did hardly change between the native state and the highest amount of denaturing agent. Thus, neither SDS nor urea substantially change the environment of the Trp residues W104 and W164, which are located in the TMD. The TMDs of BmrA are surrounded by DDM micelles and thus adding SDS to the protein detergent-solution leads to the formation of mixed DDM/SDS micelles. By increasing the amount of SDS, the mole fraction of SDS within these mixed micelles increases. SDS *per se* does typically not unfold TM α-helices [248], thus the α-helical content of the TMD did not change. Yet, increasing concentrations of SDS led to a monomerization of the TM α-helices surrounded by DDM/SDS micelles [193,247] and still no change in the environment of the Trp residues W104 and W164 could be determined. On the contrary, the membrane mimicking DDM micelles ensured the hydrophobicity of the TMD, thus the hydrophilic urea could not interact with this domain, leading to an unfolding of the water exposed more soluble parts of a protein [227].

The demonstrated differences in the isolated NBD and the isolated TMD showed that the isolated domains of the soluble and the membrane integral part of BmrA are differently affected by increasing amounts of denaturing agents. However, if the isolated NBDs and isolated TMDs were mixed together and unfolded by SDS or urea, the fluorescence spectra (Figure 23A) as well as the course of the fluorescence intensities (Figure 23B, Figure 25B) were comparable to the full-length wt ABC transporter BmrA. Identical results were obtained when the signals of the isolated domains were summed up, to gain the calculated NBD+TMD values. This finding contributes to our suggestion that the Trp environment of the full-length BmrA wt is the sum of the Trp environments of the isolated NBDs and TMDs.

As BmrA functions as a homodimer *in vivo*, within a membrane, as well as in micellar solutions [167], we evaluated the effect of dimerization on the stability of the protein. We examined the proteins via SDS PAGE analysis and neither wt BmrA nor the isolated domains formed stable dimers, when exposed to SDS. Hence, we incubated BmrA wt, NBD, TMD and the mixed NBD+TMD with BS^3-crosslinker, to obtain permanently linked proteins. The results showed that the full-length BmrA wt stably homodimerizes to some extent (Figure 24). The same, but less distinct, was found for the isolated TMD, which did dimerize as well. Whereas the isolated NBD did not dimerize, also the mixed isolated domains, showed most probably the dimerization of the isolated TMD and not a TMD connected with a NBD. This indicates a weak interaction propensity and that the connection between these domains could not be easily restored by solely adding crosslinker. Nevertheless, proteins containing a TMD or the isolated TMD itself were able to crosslink upon the addition of BS^3-crosslink.

The results obtained in our study clearly indicate that the cytosolic NBD was most prone for SDS and urea and subsequently unfolded more easily. Yet, when part of the full-length BmrA, the W413 was less vulnerable against urea and even seemed to be stabilized by non-covalent interactions at the NBD-TMD interface most likely by hydrophobic interactions [256]. Additionally, the interactions of theW413 and the CHs at this NBD-TMD interface might be crucial for the stability of BmrA as well as the proximity of the NBD to the membrane mimicking detergent.

5 Conclusion

Multidrug resistance is a major problem in human health. Thus, studying the membrane protein BmrA, as a model protein for bacterial ABC transporters involved in multidrug resistance, is of great interest. In this study, three aspects in investigating BmrA were addressed, regarding the inhibition, the dimerization and the stability.

Myristic acid, found in a fungal secondary metabolite screening, inhibited the activity of BmrA (chapter 4.1). Based on the results obtained here, myristic acid could qualify as a drug excipient and the drug export by BmrA might be reduced by applying the fatty acid together with an ABC transporter substrate.

The results maintained by investigations on the C-terminal end of BmrA, showed, that this end is crucial for the transporter's activity (chapter 4.2). Several amino acids at the C-terminus seem to interact with conserved motifs within the NBD and thereby support the dimerization of the NBDs as well as the communication between NBD and TMD during the translocation cycle of BmrA.

Unfolding BmrA showed, that the cytosolic NBD is most vulnerable against denaturing agents. Yet, the proximity of the NBD to the membrane as well as non-covalent interactions at the NBD-TMD interface of BmrA, especially W413 and the CHs, are important for the stability of the ABC transporter.

The findings regarding factors influencing dimerization and stability of BmrA might help to specifically engineer new therapeutics for diseases, which are affected by ABC transporter mediated multidrug resistance.

6 Literature

1. Janmey, P.A.; Kinnunen, P.K.J. Biophysical Properties of Lipids and Dynamic Membranes. *Trends Cell Biol.* **2006**, *16*, 538–546, doi:10.1016/j.tcb.2006.08.009.

2. Watson, H. Biological Membranes. *Essays Biochem.* **2015**, *59*, 43–70, doi:10.1042/BSE0590043.

3. van Meer, G.; Voelker, D.R.; Feigenson, G.W. Membrane Lipids: Where They Are and How They Behave. *Nat. Rev. Mol. Cell Biol.* **2008**, *9*, 112–124, doi:10.1038/nrm2330.

4. Fahy, E.; Subramaniam, S.; Brown, H.A.; Glass, C.K.; Merrill, A.H.; Murphy, R.C.; Raetz, C.R.H.; Russell, D.W.; Seyama, Y.; Shaw, W.; et al. A Comprehensive Classification System for Lipids. *J. Lipid Res.* **2005**, *46*, 839–861, doi:10.1194/jlr.E400004-JLR200.

5. Harayama, T.; Riezman, H. Understanding the Diversity of Membrane Lipid Composition. *Nat. Rev. Mol. Cell Biol.* **2018**, *19*, 281–296, doi:10.1038/nrm.2017.138.

6. Barák, I.; Muchová, K. The Role of Lipid Domains in Bacterial Cell Processes. *Int. J. Mol. Sci.* **2013**, *14*, 4050–4065, doi:10.3390/ijms14024050.

7. de Mendoza, D.; Grau, R.; Cronan, J.E. Biosynthesis and Function of Membrane Lipids. In *Bacillus subtilis and Other Gram-Positive Bacteria*; Sonenshein, A.L., Hoch, J.A., Losick, R., Eds.; ASM Press: Washington, DC, USA, 1993; pp. 411–421.

8. Moreau, P.; Bessoule, J.J.; Mongrand, S.; Testet, E.; Vincent, P.; Cassagne, C. Lipid Trafficking in Plant Cells. *Prog. Lipid Res.* **1998**, *37*, 371–391, doi:10.1016/S0163-7827(98)00016-2.

9. Hunter, A.D. ACD/ChemSketch 1.0 (Freeware); ACD/ChemSketch 2.0 and Its Tautomers, Dictionary, and 3D Plug-Ins; ACD/HNMR 2.0; ACD/CNMR 2.0. *J. Chem. Educ.* **1997**, *74*, 905–906, doi:10.1021/ed074p905.

10. Yang, N.J.; Hinner, M.J. Getting across the Cell Membrane: An Overview for Small Molecules, Peptides, and Proteins. *Methods Mol. Biol.* **2015**, *1266*, 29–53, doi:10.1007/978-1-4939-2272-7_3.

11. Saier, M.H. A Functional-Phylogenetic Classification System for Transmembrane Solute Transporters. *Microbiol. Mol. Biol. Rev.* **2000**, *64*, 354–411, doi:10.1128/MMBR.64.2.354-411.2000.

12. Skou, J.C. Enzymatic Basis for Active Transport of Na+ and K+ Across Cell Membrane.

Physiol. Rev. **1965**, *45*, 596–617, doi:10.1152/physrev.1965.45.3.596.

13. Raven, J.A.; Beardall, J. Energizing the Plasmalemma of Marine Photosynthetic Organisms: The Role of Primary Active Transport. *J. Mar. Biol. Assoc. United Kingdom* **2020**, *100*, 333–346, doi:10.1017/S0025315420000211.

14. Geck, P.; Heinz, E. Secondary Active Transport: Introductory Remarks. *Kidney Int.* **1989**, *36*, 334–341, doi:10.1038/ki.1989.201.

15. Rask-Andersen, M.; Almén, M.S.; Schiöth, H.B. Trends in the Exploitation of Novel Drug Targets. *Nat. Rev. Drug Discov.* **2011**, *10*, 579–590, doi:10.1038/nrd3478.

16. Overington, J.P.; Al-Lazikani, B.; Hopkins, A.L. How Many Drug Targets Are There? *Nat. Rev. Drug Discov.* **2006**, *5*, 993–996, doi:10.1038/nrd2199.

17. Fagerberg, L.; Jonasson, K.; Von Heijne, G.; Uhlén, M.; Berglund, L. Prediction of the Human Membrane Proteome. *Proteomics* **2010**, *10*, 1141–1149, doi:10.1002/pmic.200900258.

18. Krogh, A.; Larsson, B.; Von Heijne, G.; Sonnhammer, E.L.L. Predicting Transmembrane Protein Topology with a Hidden Markov Model: Application to Complete Genomes. *J. Mol. Biol.* **2001**, *305*, 567–580, doi:10.1006/jmbi.2000.4315.

19. Li, F.; Egea, P.F.; Vecchio, A.J.; Asial, I.; Gupta, M.; Paulino, J.; Bajaj, R.; Dickinson, M.S.; Ferguson-Miller, S.; Monk, B.C.; et al. Highlighting Membrane Protein Structure and Function: A Celebration of the Protein Data Bank. *J. Biol. Chem.* **2021**, *296*, 100557, doi:10.1016/j.jbc.2021.100557.

20. White, S.H.; Wimley, W.C. Membrane Protein Folding and Stability: Physical Principles. *Annu. Rev. Biophys. Biomol. Struct.* **1999**, *28*, 319–65, doi:10.1146/annurev.biophys.28.1.319.

21. Rigaud, J.-L.; Pitard, B.; Levy, D. Reconstitution of Membrane Proteins into Liposomes: Application to Energy-Transducing Membrane Proteins. *Biochim. Biophys. Acta - Bioenerg.* **1995**, *1231*, 223–246, doi:10.1016/0005-2728(95)00091-V.

22. Denisov, I.G.; Sligar, S.G. Nanodiscs for Structural and Functional Studies of Membrane Proteins. *Nat. Struct. Mol. Biol.* **2016**, *23*, 481–486, doi:10.1038/nsmb.3195.

23. Linke, D. Detergents: An Overview. In *Methods in Enzymology*; Burgess, R.R., Deutscher, M.P., Eds.; Elsevier Inc., 2009; Vol. 463, pp. 603–617.

24. Booth, P.J.; Clarke, J. Membrane Protein Folding Makes the Transition. *Proc. Natl.*

Acad. Sci. U. S. A. **2010**, *107*, 3947–3948, doi:10.1073/pnas.0914478107.

25. Bowie, J.U. Solving the Membrane Protein Folding Problem. *Nature* **2005**, *438*, 581–589, doi:10.1038/nature04395.

26. Bigelow, H.R.; Petrey, D.S.; Liu, J.; Przybylski, D.; Rost, B. Predicting Transmembrane Beta-Barrels in Proteomes. *Nucleic Acids Res.* **2004**, *32*, 2566–2577, doi:10.1093/nar/gkh580.

27. Cohen, C.; Parry, D.A.D. A-Helical Coiled Coils and Bundles: How to Design an A-helical Protein. *Proteins Struct. Funct. Bioinforma.* **1990**, *7*, 1–15, doi:10.1002/prot.340070102.

28. Youkharibache, P.; Veretnik, S.; Li, Q.; Stanek, K.A.; Mura, C.; Bourne, P.E. The Small β-Barrel Domain: A Survey-Based Structural Analysis. *Structure* **2019**, *27*, 6–26, doi:10.1016/j.str.2018.09.012.

29. Chaturvedi, D.; Mahalakshmi, R. Transmembrane β-Barrels: Evolution, Folding and Energetics. *Biochim. Biophys. Acta - Biomembr.* **2017**, *1859*, 2467–2482, doi:10.1016/j.bbamem.2017.09.020.

30. Schulz, G.E. Beta-Barrel Membrane Proteins. *Curr. Opin. Struct. Biol.* **2000**, *10*, 443–447, doi:10.1016/s0959-440x(00)00120-2.

31. Buchanan, S.K. Beta-Barrel Proteins from Bacterial Outer Membranes: Structure, Function and Refolding. *Curr. Opin. Struct. Biol.* **1999**, *9*, 455–461, doi:10.1016/S0959-440X(99)80064-5.

32. Sansom, M.S.P.; Kerr, I.D. Transbilayer Pores Formed by Beta-Barrels: Molecular Modeling of Pore Structures and Properties. *Biophys. J.* **1995**, *69*, 1334–1343, doi:10.1016/S0006-3495(95)80000-7.

33. Von Heijne, G. The Membrane Protein Universe: What's out There and Why Bother? *J. Intern. Med.* **2007**, *261*, 543–557, doi:10.1111/j.1365-2796.2007.01792.x.

34. Pauling, L.; Corey, R.B.; Branson, H.R. The Structure of Proteins: Two Hydrogen-Bonded Helical Configurations of the Polypeptide Chain. *Proc. Natl. Acad. Sci. U. S. A.* **1951**, *37*, 205–211, doi:10.1073/pnas.37.4.205.

35. Heyden, M.; Freites, J.A.; Ulmschneider, M.B.; White, S.H.; Tobias, D.J. Assembly and Stability of α-Helical Membrane Proteins. *Soft Matter* **2012**, *8*, 7742–7752, doi:10.1039/c2sm25402f.

36. Booth, P.J.; High, S. Polytopic Membrane Protein Folding and Assembly *in Vitro* and *in Vivo*. *Mol. Membr. Biol.* **2004**, *21*, 163–170, doi:10.1080/09687680410001697215.

37. Popot, J.-L.; Engelman, D.M. Membrane Protein Folding and Oligomerization: The Two-Stage Model. *Biochemistry* **1990**, *29*, 4031–7, doi:10.1021/bi00469a001.

38. Seddon, A.M.; Curnow, P.; Booth, P.J. Membrane Proteins, Lipids and Detergents: Not Just a Soap Opera. *Biochim. Biophys. Acta - Biomembr.* **2004**, *1666*, 105–117, doi:10.1016/j.bbamem.2004.04.011.

39. Cymer, F.; Von Heijne, G.; White, S.H. Mechanisms of Integral Membrane Protein Insertion and Folding. *J. Mol. Biol.* **2015**, *427*, 999–1022, doi:10.1016/j.jmb.2014.09.014.

40. Cymer, F.; Veerappan, A.; Schneider, D. Transmembrane Helix–Helix Interactions Are Modulated by the Sequence Context and by Lipid Bilayer Properties. *Biochim. Biophys. Acta - Biomembr.* **2012**, *1818*, 963–973, doi:10.1016/j.bbamem.2011.07.035.

41. Hong, H. Toward Understanding Driving Forces in Membrane Protein Folding. *Arch. Biochem. Biophys.* **2014**, *564*, 297–313, doi:10.1016/j.abb.2014.07.031.

42. Fiedler, S.; Broecker, J.; Keller, S. Protein Folding in Membranes. *Cell. Mol. Life Sci.* **2010**, *67*, 1779–1798, doi:10.1007/s00018-010-0259-0.

43. Langosch, D.; Heringa, J. Interaction of Transmembrane Helices by a Knobs-into-Holes Packing Characteristic of Soluble Coiled Coils. *Proteins Struct. Funct. Genet.* **1998**, *31*, 150–159, doi:10.1002/(SICI)1097-0134(19980501)31:2<150::AID-PROT5>3.0.CO;2-Q.

44. Lemmon, M.A.; Engelman, D.M. Specificity and Promiscuity in Membrane Helix Interactions. *FEBS Lett.* **1994**, *346*, 17–20, doi:10.1016/0014-5793(94)00467-6.

45. Russ, W.P.; Engelman, D.M. The GxxxG Motif: A Framework for Transmembrane Helix-Helix Association. *J. Mol. Biol.* **2000**, *296*, 911–919, doi:10.1006/jmbi.1999.3489.

46. Schneider, D.; Engelman, D.M. Involvement of Transmembrane Domain Interactions in Signal Transduction by α/β Integrins. *J. Biol. Chem.* **2004**, *279*, 9840–9846, doi:10.1074/jbc.M312749200.

47. Li, E.; Wimley, W.C.; Hristova, K. Transmembrane Helix Dimerization: Beyond the Search for Sequence Motifs. *Biochim. Biophys. Acta - Biomembr.* **2012**, *1818*, 183–193,

doi:10.1016/j.bbamem.2011.08.031.

48. Engelman, D.M.; Chen, Y.; Chin, C.-N.; Curran, A.R.; Dixon, A.M.; Dupuy, A.D.; Lee, A.S.; Lehnert, U.; Matthews, E.E.; Reshetnyak, Y.K.; et al. Membrane Protein Folding: Beyond the Two Stage Model. *FEBS Lett.* **2003**, *555*, 122–125, doi:10.1016/S0014-5793(03)01106-2.

49. Goodsell, D.S.; Olson, A.J. Structural Symmetry and Protein Function. *Annu. Rev. Biophys. Biomol. Struct.* **2000**, *29*, 105–53, doi:10.1146/annurev.biophys.29.1.105.

50. Liu, Y.; Gerstein, M.; Engelman, D.M. Transmembrane Protein Domains Rarely Use Covalent Domain Recombination as an Evolutionary Mechanism. *Proc. Natl. Acad. Sci. U. S. A.* **2004**, *101*, 3495–3497, doi:10.1073/pnas.0307330101.

51. White, S.H.; Ladokhin, A.S.; Jayasinghe, S.; Hristova, K. How Membranes Shape Protein Structure. *J. Biol. Chem.* **2001**, *276*, 32395–32398, doi:10.1074/jbc.R100008200.

52. Adamian, L.; Nanda, V.; DeGrado, W.F.; Liang, J. Empirical Lipid Propensities of Amino Acid Residues in Multispan Alpha Helical Membrane Proteins. *Proteins Struct. Funct. Genet.* **2005**, *59*, 496–509, doi:10.1002/prot.20456.

53. Stangl, M.; Schneider, D. Functional Competition within a Membrane: Lipid Recognition vs. Transmembrane Helix Oligomerization. *Biochim. Biophys. Acta - Biomembr.* **2015**, *1848*, 1886–1896, doi:10.1016/j.bbamem.2015.03.011.

54. Ali, M.H.; Imperiali, B. Protein Oligomerization: How and Why. *Bioorganic Med. Chem.* **2005**, *13*, 5013–5020, doi:10.1016/j.bmc.2005.05.037.

55. Ikebe, M.; Kambara, T.; Stafford, W.F.; Sata, M.; Katayama, E.; Ikebe, R. A Hinge at the Central Helix of the Regulatory Light Chain of Myosin Is Critical for Phosphorylation-Dependent Regulation of Smooth Muscle Myosin Motor Activity. *J. Biol. Chem.* **1998**, *273*, 17702–17707, doi:10.1074/jbc.273.28.17702.

56. Gokhale, R.S.; Khosla, C. Role of Linkers in Communication between Protein Modules. *Curr. Opin. Chem. Biol.* **2000**, *4*, 22–27, doi:10.1016/S1367-5931(99)00046-0.

57. George, R.A.; Heringa, J. An Analysis of Protein Domain Linkers: Their Classification and Role in Protein Folding. *Protein Eng.* **2002**, *15*, 871–879, doi:10.1093/protein/15.11.871.

58. Reddy Chichili, V.P.; Kumar, V.; Sivaraman, J. Linkers in the Structural Biology of

Protein-Protein Interactions. *Protein Sci.* **2013**, *22*, 153–167, doi:10.1002/pro.2206.

59. Licht, A.; Schneider, E. ATP Binding Cassette Systems: Structures, Mechanisms, and Functions. *Cent. Eur. J. Biol.* **2011**, *6*, 785–801, doi:10.2478/s11535-011-0054-4.

60. Schneider, E.; Hunke, S. ATP-Binding-Cassette (ABC) Transport Systems: Functional and Structural Aspects of the ATP-Hydrolyzing Subunits/Domains. *FEMS Microbiol. Rev.* **1998**, *22*, 1–20, doi:10.1016/S0168-6445(98)00002-3.

61. Theodoulou, F.L.; Kerr, I.D. ABC Transporter Research: Going Strong 40 Years On. *Biochem. Soc. Trans.* **2015**, *43*, 1033–1040, doi:10.1042/BST20150139.

62. ter Beek, J.; Guskov, A.; Slotboom, D.J. Structural Diversity of ABC Transporters. *J. Gen. Physiol.* **2014**, *143*, 419–435, doi:10.1085/jgp.201411164.

63. Saurin, W.; Hofnung, M.; Dassa, E. Getting in or out: Early Segregation between Importers and Exporters in the Evolution of ATP-Binding Cassette (ABC) Transporters. *J. Mol. Evol.* **1999**, *48*, 22–41, doi:10.1007/PL00006442.

64. Rice, A.J.; Park, A.; Pinkett, H.W. Diversity in ABC Transporters: Type I, II and III Importers. *Crit. Rev. Biochem. Mol. Biol.* **2014**, *49*, 426–437, doi:10.3109/10409238.2014.953626.

65. Lewinson, O.; Livnat-Levanon, N. Mechanism of Action of ABC Importers: Conservation, Divergence, and Physiological Adaptations. *J. Mol. Biol.* **2017**, *429*, 606–619, doi:10.1016/j.jmb.2017.01.010.

66. Dassa, E.; Bouige, P. The ABC of ABCs: A Phylogenetic and Functional Classification of ABC Systems in Living Organisms. *Res. Microbiol.* **2001**, *152*, 211–229, doi:10.1016/S0923-2508(01)01194-9.

67. Davidson, A.L.; Dassa, E.; Orelle, C.; Chen, J. Structure, Function, and Evolution of Bacterial ATP-Binding Cassette Systems. *Microbiol. Mol. Biol. Rev.* **2008**, *72*, 317–364, doi:10.1128/mmbr.00031-07.

68. Bouige, P.; Laurent, D.; Piloyan, L.; Dassa, E. Phylogenetic and Functional Classification of ATP-Binding Cassette (ABC) Systems. *Curr. Protein Pept. Sci.* **2002**, *3*, 541–559, doi:10.2174/1389203023380486.

69. Riordan, J.R.; Rommens, J.M.; Kerem, B.S.; Alon, N.O.A.; Rozmahel, R.; Grzelczak, Z.; Zielenski, J.; Lok, S.I.; Plavsic, N.; Chou, J.L.; et al. Identification of the Cystic Fibrosis Gene: Cloning and Characterization of Complementary DNA. *Science (80-.).*

1989, *245*, 1066–1073, doi:10.1126/science.2475911.

70. Pollock, N.L.; Rimington, T.L.; Ford, R.C. Characterizing Diverse Orthologues of the Cystic Fibrosis Transmembrane Conductance Regulator Protein for Structural Studies. *Biochem. Soc. Trans.* **2015**, *43*, 894–900, doi:10.1042/BST20150081.

71. Bose, S.J.; Scott-Ward, T.S.; Cai, Z.; Sheppard, D.N. Exploiting Species Differences to Understand the CFTR Cl- Channel. *Biochem. Soc. Trans.* **2015**, *43*, 975–982, doi:10.1042/BST20150129.

72. Allikmets, R.; Singh, N.; Sun, H.; Shroyer, N.F.; Hutchinson, A.; Chidambaram, A.; Gerrard, B.; Baird, L.; Stauffer, D.; Pfeiffer, A.; et al. A Photoreceptor Cell-Specific ATP-Binding Transporter Gene (ABCR) Is Mutated in Recessive Stargardt Macular Dystrophy. *Nat. Genet.* **1997**, *15*, 236–246.

73. Behl, T.; Kaur, I.; Sehgal, A.; Kumar, A.; Uddin, M.S.; Bungau, S. The Interplay of ABC Transporters in Aβ Translocation and Cholesterol Metabolism: Implicating Their Roles in Alzheimer's Disease. *Mol. Neurobiol.* **2021**, *58*, 1564–1582, doi:10.1007/s12035-020-02211-x.

74. Jia, Y.; Wang, N.; Zhang, Y.; Xue, D.; Lou, H.; Liu, X. Alteration in the Function and Expression of SLC and ABC Transporters in the Neurovascular Unit in Alzheimer's Disease and the Clinical Significance. *Aging Dis.* **2020**, *11*, 390–404, doi:10.14336/AD.2019.0519.

75. Tusnády, G.E.; Sarkadi, B.; Simon, I.; Váradi, A. Membrane Topology of Human ABC Proteins. *FEBS Lett.* **2006**, *580*, 1017–1022, doi:10.1016/j.febslet.2005.11.040.

76. Dean, M.; Annilo, T. Evolution of the ATP-Binding Cassette (ABC) Transporter Superfamily in Vertebrates. *Annu. Rev. Genomics Hum. Genet.* **2005**, *6*, 123–142, doi:10.1146/annurev.genom.6.080604.162122.

77. Dean, M.; Rzhetsky, A.; Allikmets, R. The Human ATP-Binding Cassette (ABC) Transporter Superfamily. *Genome Res.* **2001**, *11*, 1156–1166, doi:10.1101/gr.184901.

78. Quazi, F.; Lenevich, S.; Molday, R.S. ABCA4 Is an N-Retinylidene-Phosphatidylethanolamine and Phosphatidylethanolamine Importer. *Nat. Commun.* **2012**, *3*, doi:10.1038/ncomms1927.

79. Csanády, L.; Vergani, P.; Gadsby, D.C. Structure, Gating, and Regulation of the CFTR Anion Channel. *Physiol. Rev.* **2019**, *99*, 707–738, doi:10.1152/physrev.00007.2018.

80. Puljung, M.C. Cryo-Electron Microscopy Structures and Progress toward a Dynamic Understanding of KATP Channels. *J. Gen. Physiol.* **2018**, *150*, 653–669, doi:10.1085/jgp.201711978.

81. Choi, C.C.; Ford, R.C. ATP Binding Cassette Importers in Eukaryotic Organisms. *Biol. Rev.* **2021**, *96*, 1318–1330, doi:10.1111/brv.12702.

82. Kerr, I.D. Sequence Analysis of Twin ATP Binding Cassette Proteins Involved in Translational Control, Antibiotic Resistance, and Ribonuclease L Inhibition. *Biochem. Biophys. Res. Commun.* **2004**, *315*, 166–173, doi:10.1016/j.bbrc.2004.01.044.

83. Borst, P.; Elferink, R.O. Mammalian ABC Transporters in Health and Disease. *Annu. Rev. Biochem.* **2002**, *71*, 537–592, doi:10.1146/annurev.biochem.71.102301.093055.

84. Gottesman, M.M.; Pastan, I.; Ambudkar, S. V. P-Glycoprotein and Multidrug Resistance. *Curr. Opin. Genet. Dev.* **1996**, *6*, 610–617, doi:10.1016/S0959-437X(96)80091-8.

85. Juan-Carlos, P.D.M.; Perla-Lidia, P.P.; Stephanie-Talia, M.M.; Mónica-Griselda, A.M.; Luz-María, T.E. ABC Transporter Superfamily. An Updated Overview, Relevance in Cancer Multidrug Resistance and Perspectives with Personalized Medicine. *Mol. Biol. Rep.* **2021**, *48*, 1883–1901, doi:10.1007/s11033-021-06155-w.

86. Davidson, A.L.; Chen, J. ATP-Binding Cassette Transporters in Bacteria. *Annu. Rev. Biochem.* **2004**, *73*, 241–268, doi:10.1146/annurev.biochem.73.011303.073626.

87. Thomas, C.; Aller, S.G.; Beis, K.; Carpenter, E.P.; Chang, G.; Chen, L.; Dassa, E.; Dean, M.; Duong Van Hoa, F.; Ekiert, D.; et al. Structural and Functional Diversity Calls for a New Classification of ABC Transporters. *FEBS Lett.* **2020**, *594*, 3767–3775, doi:10.1002/1873-3468.13935.

88. Locher, K.P.; Lee, A.T.; Rees, D.C. The *E. Coli* BtuCD Structure: A Framework for ABC Transporter Architecture and Mechanism. *Science (80-.).* **2002**, *296*, 1091–1098, doi:10.1126/science.1071142.

89. Gottesman, M.M.; Ambudkar, S. V. Overview: ABC Transporters and Human Disease. *J. Bioenerg. Biomembr.* **2001**, *33*, 453–458, doi:10.1023/A:1012866803188.

90. Higgins, C.F.; Hiles, I.D.; Salmond, G.P.C.; Gill, D.R.; Downie, J.A.; Evans, I.J.; Holland, I.B.; Gray, L.; Buckel, S.D.; Bell, A.W.; et al. A Family of Related ATP-Binding Subunits Coupled to Many Distinct Biological Processes in Bacteria. *Nature*

1986, *323*, 448–450, doi:10.1038/323448a0.

91. Smith, P.C.; Karpowich, N.; Millen, L.; Moody, J.E.; Rosen, J.; Thomas, P.J.; Hunt, J.F. ATP Binding to the Motor Domain from an ABC Transporter Drives Formation of a Nucleotide Sandwich Dimer. *Mol. Cell* **2002**, *10*, 139–149, doi:10.1016/S1097-2765(02)00576-2.

92. Loo, T.W.; Claire Bartlett, M.; Clarke, D.M. The "LSGGQ" Motif in Each Nucleotide-Binding Domain of Human P-Glycoprotein Is Adjacent to the Opposing Walker A Sequence. *J. Biol. Chem.* **2002**, *277*, 41303–41306, doi:10.1074/jbc.C200484200.

93. Ward, A.B.; Reyes, C.L.; Yu, J.; Roth, C.B.; Chang, G. Flexibility in the ABC Transporter MsbA: Alternating Access with a Twist. *Proc. Natl. Acad. Sci. U. S. A.* **2007**, *104*, 19005–19010, doi:10.1073/pnas.0709388104.

94. Buchaklian, A.H.; Klug, C.S. Characterization of the LSGGQ and H Motifs from the *Escherichia Coli* Lipid A Transporter MsbA. *Biochemistry* **2006**, *45*, 12539–12546, doi:10.1021/bi060830a.

95. Dawson, R.J.P.; Locher, K.P. Structure of a Bacterial Multidrug ABC Transporter. *Nature* **2006**, *443*, 180–185, doi:10.1038/nature05155.

96. Walker, J.E.; Saraste, M.; Runswick, M.J.; Gay, N.J. Distantly Related Sequences in the Alpha- and Beta-Subunits of ATP Synthase, Myosin, Kinases and Other ATP-Requiring Enzymes and a Common Nucleotide Binding Fold. *EMBO J.* **1982**, *1*, 945–51.

97. Schmitt, L.; Tampé, R. Structure and Mechanism of ABC Transporters. *Curr. Opin. Struct. Biol.* **2002**, *12*, 754–760, doi:10.1016/s0959-440x(02)00399-8.

98. Senior, A.E.; Bhagat, S. P-Glycoprotein Shows Strong Catalytic Cooperativity between the Two Nucleotide Sites. *Biochemistry* **1998**, *37*, 831–836, doi:10.1021/bi9719962.

99. Chen, J.; Sharma, S.; Quiocho, F.A.; Davidson, A.L. Trapping the Transition State of an ATP-Binding Cassette Transporter: Evidence for a Concerted Mechanism of Maltose Transport. *Proc. Natl. Acad. Sci. U. S. A.* **2001**, *98*, 1525–1530, doi:10.1073/pnas.98.4.1525.

100. Zaitseva, J.; Jenewein, S.; Wiedenmann, A.; Benabdelhak, H.; Holland, I.B.; Schmitt, L. Functional Characterization and ATP-Induced Dimerization of the Isolated ABC-Domain of the Haemolysin B Transporter. *Biochemistry* **2005**, *44*, 9680–9690, doi:10.1021/bi0506122.

101. Zoghbi, M.E.; Altenberg, G.A. ATP Binding to Two Sites Is Necessary for Dimerization of Nucleotide-Binding Domains of ABC Proteins. *Biochem. Biophys. Res. Commun.* **2014**, *443*, 97–102, doi:10.1016/j.bbrc.2013.11.050.

102. Dalmas, O.; Do Cao, M.-A.; Lugo, M.R.; Sharom, F.J.; Di Pietro, A.; Jault, J.-M. Time-Resolved Fluorescence Resonance Energy Transfer Shows That the Bacterial Multidrug ABC Half-Transporter BmrA Functions as a Homodimer. *Biochemistry* **2005**, *44*, 4312–4321, doi:10.1021/bi0482809.

103. Barth, K.; Hank, S.; Spindler, P.E.; Prisner, T.F.; Tampé, R.; Joseph, B. Conformational Coupling and Trans-Inhibition in the Human Antigen Transporter Ortholog TmrAB Resolved with Dipolar EPR Spectroscopy. *J. Am. Chem. Soc.* **2018**, *140*, 4527–4533, doi:10.1021/jacs.7b12409.

104. Collauto, A.; Mishra, S.; Litvinov, A.; Mchaourab, H.S.; Goldfarb, D. Direct Spectroscopic Detection of ATP Turnover Reveals Mechanistic Divergence of ABC Exporters. *Structure* **2017**, *25*, 1264-1274.e3, doi:10.1016/j.str.2017.06.014.

105. Stefan, E.; Hofmann, S.; Tampé, R. A Single Power Stroke by ATP Binding Drives Substrate Translocation in a Heterodimeric ABC Transporter. *Elife* **2020**, *9*, 1–17, doi:10.7554/eLife.55943.

106. Zutz, A.; Hoffmann, J.; Hellmich, U.A.; Glaubitz, C.; Ludwig, B.; Brutschy, B.; Tampé, R. Asymmetric ATP Hydrolysis Cycle of the Heterodimeric Multidrug ABC Transport Complex TmrAB from *Thermus Thermophilus*. *J. Biol. Chem.* **2011**, *286*, 7104–7115, doi:10.1074/jbc.M110.201178.

107. Thomas, C.; Tampé, R. Structural and Mechanistic Principles of ABC Transporters. *Annu. Rev. Biochem.* **2020**, *89*, 605–636, doi:10.1146/annurev-biochem-011520-105201.

108. Ambudkar, S. V.; Kim, I.W.; Xia, D.; Sauna, Z.E. The A-Loop, a Novel Conserved Aromatic Acid Subdomain Upstream of the Walker A Motif in ABC Transporters, Is Critical for ATP Binding. *FEBS Lett.* **2006**, *580*, 1049–1055, doi:10.1016/j.febslet.2005.12.051.

109. Geourjon, C.; Orelle, C.; Steinfels, E.; Blanchet, C.; Deléage, G.; Di Pietro, A.; Jault, J.-M. A Common Mechanism for ATP Hydrolysis in ABC Transporter and Helicase Superfamilies. *Trends Biochem. Sci.* **2001**, *26*, 539–544, doi:10.1016/S0968-0004(01)01907-7.

110. Saraste, M.; Sibbald, P.R.; Wittinghofer, A. The P-Loop - a Common Motif in ATP- and GTP-Binding Proteins. *Trends Biochem. Sci.* **1990**, *15*, 430–434, doi:10.1016/0968-0004(90)90281-F.

111. Orelle, C.; Gubellini, F.; Durand, A.; Marco, S.; Lévy, D.; Gros, P.; Di Pietro, A.; Jault, J.-M. Conformational Change Induced by ATP Binding in the Multidrug ATP-Binding Cassette Transporter BmrA. *Biochemistry* **2008**, *47*, 2404–2412, doi:10.1021/bi702303s.

112. Yang, R.; Hou, Y.X.; Campbell, C.A.; Palaniyandi, K.; Zhao, Q.; Bordner, A.J.; Chang, X.B. Glutamine Residues in Q-Loops of Multidrug Resistance Protein MRP1 Contribute to ATP Binding via Interaction with Metal Cofactor. *Biochim. Biophys. Acta - Biomembr.* **2011**, *1808*, 1790–1796, doi:10.1016/j.bbamem.2011.02.004.

113. Zolnerciks, J.K.; Akkaya, B.G.; Snippe, M.; Chiba, P.; Seelig, A.; Linton, K.J. The Q Loops of the Human Multidrug Resistance Transporter ABCB1 Are Necessary to Couple Drug Binding to the ATP Catalytic Cycle. *FASEB J.* **2014**, *28*, 4335–4346, doi:10.1096/fj.13-245639.

114. Dalmas, O.; Orelle, C.; Foucher, A.E.; Geourjon, C.; Crouzy, S.; Di Pietro, A.; Jault, J.M. The Q-Loop Disengages from the First Intracellular Loop during the Catalytic Cycle of the Multidrug ABC Transporter BmrA. *J. Biol. Chem.* **2005**, *280*, 36857–36864, doi:10.1074/jbc.M503266200.

115. Schmees, G.; Stein, A.; Hunke, S.; Landmesser, H.; Schneider, E. Functional Consequences of Mutations in the Conserved "signature Sequence" of the ATP-Binding-Cassette Protein MalK. *Eur. J. Biochem.* **1999**, *266*, 420–430, doi:10.1046/j.1432-1327.1999.00871.x.

116. Oldham, M.L.; Chen, J. Snapshots of the Maltose Transporter during ATP Hydrolysis. *Proc. Natl. Acad. Sci. U. S. A.* **2011**, *108*, 15152–15156, doi:10.1073/pnas.1108858108.

117. Orelle, C.; Dalmas, O.; Gros, P.; Di Pietro, A.; Jault, J.-M. The Conserved Glutamate Residue Adjacent to the Walker-B Motif Is the Catalytic Base for ATP Hydrolysis in the ATP-Binding Cassette Transporter BmrA. *J. Biol. Chem.* **2003**, *278*, 47002–47008, doi:10.1074/jbc.M308268200.

118. Sauna, Z.E.; Kim, I.-W.; Nandigama, K.; Kopp, S.; Chiba, P.; Ambudkar, S. V. Catalytic Cycle of ATP Hydrolysis by P-Glycoprotein: Evidence for Formation of the E·S Reaction Intermediate with ATP-γ-S, a Nonhydrolyzable Analogue of ATP. *Biochemistry* **2007**, *46*, 13787–13799, doi:10.1021/bi701385t.

119. Mehmood, S.; Domene, C.; Forest, E.; Jault, J.-M. Dynamics of a Bacterial Multidrug ABC Transporter in the Inward- and Outward-Facing Conformations. *Proc. Natl. Acad. Sci. U. S. A.* **2012**, *109*, 10832–10836, doi:10.1073/pnas.1204067109.

120. Moody, J.E.; Millen, L.; Binns, D.; Hunt, J.F.; Thomas, P.J. Cooperative, ATP-Dependent Association of the Nucleotide Binding Cassettes during the Catalytic Cycle of ATP-Binding Cassette Transporters. *J. Biol. Chem.* **2002**, *277*, 21111–4, doi:10.1074/jbc.C200228200.

121. Grossmann, N.; Vakkasoglu, A.S.; Hulpke, S.; Abele, R.; Gaudet, R.; Tampé, R. Mechanistic Determinants of the Directionality and Energetics of Active Export by a Heterodimeric ABC Transporter. *Nat. Commun.* **2014**, *5*, doi:10.1038/ncomms6419.

122. Jones, P.M.; George, A.M. Role of the D-Loops in Allosteric Control of ATP Hydrolysis in an ABC Transporter. *J. Phys. Chem. A* **2012**, *116*, 3004–3013, doi:10.1021/jp211139s.

123. Vakkasoglu, A.S.; Srikant, S.; Gaudet, R. D-Helix Influences Dimerization of the ATP-Binding Cassette (ABC) Transporter Associated with Antigen Processing 1 (TAP1) Nucleotide-Binding Domain. *PLoS One* **2017**, *12*, 1–14, doi:10.1371/journal.pone.0178238.

124. Zaitseva, J.; Jenewein, S.; Jumpertz, T.; Holland, I.B.; Schmitt, L. H662 Is the Linchpin of ATP Hydrolysis in the Nucleotide-Binding Domain of the ABC Transporter HlyB. *EMBO J.* **2005**, *24*, 1901–1910, doi:10.1038/sj.emboj.7600657.

125. Ernst, R.; Kueppers, P.; Klein, C.M.; Schwarzmueller, T.; Kuchler, K.; Schmitt, L. A Mutation of the H-Loop Selectively Affects Rhodamine Transport by the Yeast Multidrug ABC Transporter Pdr5. *Proc. Natl. Acad. Sci. U. S. A.* **2008**, *105*, 5069–5074, doi:10.1073/pnas.0800191105.

126. Prieß, M.; Göddeke, H.; Groenhof, G.; Schäfer, L. V. Molecular Mechanism of ATP Hydrolysis in an ABC Transporter. *ACS Cent. Sci.* **2018**, *4*, 1334–1343, doi:10.1021/acscentsci.8b00369.

127. Oancea, G.; O'Mara, M.L.; Bennett, W.F.D.; Tieleman, D.P.; Abele, R.; Tampé, R. Structural Arrangement of the Transmission Interface in the Antigen ABC Transport Complex TAP. *Proc. Natl. Acad. Sci. U. S. A.* **2009**, *106*, 5551–5556, doi:10.1073/pnas.0811260106.

128. Kluth, M.; Stindt, J.; Dröge, C.; Linnemann, D.; Kubitz, R.; Schmitt, L. A Mutation within the Extended X Loop Abolished Substrateinduced ATPase Activity of the Human

Liver ATP-Binding Cassette (ABC) Transporter MDR3. *J. Biol. Chem.* **2015**, *290*, 4896–4907, doi:10.1074/jbc.M114.588566.

129. Orelle, C.; Mathieu, K.; Jault, J.-M. Multidrug ABC Transporters in Bacteria. *Res. Microbiol.* **2019**, *170*, 381–391, doi:10.1016/j.resmic.2019.06.001.

130. Rees, D.C.; Johnson, E.; Lewinson, O. ABC Transporters: The Power to Change. *Nat. Rev. Mol. Cell Biol.* **2009**, *10*, 218–227, doi:10.1038/nrm2646.

131. Locher, K.P. Mechanistic Diversity in ATP-Binding Cassette (ABC) Transporters. *Nat. Struct. Mol. Biol.* **2016**, *23*, 487–493, doi:10.1038/nsmb.3216.

132. Bonifer, C.; Glaubitz, C. MsbA: An ABC Transporter Paradigm. *Biochem. Soc. Trans.* **2021**, *49*, 2917–2927, doi:10.1042/BST20211030.

133. Wilkens, S. Structure and Mechanism of ABC Transporters. *F1000Prime Rep.* **2015**, *7*, 1–9, doi:10.12703/P7-14.

134. Gutmann, D.A.P.; Ward, A.B.; Urbatsch, I.L.; Chang, G.; van Veen, H.W. Understanding Polyspecificity of Multidrug ABC Transporters: Closing in on the Gaps in ABCB1. *Trends Biochem. Sci.* **2010**, *35*, 36–42, doi:10.1016/j.tibs.2009.07.009.

135. Chufan, E.E.; Sim, H.-M.; Ambudkar, S. V. Molecular Basis of the Polyspecificity of P-Glycoprotein (ABCB1): Recent Biochemical and Structural Studies. *Adv. Cancer Res.* **2015**, *125*, 71–96, doi:10.1016/bs.acr.2014.10.003.

136. Loo, T.W.; Clarke, D.M. Mutational Analysis of ABC Proteins. *Arch. Biochem. Biophys.* **2008**, *476*, 51–64, doi:10.1016/j.abb.2008.02.025.

137. Higgins, C.F. ABC Transporters: Physiology, Structure and Mechanism – an Overview. *Res. Microbiol.* **2001**, *152*, 205–210, doi:10.1016/S0923-2508(01)01193-7.

138. Holland, I.B.; Blight, M.A. ABC-ATPases, Adaptable Energy Generators Fuelling Transmembrane Movement of a Variety of Molecules in Organisms from Bacteria to Humans. *J. Mol. Biol.* **1999**, *293*, 381–399, doi:10.1006/jmbi.1999.2993.

139. Esser, L.; Zhou, F.; Pluchino, K.M.; Shiloach, J.; Ma, J.; Tang, W.K.; Gutierrez, C.; Zhang, A.; Shukla, S.; Madigan, J.P.; et al. Structures of the Multidrug Transporter P-Glycoprotein Reveal Asymmetric ATP Binding and the Mechanism of Polyspecificity. *J. Biol. Chem.* **2017**, *292*, 446–461, doi:10.1074/jbc.M116.755884.

140. Aller, S.G.; Yu, J.; Ward, A.B.; Weng, Y.; Chittaboina, S.; Zhuo, R.; Harrell, P.M.; Trinh, Y.T.; Zhang, Q.; Urbatsch, I.L.; et al. Structure of P-Glycoprotein Reveals a

Molecular Basis for Poly-Specific Drug Binding. *Science (80-.).* **2009**, *323*, 1718–1722, doi:10.1126/science.1168750.

141. Callaghan, R. Providing a Molecular Mechanism for P-Glycoprotein; Why Would i Bother? *Biochem. Soc. Trans.* **2015**, *43*, 995–1002, doi:10.1042/BST20150131.

142. Loo, T.W.; Bartlett, M.C.; Clarke, D.M. Simultaneous Binding of Two Different Drugs in the Binding Pocket of the Human Multidrug Resistance P-Glycoprotein. *J. Biol. Chem.* **2003**, *278*, 39706–39710, doi:10.1074/jbc.M308559200.

143. Dönmez Cakil, Y.; Khunweeraphong, N.; Parveen, Z.; Schmid, D.; Artaker, M.; Ecker, G.F.; Sitte, H.H.; Pusch, O.; Stockner, T.; Chiba, P. Pore-Exposed Tyrosine Residues of P-Glycoprotein Are Important Hydrogen-Bonding Partners for Drugs. *Mol. Pharmacol.* **2014**, *85*, 420–428, doi:10.1124/mol.113.088526.

144. Chaptal, V.; Zampieri, V.; Wiseman, B.; Orelle, C.; Martin, J.; Nguyen, K.; Gobet, A.; Di Cesare, M.; Magnard, S.; Javed, W.; et al. Substrate-Bound and Substrate-Free Outward-Facing Structures of a Multidrug ABC Exporter. *Sci. Adv.* **2022**, *8*, 1–11, doi:10.1126/sciadv.abg9215.

145. Szöllősi, D.; Rose-Sperling, D.; Hellmich, U.A.; Stockner, T. Comparison of Mechanistic Transport Cycle Models of ABC Exporters. *Biochim. Biophys. Acta - Biomembr.* **2018**, *1860*, 818–832, doi:10.1016/j.bbamem.2017.10.028.

146. Higgins, C.F.; Linton, K.J. The ATP Switch Model for ABC Transporters. *Nat. Struct. Mol. Biol.* **2004**, *11*, 918–926, doi:10.1038/nsmb836.

147. van der Does, C.; Tampé, R. How Do ABC Transporters Drive Transport? *Biol. Chem.* **2004**, *385*, 927–933, doi:10.1515/BC.2004.121.

148. Linton, K.J.; Higgins, C.F. Structure and Function of ABC Transporters: The ATP Switch Provides Flexible Control. *Pflugers Arch. Eur. J. Physiol.* **2007**, *453*, 555–567, doi:10.1007/s00424-006-0126-x.

149. Chen, J.; Lu, G.; Lin, J.; Davidson, A.L.; Quiocho, F.A. A Tweezers-like Motion of the ATP-Binding Cassette Dimer in an ABC Transport Cycle. *Mol. Cell* **2003**, *12*, 651–661, doi:10.1016/j.molcel.2003.08.004.

150. Senior, A.E.; Al-Shawi, M.K.; Urbatsch, I.L. The Catalytic Cycle of P-Glycoprotein. *FEBS Lett.* **1995**, *377*, 285–289, doi:10.1016/0014-5793(95)01345-8.

151. Jones, P.M.; George, A.M. Opening of the ADP-Bound Active Site in the ABC

Transporter ATPase Dimer: Evidence for a Constant Contact, Alternating Sites Model for the Catalytic Cycle. *Proteins Struct. Funct. Bioinforma.* **2009**, *75*, 387–396, doi:10.1002/prot.22250.

152. Jones, P.M.; George, A.M. Subunit Interactions in ABC Transporters: Towards a Functional Architecture. *FEMS Microbiol. Lett.* **1999**, *179*, 187–202, doi:10.1016/S0378-1097(99)00411-5.

153. Zoghbi, M.E.; Altenberg, G.A. Hydrolysis at One of the Two Nucleotide-Binding Sites Drives the Dissociation of ATP-Binding Cassette Nucleotide-Binding Domain Dimers. *J. Biol. Chem.* **2013**, *288*, 34259–34265, doi:10.1074/jbc.M113.500371.

154. Loo, T.W.; Bartlett, M.C.; Clarke, D.M. Human P-Glycoprotein Contains a Greasy Ball-and-Socket Joint at the Second Transmission Interface. *J. Biol. Chem.* **2013**, *288*, 20326–20333, doi:10.1074/jbc.M113.484550.

155. Jin, M.S.; Oldham, M.L.; Zhang, Q.; Chen, J. Crystal Structure of the Multidrug Transporter P-Glycoprotein from *Caenorhabditis Elegans*. *Nature* **2012**, *490*, 566–9, doi:10.1038/nature11448.

156. Hollenstein, K.; Dawson, R.J.P.; Locher, K.P. Structure and Mechanism of ABC Transporter Proteins. *Curr. Opin. Struct. Biol.* **2007**, *17*, 412–418, doi:10.1016/j.sbi.2007.07.003.

157. Damas, J.M.; Oliveira, A.S.F.; Baptista, A.M.; Soares, C.M. Structural Consequences of ATP Hydrolysis on the ABC Transporter NBD Dimer: Molecular Dynamics Studies of HlyB. *Protein Sci.* **2011**, *20*, 1220–1230, doi:10.1002/pro.650.

158. Locher, K.P. Structure and Mechanism of ATP-Binding Cassette Transporters. *Philos. Trans. R. Soc. B Biol. Sci.* **2009**, *364*, 239–245, doi:10.1098/rstb.2008.0125.

159. Doshi, R.; Ali, A.; Shi, W.; Freeman, E. V.; Fagg, L.A.; Van Veen, H.W. Molecular Disruption of the Power Stroke in the ATP-Binding Cassette Transport Protein MsbA. *J. Biol. Chem.* **2013**, *288*, 6801–6813, doi:10.1074/jbc.M112.430074.

160. Hanekop, N.; Zaitseva, J.; Jenewein, S.; Holland, I.B.; Schmitt, L. Molecular Insights into the Mechanism of ATP-Hydrolysis by the NBD of the ABC-Transporter HlyB. *FEBS Lett.* **2006**, *580*, 1036–1041, doi:10.1016/j.febslet.2005.11.012.

161. Johnson, Z.L.; Chen, J. ATP Binding Enables Substrate Release from Multidrug Resistance Protein 1. *Cell* **2018**, *172*, 81-89.e10, doi:10.1016/j.cell.2017.12.005.

162. Chaptal, V.; Zampieri, V.; Wiseman, B.; Orelle, C.; Martin, J.; Nguyen, K.-A.; Magnard, S.; Gobet, A.; Di Cesare, M.; Javed, W.; et al. Drug-Bound and -Free Outward-Facing Structures of a Multidrug ABC Exporter Point to a Swing Mechanism. **2021**, doi:10.1101/2021.03.12.435132.

163. Quentin, Y.; Fichant, G.; Denizot, F. Inventory, Assembly and Analysis of *Bacillus Subtilis* ABC Transport Systems. *J. Mol. Biol.* **1999**, *287*, 467–484, doi:10.1006/jmbi.1999.2624.

164. Steinfels, E.; Orelle, C.; Dalmas, O.; Penin, F.; Miroux, B.; Di Pietro, A.; Jault, J.-M. Highly Efficient Over-Production in *E. Coli* of YvcC, a Multidrug-like ATP-Binding Cassette Transporter from *Bacillus Subtilis*. *Biochim. Biophys. Acta - Biomembr.* **2002**, *1565*, 1–5, doi:10.1016/S0005-2736(02)00515-1.

165. Steinfels, E.; Orelle, C.; Fantino, J.-R.; Dalmas, O.; Rigaud, J.-L.; Denizot, F.; Di Pietro, A.; Jault, J.-M. Characterization of YvcC (BmrA), a Multidrug ABC Transporter Constitutively Expressed in *Bacillus Subtilis*. *Biochemistry* **2004**, *43*, 7491–7502, doi:10.1021/bi0362018.

166. Krügel, H.; Licht, A.; Biedermann, G.; Petzold, A.; Lassak, J.; Hupfer, Y.; Schlott, B.; Hertweck, C.; Platzer, M.; Brantl, S.; et al. Cervimycin C Resistance in *Bacillus Subtilis* Is Due to a Promoter Up-Mutation and Increased MRNA Stability of the Constitutive ABC-Transporter Gene BmrA. *FEMS Microbiol. Lett.* **2010**, *313*, 155–163, doi:10.1111/j.1574-6968.2010.02143.x.

167. Ravaud, S.; Do Cao, M.-A.; Jidenko, M.; Ebel, C.; Le Maire, M.; Jault, J.-M.; Di Pietro, A.; Haser, R.; Aghajari, N. The ABC Transporter BmrA from *Bacillus Subtilis* Is a Functional Dimer When in a Detergent-Solubilized State. *Biochem. J.* **2006**, *395*, 345–353, doi:10.1042/BJ20051719.

168. Chami, M.; Steinfels, E.; Orelle, C.; Jault, J.-M.; Di Pietro, A.; Rigaud, J.-L.; Marco, S. Three-Dimensional Structure by Cryo-Electron Microscopy of YvcC, an Homodimeric ATP-Binding Cassette Transporter from *Bacillus Subtilis*. *J. Mol. Biol.* **2002**, *315*, 1075–1085, doi:10.1006/jmbi.2001.5309.

169. Lacabanne, D.; Orelle, C.; Lecoq, L.; Kunert, B.; Chuilon, C.; Wiegand, T.; Ravaud, S.; Jault, J.-M.; Meier, B.H.; Böckmann, A. Flexible-to-Rigid Transition Is Central for Substrate Transport in the ABC Transporter BmrA from *Bacillus Subtilis*. *Commun. Biol.* **2019**, *2*, 1–9, doi:10.1038/s42003-019-0390-x.

170. Hutter, C.A.J.; Timachi, M.H.; Hürlimann, L.M.; Zimmermann, I.; Egloff, P.; Göddeke, H.; Kucher, S.; Štefanić, S.; Karttunen, M.; Schäfer, L. V.; et al. The Extracellular Gate Shapes the Energy Profile of an ABC Exporter. *Nat. Commun.* **2019**, *10*, doi:10.1038/s41467-019-09892-6.

171. Ambudkar, S. V.; Kimchi-Sarfaty, C.; Sauna, Z.E.; Gottesman, M.M. P-Glycoprotein: From Genomics to Mechanism. *Oncogene* **2003**, *22*, 7468–7485, doi:10.1038/sj.onc.1206948.

172. Gottesman, M.M.; Pastan, I. Biochemistry of Multidrug Resistance Mediated by the Multidrug Transporter. *Annu. Rev. Biochem.* **1993**, *62*, 385–427, doi:10.1146/annurev.bi.62.070193.002125.

173. Martinez, L.; Arnaud, O.; Henin, E.; Tao, H.; Chaptal, V.; Doshi, R.; Andrieu, T.; Dussurgey, S.; Tod, M.; Di Pietro, A.; et al. Understanding Polyspecificity within the Substrate-Binding Cavity of the Human Multidrug Resistance P-Glycoprotein. *FEBS J.* **2014**, *281*, 673–682, doi:10.1111/febs.12613.

174. Nöll, A.; Thomas, C.; Herbring, V.; Zollmann, T.; Barth, K.; Mehdipour, A.R.; Tomasiak, T.M.; Brüchert, S.; Joseph, B.; Abele, R.; et al. Crystal Structure and Mechanistic Basis of a Functional Homolog of the Antigen Transporter TAP. *Proc. Natl. Acad. Sci. U. S. A.* **2017**, *114*, E438–E447, doi:10.1073/pnas.1620009114.

175. Schneider, C.A.; Rasband, W.S.; Eliceiri, K.W. NIH Image to ImageJ: 25 Years of Image Analysis. *Nat. Methods* **2012**, *9*, 671–675, doi:10.1038/nmeth.2089.

176. Chung, C.T.; Niemela, S.L.; Miller, R.H. One-Step Preparation of Competent *Escherichia Coli*: Transformation and Storage of Bacterial Cells in the Same Solution. *Proc. Natl. Acad. Sci.* **1989**, *86*, 2172–2175, doi:10.1073/pnas.86.7.2172.

177. Gasteiger, E.; Hoogland, C.; Gattiker, A.; Duvaud, S.; Wilkins, M.R.; Appel, R.D.; Bairoch, A. *Protein Identification and Analysis Tools on the ExPASy Server*; Walker, J.M., Ed.; Humana Press: Totowa, NJ, 2005; ISBN 978-1-58829-343-5.

178. Laemmli, U.K. Cleavage of Structural Proteins during the Assembly of the Head of Bacteriophage T4. *Nature* **1970**, *227*, 680–5, doi:10.1038/227680a0.

179. Hellmann, N.; Schneider, D. Hands On: Using Tryptophan Fluorescence Spectroscopy to Study Protein Structure. In *Protein Supersecondary Structures: Methods and Protocols*; Kister, A.E., Ed.; Springer New York: New York, NY, 2019; pp. 379–401 ISBN 978-1-4939-9161-7.

180. Oepen, K.; Özbek, H.; Schüffler, A.; Liermann, J.C.; Thines, E.; Schneider, D. Myristic Acid Inhibits the Activity of the Bacterial ABC Transporter BmrA. *Int. J. Mol. Sci.* **2021**, *22*, doi:10.3390/ijms222413565.

181. Hediger, M.A.; Romero, M.F.; Peng, J.-B.; Rolfs, A.; Takanaga, H.; Bruford, E.A. The ABCs of Solute Carriers: Physiological, Pathological and Therapeutic Implications of Human Membrane Transport Proteins. *Pflugers Arch. Eur. J. Physiol.* **2004**, *447*, 465–468, doi:10.1007/s00424-003-1192-y.

182. Higgins, C.F. ABC Transporters: From Microorganisms to Man. *Annu. Rev. Cell Biol.* **1992**, *8*, 67–113, doi:10.1146/annurev.cb.08.110192.000435.

183. Falasca, M.; Linton, K.J. Investigational ABC Transporter Inhibitors. *Expert Opin. Investig. Drugs* **2012**, *21*, 657–666, doi:10.1517/13543784.2012.679339.

184. Neyfakh, A.A.; Bidnenko, V.E.; Chen, L.B. Efflux-Mediated Multidrug Resistance in *Bacillus Subtilis*: Similarities and Dissimilarities with the Mammalian System. *Proc. Natl. Acad. Sci. U. S. A.* **1991**, *88*, 4781–4785, doi:10.1073/pnas.88.11.4781.

185. Lacabanne, D.; Lends, A.; Danis, C.; Kunert, B.; Fogeron, M.L.; Jirasko, V.; Chuilon, C.; Lecoq, L.; Orelle, C.; Chaptal, V.; et al. Gradient Reconstitution of Membrane Proteins for Solid-State NMR Studies. *J. Biomol. NMR* **2017**, *69*, 81–91, doi:10.1007/s10858-017-0135-4.

186. Sharom, F.J. Characterization and Functional Reconstitution of the Multidrug Transporter. *J. Bioenerg. Biomembr.* **1995**, *27*, 15–22, doi:10.1007/BF02110326.

187. Ambudkar, S. V.; Lelong, I.H.; Zhang, J.; Cardarelli, C.O.; Gottesman, M.M.; Pastan, I. Partial Purification and Reconstitution of the Human Multidrug-Resistance Pump: Characterization of the Drug-Stimulatable ATP Hydrolysis. *Proc. Natl. Acad. Sci. U. S. A.* **1992**, *89*, 8472–8476, doi:10.1073/pnas.89.18.8472.

188. de Athayde Moncorvo Collado, A.; Corbalán, N.; Homolya, L.; Morero, R.; Minahk, C. Resveratrol Modulates ATPase Activity of Liposome-Reconstituted ABCG1. *FEBS Lett.* **2013**, *587*, 2359–2363, doi:10.1016/j.febslet.2013.06.001.

189. Fameau, A.-L.; Ventureira, J.; Novales, B.; Douliez, J.-P. Foaming and Emulsifying Properties of Fatty Acids Neutralized by Tetrabutylammonium Hydroxide. *Colloids Surfaces A Physicochem. Eng. Asp.* **2012**, *403*, 87–95, doi:10.1016/j.colsurfa.2012.03.059.

190. Veerappan, A.; Cymer, F.; Klein, N.; Schneider, D. The Tetrameric α-Helical Membrane Protein GlpF Unfolds via a Dimeric Folding Intermediate. *Biochemistry* **2011**, *50*, 10223–10230, doi:10.1021/bi201266m.

191. Anbazhagan, V.; Cymer, F.; Schneider, D. Unfolding a Transmembrane Helix Dimer: A FRET Study in Mixed Micelles. *Arch. Biochem. Biophys.* **2010**, *495*, 159–164, doi:10.1016/j.abb.2010.01.006.

192. Sehgal, P.; Mogensen, J.E.; Otzen, D.E. Using Micellar Mole Fractions to Assess Membrane Protein Stability in Mixed Micelles. *Biochim. Biophys. Acta - Biomembr.* **2005**, *1716*, 59–68, doi:10.1016/j.bbamem.2005.08.006.

193. Hellmann, N.; Schneider, D. A Complex Unfolding Pathway of α-Helical Membrane Proteins in SDS-Containing Micelles. *Biophys. J.* **2021**, *120*, 3857–3859, doi:10.1016/j.bpj.2021.08.002.

194. Otzen, D.E.; Nedergaard Pedersen, J.; Kumar Somavarapu, A.; Clement, A.; Ji, M.; Hartvig Petersen, E.; Skov Pedersen, J.; Urban, S.; Schafer, N.P. Cys-Labeling Kinetics of Membrane Protein GlpG: A Role for Specific SDS Binding and Micelle Changes? *Biophys. J.* **2021**, *120*, 4115–4128, doi:10.1016/J.BPJ.2021.08.001.

195. Shapiro, A.B.; Ling, V. Reconstitution of Drug Transport by Purified P-Glycoprotein. *J. Biol. Chem.* **1995**, *270*, 16167–16175, doi:10.1074/jbc.270.27.16167.

196. Burdock, G.A.; Carabin, I.G. Safety Assessment of Myristic Acid as a Food Ingredient. *Food Chem. Toxicol.* **2007**, *45*, 517–529, doi:10.1016/j.fct.2006.10.009.

197. Bishop, D.G.; Rutberg, L.; Samuelsson, B. The Chemical Composition of the Cytoplasmic Membrane of *Bacillus Subtilis*. *Eur. J Biochem* **1967**, *2*, 448–453.

198. Doige, C.A.; Yu, X.; Sharom, F.J. The Effects of Lipids and Detergents on ATPase-Active P-Glycoprotein. *Biochim. Biophys. Acta* **1993**, *1146*, 65–72, doi:10.1016/0005-2736(93)90339-2.

199. Sharom, F.J. The P-Glycoprotein Efflux Pump: How Does It Transport Drugs? *J. Membr. Biol.* **1997**, *160*, 161–175, doi:10.1007/s002329900305.

200. Neumann, J.; Rose-Sperling, D.; Hellmich, U.A. Diverse Relations between ABC Transporters and Lipids: An Overview. *Biochim. Biophys. Acta - Biomembr.* **2017**, *1859*, 605–618, doi:10.1016/j.bbamem.2016.09.023.

201. Reuter, G.; Janvilisri, T.; Venter, H.; Shahi, S.; Balakrishnan, L.; van Veen, H.W. The

ATP Binding Cassette Multidrug Transporter LmrA and Lipid Transporter MsbA Have Overlapping Substrate Specificities. *J. Biol. Chem.* **2003**, *278*, 35193–35198, doi:10.1074/jbc.M306226200.

202. Woebking, B.; Reuter, G.; Shilling, R.A.; Velamakanni, S.; Shahi, S.; Venter, H.; Balakrishnan, L.; van Veen, H.W. Drug-Lipid A Interactions on The. *J. Bacteriol.* **2005**, *187*, 6363–6369, doi:10.1128/JB.187.18.6363-6369.2005.

203. Lee, A.. Lipid–Protein Interactions in Biological Membranes: A Structural Perspective. *Biochim. Biophys. Acta - Biomembr.* **2003**, *1612*, 1–40, doi:10.1016/S0005-2736(03)00056-7.

204. Tiefenauer, L.; Demarche, S. Challenges in the Development of Functional Assays of Membrane Proteins. *Materials (Basel).* **2012**, *5*, 2205–2242, doi:10.3390/ma5112205.

205. Hyde, S.C.; Emsley, P.; Hartshorn, M.J.; Mimmack, M.M.; Gileadi, U.; Pearce, S.R.; Gallagher, M.P.; Gill, D.R.; Hubbard, R.E.; Higgins, C.F. Structural Model of ATP-Binding Proteins Associated with Cystic Fibrosis, Multidrug Resistance and Bacterial Transport. *Nature* **1990**, *346*, 362–365, doi:10.1038/346362a0.

206. Bolhuis, H.; van Veen, H.W.; Molenaar, D.; Poolman, B.; Driessen, A.J.M.; Konings, W.N. Multidrug Resistance in *Lactococcus Lactis*: Evidence for ATP-Dependent Drug Extrusion from the Inner Leaflet of the Cytoplasmic Membrane. *EMBO J.* **1996**, *15*, 4239–4245, doi:10.1002/j.1460-2075.1996.tb00798.x.

207. Putman, M.; van Veen, H.W.; Konings, W.N. Molecular Properties of Bacterial Multidrug Transporters. *Microbiol. Mol. Biol. Rev.* **2000**, *64*, 672–693, doi:10.1128/mmbr.64.4.672-693.2000.

208. Alam, A.; Kowal, J.; Broude, E.; Roninson, I.; Locher, K.P. Structural Insight into Substrate and Inhibitor Discrimination by Human P-Glycoprotein. *Science (80-.).* **2019**, *363*, 753–756, doi:10.1126/science.aav7102.

209. Jones, P.M.; George, A.M. The ABC Transporter Structure and Mechanism: Perspectives on Recent Research. *Cell. Mol. Life Sci.* **2004**, *61*, 682–699, doi:10.1007/s00018-003-3336-9.

210. Janas, E.; Hofacker, M.; Chen, M.; Gompf, S.; Van der Does, C.; Tampé, R. The ATP Hydrolysis Cycle of the Nucleotide-Binding Domain of the Mitochondrial ATP-Binding Cassette Transporter Mdl1p. *J. Biol. Chem.* **2003**, *278*, 26862–26869, doi:10.1074/jbc.M301227200.

211. Ford, R.C.; Hellmich, U.A. What Monomeric Nucleotide Binding Domains Can Teach Us about Dimeric ABC Proteins. *FEBS Lett.* **2020**, *594*, 3857–3875, doi:10.1002/1873-3468.13921.

212. Lu, G.; Westbrooks, J.M.; Davidson, A.L.; Chen, J. ATP Hydrolysis Is Required to Reset the ATP-Binding Cassette Dimer into the Resting-State Conformation. *Proc. Natl. Acad. Sci. U. S. A.* **2005**, *102*, 17969–17974, doi:10.1073/pnas.0506039102.

213. Diederichs, K.; Diez, J.; Greller, G.; Müller, C.; Breed, J.; Schnell, C.; Vonrhein, C.; Boos, W.; Welte, W. Crystal Structure of Malk, the ATPase Subunit of the Trehalose/Maltose ABC Transporter of the Archaeon *Thermococcus Litoralis*. *EMBO J.* **2000**, *19*, 5951–5961, doi:10.1093/emboj/19.22.5951.

214. Hollenstein, K.; Frei, D.C.; Locher, K.P. Structure of an ABC Transporter in Complex with Its Binding Protein. *Nature* **2007**, *446*, 213–216, doi:10.1038/nature05626.

215. Srinivasan, V.; Pierik, A.J.; Lill, R. Crystal Structures of Nucleotide-Free and Glutathione-Bound Mitochondrial ABC Transporter Atm1. *Science (80-.).* **2014**, *343*, 1137–1140, doi:10.1126/science.1246729.

216. Schaedler, T.A.; Faust, B.; Shintre, C.A.; Carpenter, E.P.; Srinivasan, V.; Van Veen, H.W.; Balk, J. Structures and Functions of Mitochondrial ABC Transporters. *Biochem. Soc. Trans.* **2015**, *43*, 943–51, doi:10.1042/BST20150118.

217. Timachi, M.H.; Hutter, C.A.J.; Hohl, M.; Assafa, T.; Böhm, S.; Mittal, A.; Seeger, M.A.; Bordignon, E. Exploring Conformational Equilibria of a Heterodimeric ABC Transporter. *Elife* **2017**, *6*, 1–28, doi:10.7554/eLife.20236.

218. Davidson, A.L.; Sharma, S. Mutation of a Single MalK Subunit Severely Impairs Maltose Transport Activity in *Escherichia Coli*. *J. Bacteriol.* **1997**, *179*, 5458–5464, doi:10.1128/jb.179.17.5458-5464.1997.

219. Nikaido, K.; Ames, G.F.-L. One Intact ATP-Binding Subunit Is Sufficient to Support ATP Hydrolysis and Translocation in an ABC Transporter, the Histidine Permease. *J. Biol. Chem.* **1999**, *274*, 26727–26735, doi:10.1074/jbc.274.38.26727.

220. De La Rosa, M.B.; Nelson, S.W. An Interaction between the Walker A and D-Loop Motifs Is Critical to ATP Hydrolysis and Cooperativity in Bacteriophage T4 Rad50. *J. Biol. Chem.* **2011**, *286*, 26258–26266, doi:10.1074/jbc.M111.256305.

221. Zaitseva, J.; Oswald, C.; Jumpertz, T.; Jenewein, S.; Wiedenmann, A.; Holland, I.B.;

Schmitt, L. A Structural Analysis of Asymmetry Required for Catalytic Activity of an ABC-ATPase Domain Dimer. *EMBO J.* **2006**, *25*, 3432–3443, doi:10.1038/sj.emboj.7601208.

222. Pérez Carrillo, V.H.; Rose-Sperling, D.; Tran, M.A.; Wiedemann, C.; Hellmich, U.A. Backbone NMR Assignment of the Nucleotide Binding Domain of the *Bacillus Subtilis* ABC Multidrug Transporter BmrA in the Post-Hydrolysis State. *Biomol. NMR Assign.* **2022**, doi:10.1007/s12104-021-10063-2.

223. Harakalova, M.; Van Harssel, J.J.T.; Terhal, P.A.; Van Lieshout, S.; Duran, K.; Renkens, I.; Amor, D.J.; Wilson, L.C.; Kirk, E.P.; Turner, C.L.S.; et al. Dominant Missense Mutations in ABCC9 Cause Cantúsyndrome. *Nat. Genet.* **2012**, *44*, 793–796, doi:10.1038/ng.2324.

224. Sanders, C.R.; Myers, J.K. Disease-Related Misassembly of Membrane Proteins. *Annu. Rev. Biophys. Biomol. Struct.* **2004**, *33*, 25–51, doi:10.1146/annurev.biophys.33.110502.140348.

225. Nagy, J.K.; Lonzer, W.L.; Sanders, C.R. Kinetic Study of Folding and Misfolding of Diacylglycerol Kinase in Model Membranes. *Biochemistry* **2001**, *40*, 8971–8980, doi:10.1021/bi010202n.

226. Marinko, J.T.; Huang, H.; Penn, W.D.; Capra, J.A.; Schlebach, J.P.; Sanders, C.R. Folding and Misfolding of Human Membrane Proteins in Health and Disease: From Single Molecules to Cellular Proteostasis. *Chem. Rev.* **2019**, *119*, 5537–5606, doi:10.1021/acs.chemrev.8b00532.

227. Harris, N.J.; Booth, P.J. Folding and Stability of Membrane Transport Proteins *in Vitro*. *Biochim. Biophys. Acta - Biomembr.* **2012**, *1818*, 1055–1066, doi:10.1016/j.bbamem.2011.11.006.

228. Phillips, B.P.; Miller, E.A. Membrane Protein Folding and Quality Control. *Curr. Opin. Struct. Biol.* **2021**, *69*, 50–54, doi:10.1016/j.sbi.2021.03.003.

229. Booth, P.J.; Curnow, P. Membrane Proteins Shape up: Understanding *in Vitro* Folding. *Curr. Opin. Struct. Biol.* **2006**, *16*, 480–488, doi:10.1016/j.sbi.2006.06.004.

230. Di Bartolo, N.D.; Hvorup, R.N.; Locher, K.P.; Booth, P.J. *In Vitro* Folding and Assembly of the *Escherichia Coli* ATP-Binding Cassette Transporter, BtuCD. *J. Biol. Chem.* **2011**, *286*, 18807–18815, doi:10.1074/jbc.M110.176891.

231. Popot, J.-L. Folding Membrane Proteins *in Vitro*: A Table and Some Comments. *Arch. Biochem. Biophys.* 2014.

232. Lorch, M.; Booth, P.J. Insertion Kinetics of a Denatured α Helical Membrane Protein into Phospholipid Bilayer Vesicles. *J. Mol. Biol.* **2004**, *344*, 1109–1121, doi:10.1016/j.jmb.2004.09.090.

233. Booth, P.J.; Paulsen, H. Assembly of Light-Harvesting Chlorophyll a/b Complex *in Vitro*. Time-Resolved Fluorescence Measurements. *Biochemistry* **1996**, *35*, doi:10.1021/bi953053f.

234. Booth, P.J.; Flitsch, S.L.; Stern, L.J.; Greenhalgh, D.A.; Kim, P.S.; Khorana, H.G. Intermediates in the Folding of the Membrane Protein Bacteriorhodopsin. *Nat. Struct. Mol. Biol.* **1995**, *2*, 139–143, doi:10.1038/nsb0295-139.

235. London, E.; Khorana, H.G. Denaturation and Renaturation of Bacteriorhodopsin in Detergents and Lipid-Detergent Mixtures. *J. Biol. Chem.* **1982**, *257*, 7003–7011, doi:10.1016/s0021-9258(18)34529-0.

236. Gorzelle, B.M.; Nagy, J.K.; Oxenoid, K.; Lonzer, W.L.; Cafiso, D.S.; Sanders, C.R. Reconstitutive Refolding of Diacylglycerol Kinase, an Integral Membrane Protein. *Biochemistry* **1999**, *38*, 16373–16382, doi:10.1021/bi991292n.

237. Lau, F.W.; Bowie, J.U. A Method for Assessing the Stability of a Membrane Protein. *Biochemistry* **1997**, *36*, 5884–5892, doi:10.1021/bi963095j.

238. Miller, D.; Charalambous, K.; Rotem, D.; Schuldiner, S.; Curnow, P.; Booth, P.J. *In Vitro* Unfolding and Refolding of the Small Multidrug Transporter EmrE. *J. Mol. Biol.* **2009**, *393*, 815–832, doi:10.1016/j.jmb.2009.08.039.

239. Curnow, P.; Lorch, M.; Charalambous, K.; Booth, P.J. The Reconstitution and Activity of the Small Multidrug Transporter EmrE Is Modulated by Non-Bilayer Lipid Composition. *J. Mol. Biol.* **2004**, *343*, 213–222, doi:10.1016/j.jmb.2004.08.032.

240. Renart, M.L.; Barrera, F.N.; Molina, M.L.; Encinar, J.A.; Poveda, J.A.; Fernández, A.M.; Gómez, J.; González-Ros, J.M. Effects of Conducting and Blocking Ions on the Structure and Stability of the Potassium Channel KcsA. *J. Biol. Chem.* **2006**, *281*, 29905–29915, doi:10.1074/jbc.M602636200.

241. Shenkarev, Z.O.; Lyukmanova, E.N.; Butenko, I.O.; Petrovskaya, L.E.; Paramonov, A.S.; Shulepko, M.A.; Nekrasova, O. V.; Kirpichnikov, M.P.; Arseniev, A.S. Lipid-

Protein Nanodiscs Promote *in Vitro* Folding of Transmembrane Domains of Multi-Helical and Multimeric Membrane Proteins. *Biochim. Biophys. Acta - Biomembr.* **2013**, *1828*, 776–784, doi:10.1016/j.bbamem.2012.11.005.

242. Renthal, R. An Unfolding Story of Helical Transmembrane Proteins. *Biochemistry* **2006**, *45*, 14559–14566, doi:10.1021/bi0620454.

243. Stanley, A.M.; Fleming, K.G. The Process of Folding Proteins into Membranes: Challenges and Progress. *Arch. Biochem. Biophys.* **2008**, *469*, 46–66, doi:10.1016/j.abb.2007.09.024.

244. Bennion, B.J.; Daggett, V. The Molecular Basis for the Chemical Denaturation of Proteins by Urea. *Proc. Natl. Acad. Sci. U. S. A.* **2003**, *100*, 5142–5147, doi:10.1073/pnas.0930122100.

245. Pace, C.N.; Grimsley, G.R.; Scholtz, J.M. Denaturation of Proteins by Urea and Guanidine Hydrochloride. In *Protein Folding Handbook*; Buchner, J., Kiefhaber, T., Eds.; Wiley-VCH Verlag GmbH & Co. KGaA, Weinheim, 2005; Vol. 1, pp. 45–69 ISBN 3-527-30784-2.

246. Curnow, P.; Booth, P.J. Combined Kinetic and Thermodynamic Analysis of α-Helical Membrane Protein Unfolding. *Proc. Natl. Acad. Sci. U. S. A.* **2007**, *104*, 18970–18975, doi:10.1073/pnas.0705067104.

247. Fisher, L.E.; Engelman, D.M.; Sturgis, J.N. Effect of Detergents on the Association of the Glycophorin A Transmembrane Helix. *Biophys. J.* **2003**, *85*, 3097–3105, doi:10.1016/S0006-3495(03)74728-6.

248. Mattice, W.L.; Riser, J.M.; Clark, D.S. Conformational Properties of the Complexes Formed by Proteins and Sodium Dodecyl Sulfate. *Biochemistry* **1976**, *15*, 4264–4272, doi:10.1021/bi00664a020.

249. Di Bartolo, N.D.; Booth, P.J. Unravelling the Folding and Stability of an ABC (ATP-Binding Cassette) Transporter. *Biochem Soc Trans* **2011**, *39*, 751–760, doi:10.1042/BST0390751.

250. Rumfeldt, J.A.O.; Galvagnion, C.; Vassall, K.A.; Meiering, E.M. Conformational Stability and Folding Mechanisms of Dimeric Proteins. *Prog. Biophys. Mol. Biol.* **2008**, *98*, 61–84, doi:10.1016/j.pbiomolbio.2008.05.004.

251. Van Veen, H.W.; Konings, W.N. Multidrug Transporters from Bacteria to Man:

Similarities in Structure and Function. *Semin. Cancer Biol.* **1997**, *8*, 183–191, doi:10.1006/scbi.1997.0064.

252. Eftink, M.R. The Use of Fluorescence Methods to Monitor Unfolding Transitions in Proteins. *Biophys. J.* **1994**, *66*, 482–501, doi:10.1016/S0006-3495(94)80799-4.

253. Roman, E.A.; Flecha, F.L.G. Kinetics and Thermodynamics of Membrane Protein Folding. *Biomolecules* **2014**, *4*, 354–373, doi:10.3390/biom4010354.

254. Timasheff, S.N.; Xie, G. Preferential Interactions of Urea with Lysozyme and Their Linkage to Protein Denaturation. *Biophys. Chem.* **2003**, *105*, 421–448, doi:10.1016/S0301-4622(03)00106-6.

255. Vivian, J.T.; Callis, P.R. Mechanisms of Tryptophan Fluorescence Shifts in Proteins. *Biophys. J.* **2001**, *80*, 2093–2109, doi:10.1016/S0006-3495(01)76183-8.

256. Lijnzaad, P.; Argos, P. Hydrophobic Patches on Protein Subunit Interfaces: Characteristics and Prediction. *Proteins Struct. Funct. Genet.* **1997**, *28*, 333–343, doi:10.1002/(SICI)1097-0134(199707)28:3<333::AID-PROT4>3.0.CO;2-D.

257. Gottlieb, H.E.; Kotlyar, V.; Nudelman, A. NRM Chemicals Shifts of Common Laboratory Solvents as Traces Imputities. *J. org. Chem* **1997**, *62*, 7512–7515, doi:10.1021/JO971176V.

258. Murray, A.T.; Matton, P.; Fairhurst, N.W.G.; John, M.P.; Carbery, D.R. Biomimetic Flavin-Catalyzed Aldehyde Oxidation. *Org. Lett.* **2012**, *14*, 3656–3659, doi:10.1021/ol301496m.

7 Abbreviations

λ	Wavelength
<λ>	Average emission wavelength
°C	Degree Celsius
Å	Ångström
ABC	ATP-binding cassette
ADP	Adenosine diphosphate
Ala/A	Alanine
approx.	Approximately
Arg/R	Arginine
Asn/N	Asparagine
Asp/D	Aspartic acid
ATP	Adenosine triphosphate
B. subtilis	*Bacillus subtilis*
BmrA	*Bacillus* multidrug resistance ATP
cal	Calculated
CH	Coupling helix
Cys/C	Cysteine
Da	Dalton
DDM	n-dodecyl-β-D-maltoside
DMPC	1,2-dimyristoyl-sn- glycero-3-phosphocholin
DNA	Deoxyribonucleic acid
dNTP	Deoxynucleoside triphosphate
DTT	Dithiothreitol
E. coli	*Escherichia coli*
e.g.	Lat. exempli gratia
Gln/Q	Glutamine
Glu/E	Glutamic acid
Gly/G	Glycine
h	Hour
Hoechst 33342	2'-[4-ethoxyphenyl]-5-[4-methyl-1-piperazinyl]-2,5'-bis-1H-benzimidazole
i.e.	Lat. id est
IF	Inward-facing
kDa	Kilo Dalton
LDH	Lactate dehydrogenase
Leu/L	Leucine
Lys/K	Lysine
M	Molarity / Marker
MDR	Multidrug resistance
Met/M	Methionine
min	Minute
n	Number of samples
NADH	β-nicotinamide adenine dinucleotide
NBD	Nucleotide-binding site

NBS	Nucleotide-binding domain
OD	Optical density
OF	Outward-facing conformation
PCR	Polymerase chain reaction
PDB	Protein data bank
P-gp	P-glycoprotein
Phe/F	Phenylalanine
Pi	inorganic phosphate
PK	Pyruvate kinase
Pro	Proline
PSI	Pound-force per square inch
rel	Relative
rpm	Revolutions per minute
s	Seconds
SD	Standard derivation
SDS	Sodium dodecyl sulfate
PAGE	Polyacrylamide gel electrophoresis
SEM	Standard error of the mean
Ser/S	Serine
Thr/T	Threonine
TM	Transmembrane
TMD	Transmembrane domain
Trp/W	Tryptophan
Tyr/Y	Tyrosine
Val/V	Valine
wt	Wild type
χ_{SDS}	SDS mole fraction

8 List of Figures

9 List of Tables

10 Author affiliations

11 Appendix

11.1 Plasmid

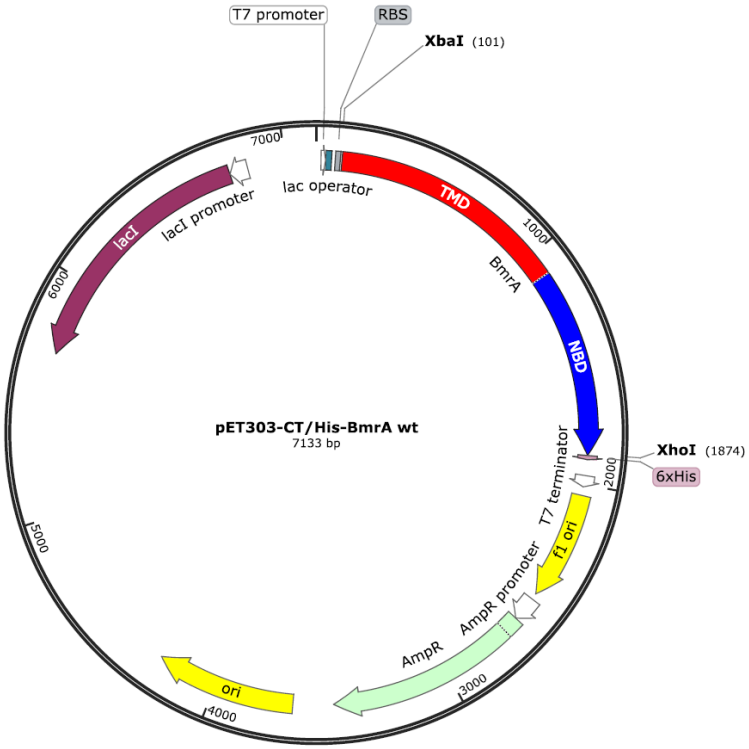

Figure 26: pET303-CT/His BmrA wt plasmid. This plasmid contains an ampicillin resistance (AmpR, green). The area coding for BmrA was separated in TMD (red) and NBD (blue). BmrA was inserted into the plasmid using the enzymes XbaI and XhoI. The plasmid map was created using SnapGene Viewer (SnapGene software (from Insightful Science; available at snapgene.com; version 6.0.2)

11.2 Methods

11.2.1 Screening for BmrA inhibitors using fungal extracts and isolation of myristic acid from IBWF 030-11

This method was performed by [redacted] and [redacted]. This is an unmodified "Methods" section published in the article "Myristic acid inhibits the activity of the bacterial ABC transporter BmrA". The article can be found in chapter 11.3.

448 fungal extracts dissolved in DMSO were tested in 384 well plate format in accordance to assay methodology described in 3.4.1 at a concentration of 0.5 mg/mL in initial screens. NADH decrease was monitored with a multilabel reader (Perkin Elmer Envision 2104). Among the active extracts was one isolated from the mycelium of strain IBWF 030-11 (*Clavicipitaceae*). This strain is deposited in the strain collection at the *Institut für Biotechnologie und Wirkstoff-*

Forschung (IBWF), Mainz. The active principle was identified by subfractionation of the initial extract and retesting whereby the activity was tracked to a natural product which was unknown to the IBWF compound library. To isolate the active principle for structure elucidation and natural product characterization, strain IBWF 030-11 was regrown and cultivated in a 20 L fermenter in YMG medium (YMG: 4 g yeast extract, 10 g malt extract, 10 g glucose, pH was adjusted to 5.5 before autoclaving). For inoculation a well-grown flask culture in the same medium was used. The mycelium was separated from the culture by filtration 16 days after inoculation, freeze-dried (dry weight 122 g) and subsequently extracted with MeOH to yield 24 g crude extract. Flash chromatography on silica gel 60 (0.04–0.063 mm; Macherey-Nagel) yielded a subfraction (750 mg) which was applied to a second silica gel fractionation to yield intermediate 1 (628 mg). Preparative HPLC (PrepHT Zorbax Eclipse XDB-Phenyl, 5 µm, 21 x 250 mm, Agilent Technologies, MeCN: 0.1% TFA in H_2O gradient from 50% MeCN to 70% MeCN in 20 min, 21 mL/min) of intermediate 1 yielded 5 mg of the active substance (myristic acid (RT 11.5 min)). The purity of the active substance was checked with mass spectrometry.

11.2.2 NMR analysis

This method was performed by [redacted]. This is an unmodified "Methods" section published in the article "Myristic acid inhibits the activity of the bacterial ABC transporter BmrA". The article can be found in chapter 11.3.

Myristic acid was identified by ^{1}H, ^{13}C, COSY, HSQC, and HMBC NMR using a Bruker Avance III 600 MHz spectrometer, equipped with an inverse Helium-cooled cryoprobe. All shifts are given relative to TMS, using the residual $CHCl_3$ shift as reference (7.26 ppm) [257].

^{1}H NMR (600 MHz, $CDCl_3$) δ = 2.36 (t, J = 7.5 Hz, 2H, H-2), 1.63 (pseudo quin, J = 7.5 Hz, 2H, H-3), 1.44–1.19 (m, 20H, H-4 to H-13), 0.88 (dist. t, J = 6.9 Hz, 3H, H-14) ppm. ^{13}C NMR (151 MHz, $CDCl_3$) δ = 176.6* (C-1, by HMBC), 33.4 (C-2), 31.9 (C-12), 29.8–29.0 (C-4 to C-11), 24.7 (C-3), 22.7 (C-13), 14.2 (C-14) ppm. Shifts are in accordance with literature [258].

11.3 Published article

Myristic Acid Inhibits the Activity of the Bacterial ABC Transporter BmrA

Kristin Oepen[1], Hüseyin Özbek[2], Anja Schüffler[2], Johannes C. Liermann[1], Eckhard Thines[2,3] and Dirk Schneider[1,3,*]

[1] Department of Chemistry, Johannes Gutenberg-University, 55128 Mainz, Germany; khackme@uni-mainz.de (K.O.); liermann@uni-mainz.de (J.C.L.)

[2] Institut für Biotechnologie und Wirkstoff-Forschung gGmbH (IBWF), 55128 Mainz, Germany; Hozbek@tutanota.com (H.Ö.); schueffler@ibwf.de (A.S.); thines@uni-mainz.de (E.T.)

[3] Institute of Molecular Physiology, Johannes Gutenberg-University, 55128 Mainz, Germany

[*] **Correspondence**: Dirk.Schneider@uni-mainz.de; Tel.: +49-6131-39-25833

Received: 8 November 2021, **Accepted:** 14 December 2021, **Published:** 17 December 2021

Academic Editor(s): Stathis Frillingos and Maria Botou

Keywords: ABC transporter; BmrA; membrane transport; myristic acid; inhibitor

Abstract: ATP-binding cassette (ABC) transporters are conserved in all kingdoms of life, where they transport substrates against a concentration gradient across membranes. Some ABC transporters are known to cause multidrug resistances in humans and are able to transport chemotherapeutics across cellular membranes. Similarly, BmrA, the ABC transporter of *Bacillus subtilis*, is involved in excretion of certain antibiotics out of bacterial cells. Screening

of extract libraries isolated from fungi revealed that the C14 fatty acid myristic acid has an inhibitory effect on the BmrA ATPase as well as the transport activity. Thus, a natural membrane constituent inhibits the BmrA activity, a finding with physiological consequences as to the activity and regulation of ABC transporter activities in biological membranes.

1. Introduction

Membrane integral transport proteins mediate and control the translocation of essential compounds across biological membranes, involving the uptake and efflux of sugars, inorganic ions, nucleotides or drugs [1]. Primary active transporters use the energy gained via ATP hydrolysis for transport [1,2], and such transport ATPases are typically represented by ion pumps and ATP-binding cassette (ABC) transporters [2]. ABC transporters can be found in all kingdoms of life and they either import or export substrates against a concentration gradient. While, in bacteria, ABC importers and exporters can be found, eukaryotes mainly contain exporters [1,3]. Structurally, all ABC transporters consist of two nucleotide binding domains (NBDs) and two transmembrane domains (TMDs). The TMDs consist of α-helix bundles that mediate the actual TM flux of the substrates, whereas ATP is hydrolyzed in the NBDs [3–5]. In contrast to the NBD, the sequences of the TMDs are typically less conserved and the TM topology can vary. The four domains of an ABC transporter can be part of a single polypeptide chain, or the transporter assembles from two to four individual subunits [5,6]. One TMD and one NBD can be fused to form a so-called half-transporter, which can either form a homodimeric (identical half-transporters) or assemble as a heterodimeric (different half-transporters) full-transporter [1,3,7,8].

Many ABC transporters appear to be involved in bacterial multidrug resistances [9]. For example, in cervimycin C resistant *Bacillus subtilis* colonies the *bmrA* gene, encoding an ABC half-transporter, was strongly overexpressed, which led to the assumption that BmrA (Bacillus multidrug-resistance ATP) is able to effectively transport this antibiotic out of the cell [10,11]. Besides cervimycin C, BmrA can transport a broad range of substrates, which include Hoechst 33342, doxorubicin as well as 7-aminoactinomycin D [11].

BmrA, a homodimeric ABC transporter with a molecular mass of 64.9 kDa, is homologous to the bacterial ABC transporters LmrA and MsbA [6,12] as well as to the human P-glycoprotein [3,11]. In recent years, BmrA became a paradigm for studying ABC transporters, mostly due to the vast number of seemingly unrelated substrates as well as its homology to the human P-glycoprotein [11–13].

As BmrA is involved in excretion of certain antibiotics out of bacterial cells, we aimed at identifying small molecules which inhibit the BmrA transport activity and thus might be used to modulate the BmrA transport activity. Screening of extract libraries isolated from fungi revealed that the C14 fatty acid myristic acid has an inhibitory effect on the BmrA ATPase as well as the transport activity. Thus, BmrA "sleeps with the enemy", as a natural membrane constituent inhibits its activity, a finding with physiological consequences as to the activity and regulation of ABC transporter activities in biological membranes.

2. Results

2.1. Myristic Acid Inhibits the ATPase Activity of the ABC Transporter BmrA

In total, 448 fungal extracts were tested for an inhibitory effect on the BmrA ATPase activity and 22 were found to be active. One of the most promising candidates, the mycelial extract of strain IBWF 030-11, was selected for further characterization. To identify the natural product responsible for the inhibitory effect, the fungus was cultivated in a 20 L scale and the active principle was isolated. Based on NMR analysis, the isolated substance was identified as the C14 fatty acid myristic acid (Figure 1a), 0.25 mg of which was isolated per L axenic fungus culture.

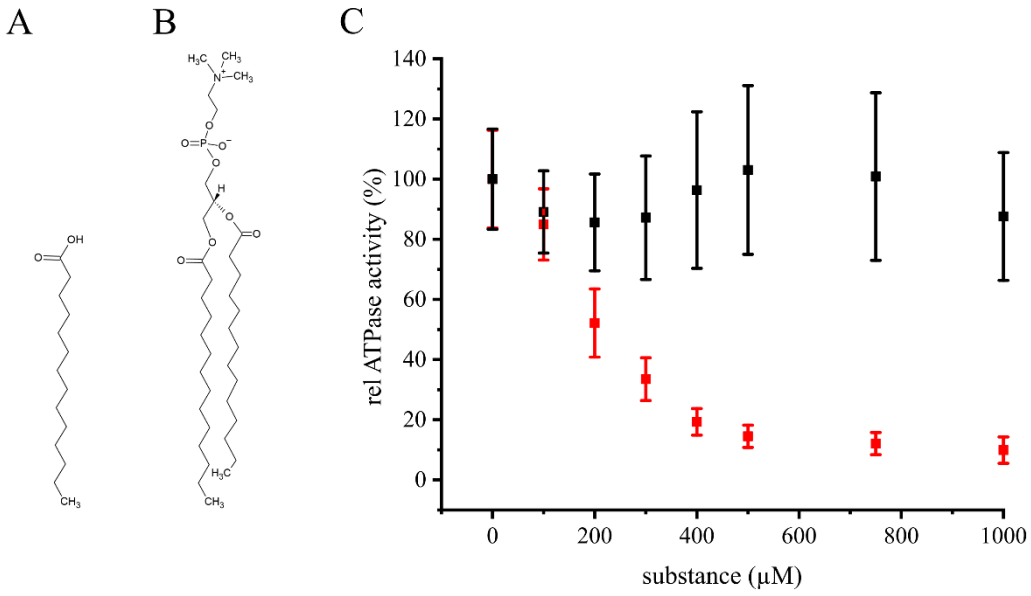

Figure 1. Inhibition of the BmrA ATPase activity by myristic acid. (a) Structure of the fatty acid myristic acid ($C_{14}H_{28}O_2$). (b) Structure of 1,2-dimyristoyl-sn-glycero-3-phosphocholine (DMPC), a membrane phospholipid containing two myristic acids as fatty acids. The structures were created using ChemSketch [14]. (c): Myristic acid ($n \geq 6$, ± SEM; red) inhibits the in vitro ATPase activity of detergent solubilized BmrA, whereas the lipid 1,2-dimyristoyl-sn-glycero-3-phosphocholin (DMPC, $n = 12$, ± SEM; black) does not.

To quantitatively evaluate the inhibitory potential of myristic acid, we next examined the in vitro ATPase activity of BmrA at increasing myristic acid concentrations (Figure 1c, red). The BmrA ATPase activity was determined in buffer containing myristic acid concentrations ranging from 0 to 1000 µM to calculate the IC_{50} value, i.e., the substance concentration required to inhibit 50% of the protein's ATPase activity. The ATPase activity of BmrA in pure 5 mM DDM was 1.0 ± 0.16 µmol/min per mg protein, a value comparable to values previously determined under slightly different experimental conditions [15,16]. As expected in the presence of an inhibitor, the ATPase activity constantly decreased with increasing myristic acid concentrations, until at ~500 µM myristic acid the activity levelled off to about 12%. Based on this analysis, the turning point, i.e., the IC_{50}, is at approximately 200 µM myristic acid. Furthermore, these results additionally indicate that myristic acid is not a BmrA substrate that stimulates the ATPase activity, as has been observed with other ABC transporter substrates [17–19].

Nevertheless, the concentration for free myristic acid within the membrane is low *in vivo*, as myristic acid typically is part of diacylglycerol lipids. This now raised the question whether the ATPase activity of BmrA is also affected by myristic acid-containing phospholipids. Thus, we next tested the in vitro ATPase activity of isolated BmrA in the presence of increasing concentrations of 1,2-dimyristoyl-sn-glycero-3-phosphocholine (DMPC, Figure 1b,c black). DMPC is a glycerophospholipid, containing two myristic acids as fatty acids attached to the glycerol backbone. As the determined ATPase activity of BmrA is not significantly affected by DMPC, the inhibitory effects observed before can clearly be linked to the isolated myristic acid.

2.2. The Stability of BmrA in Micelles Is Not Affected by Myristic Acid

Myristic acid has detergent properties and can form micelles in solution [20]. As harsh detergents can unfold (membrane) proteins [21], at least to some extent, the question arose whether myristic acid does not inhibit the BmrA ATPase activity via binding but via denaturation of the protein structure, resulting in a diminished protein activity.

As changes in a local tryptophan environment, e.g., caused by protein denaturation, result in a different fluorescence emission spectrum, the stability of purified BmrA in DDM micelles can be determined by fluorescence spectroscopy. A well-established approach to unfold membrane proteins is to solubilize the protein in a mild detergent, such as DDM, and to subsequently titrate in increasing amounts of a harsh detergent, typically SDS [22,23]. Addition of SDS results in formation of mixed DDM/SDS micelles, which eventually unfold α-helical membrane proteins. It is noteworthy that, while the mixed micelles can indeed unfold soluble regions or domains of

membrane proteins, the membrane integral protein parts typically retain their helical structure, and the term “unfolding” here in fact describes the separation of previously interacting individual TM α-helices [24].

When the purified protein was exposed to increasing SDS concentrations, the average emission wavelength (<λ>) decreased (Figure 2, black). At a low SDS mole fraction of χSDS = 0.04 the <λ> slightly increased, a behavior also observed with other TM proteins [25], whereas higher SDS concentrations led to a dramatic decrease in the average emission wavelength. In contrast, while addition of low myristic acid concentration also resulted in a slight increase in the <λ>, further increasing the myristic acid concentration resulted in a slightly decrease, albeit the <λ> myristic acid never changed to an extent as observed with SDS. This indicates that myristic acid does not substantially destabilize the protein, in contrast to SDS.

2.3. Myristic Acid Inhibits the BmrA-Mediated Transport of Hoechst 33342 in Inverted Membrane Vesicles

Hoechst 33342 is a substrate commonly used when the BmrA activity is studied in inverted membrane vesicles. Upon spontaneous membrane partitioning, the dye’s fluorescence increases. When the dye is actively transported out of the lipid membrane by BmrA and expelled to the liquid surrounding, the fluorescence decreases again. Importantly, the transport of Hoechst 33342 depends on the BmrA ATPase activity [11].

At first, the initial fluorescence of the inverted membrane vesicles was monitored in absence of Hoechst 33342 (Figure 3a). Subsequently, upon addition (Figure 3a, 1) and membrane incorporation of Hoechst 33342, the fluorescence increased tremendously due to membrane partitioning of the dye [26]. After addition of ATP the fluorescence intensity decreased again due to the removal of Hoechst 33342 from the membrane. The decrease in the fluorescence intensity thus directly correlates with the BmrA transport activity [26]. When the BmrA-mediated Hoechst 33342 transport was measured in inverted membrane vesicles pre-incubated with myristic acid, the initial fluorescence intensities were similar. Upon ATP addition (Figure 3a, 2), the fluorescence intensity first decreased, as observed in absence of myristic acid, yet remained on a higher fluorescence level. This implies that more Hoechst 33342 molecules remained incorporated within the lipid bilayer, and thus, less Hoechst 33342 molecules were transported by the ABC transporter (Figure 3a, red). For comparison, the absolute value of the slope was used to quantify the transport activity. The BmrA wild type transport activity was set as 100% and the generated values at increasing myristic acid concentrations were normalized to the wild type (Figure 3b).

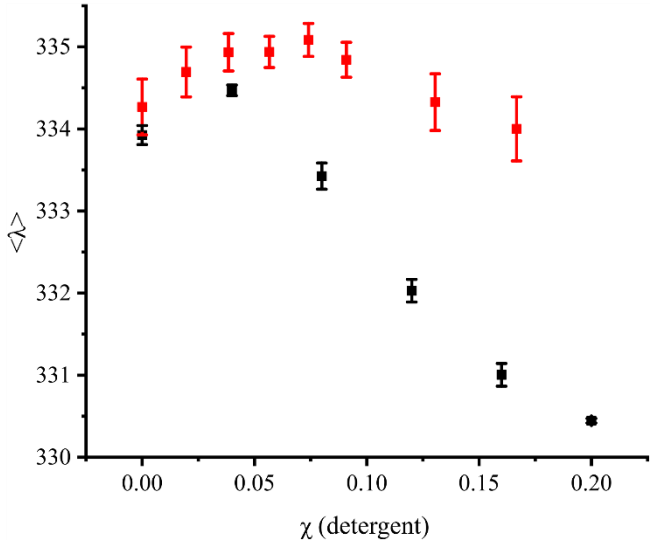

Figure 2. Myristic acid does not destabilize the BmrA structure as SDS. Increasing amounts of myristic acid (n = 9, ± SEM; red) or SDS (n = 7, ± SEM black) were titrated to BmrA solubilized in DDM micelles. While addition of SDS leads to a larger decrease in the average emission wavelength (<λ>), this was not observed when myristic acid was added.

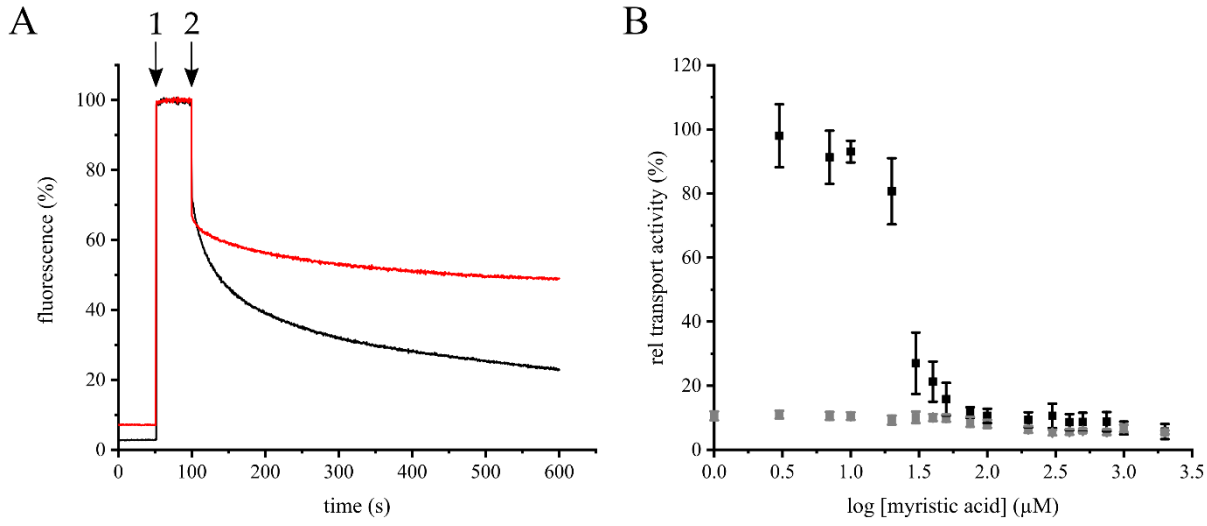

Figure 3. Myristic acid inhibits Hoechst 33342 transport in inverted C41(DE3) *E. coli* membrane vesicles. (a) Kinetics of Hoechst 33342 transport followed in absence (black) or presence of 1000 µM myristic acid (red), 1: addition of Hoechst 33342, 2: addition of ATP. (b) 3–1000 µM myristic acid was added to inverted membrane vesicles prepared from BmrA expressing cells (black) or *E. coli* C41(DE3) cells transformed with an empty vector (grey) and Hoechst 33342 transport was quantified (n = 3, ± SEM).

To test a (potential) inhibition of the BmrA transport activity, myristic acid was added to inverted membrane vesicles at increasing concentrations (3–1000 µM) and the Hoechst 33342 transport was quantified (Figure 3b). The BmrA transport activity was essentially not affected

up to myristic acid concentrations of 10 µM. However, at 20–50 µM myristic acid, the transport activity of BmrA massively decreased, and at around 100 µM myristic acid a plateau was reached. Based on a Boltzmann fit, an IC_{50} value of about 25 µM myristic acid was determined for the Hoechst transport using inverted vesicles. As expected, the inverted vesicles prepared from *E. coli* C41(DE3) cells transformed with an empty vector did not show activity at any given myristic acid concentration.

Yet, myristic acid might not inhibit the BmrA transport activity, but in fact is a substrate that simply competes with Hoechst 33342 for transport. To test this assumption, inverted vesicles were first exposed to 0.2 mM myristic acid, and the Hoechst 33342 transport was measured as before, but at different Hoechst 33342 concentrations. Upon addition of ATP, the absolute value of the slope of the fluorescence decrease was determined at each Hoechst 33342 concentration (Figure 4). When Hoechst 33342 and myristic acid compete for transport, addition of small amounts of Hoechst 33342 should not result in a measurable transport activity, and only at rather high Hoechst 33342 concentrations is an activity expected to be observed. As can be seen in Figure 4, the absolute value of the slope increased linearly with increasing Hoechst 33342 concentrations for the control (no myristic acid). In contrast, the activity of the inverted vesicles containing a constant myristic acid concentration but increasing Hoechst 33342 concentrations increased linearly up to a concentration of ~0.6 µM Hoechst 33342. At higher Hoechst 33342 concentrations, the initial slope remained more or less constant. If Hoechst 33342 and myristic acid were both substrates competing for binding and translocation, an initial significantly slowed down Hoechst 33342 transport would be expected at the (high) constant myristic acid concentration. However, this was not observed. Instead, the transport activity leveled off at a rather low Hoechst concentration. Consequently, the data indicate that there is no simple competitive or non- or uncompetitive inhibition of BmrA by myristic acid. The BmrA activity is inhibited by myristic acid via a rather complex mechanism. Noteworthy, the fluorescence intensities (without ATP added) of the control and the myristic acid-incubated inverted vesicles were more or less equal for each Hoechst 33342 concentration. The increasing amounts of Hoechst 33342 lead to a linearly increasing slope (data not shown).

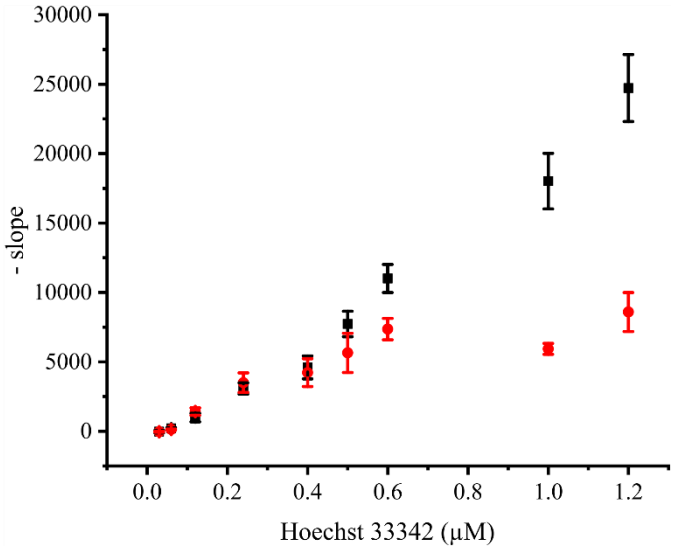

Figure 4. BmrA-mediated Hoechst 33342 transport at a constant myristic acid concentration. 0.2 mM myristic acid (red) or methanol (control; black) were added to inverted membrane vesicles and Hoechst 33342 transport was tested at increasing Hoechst 33342 concentrations (n = 3, ± SEM).

2.4. Myristic Acid Does Not Solubilize Overexpressed BmrA in Inverted Vesicles

Due to the detergent properties of myristic acid, it was possible that the fatty acid solubilized the overexpressed protein in the inverted vesicles, resulting in the observed decreased BmrA transport activity. To finally exclude this, vesicles were incubated with the detergent SDS or myristic acid for 1 h. Subsequently, solubilized protein was separated from membranes via ultracentrifugation, and solubilized proteins were analyzed via SDS PAGE. As can be seen in Figure 5, while BmrA was properly solubilized by SDS, neither at low nor at high myristic acid concentrations BmrA was extracted from the membranes. Thus, the inverted vesicles remained intact at the here analyzed myristic acid concentrations.

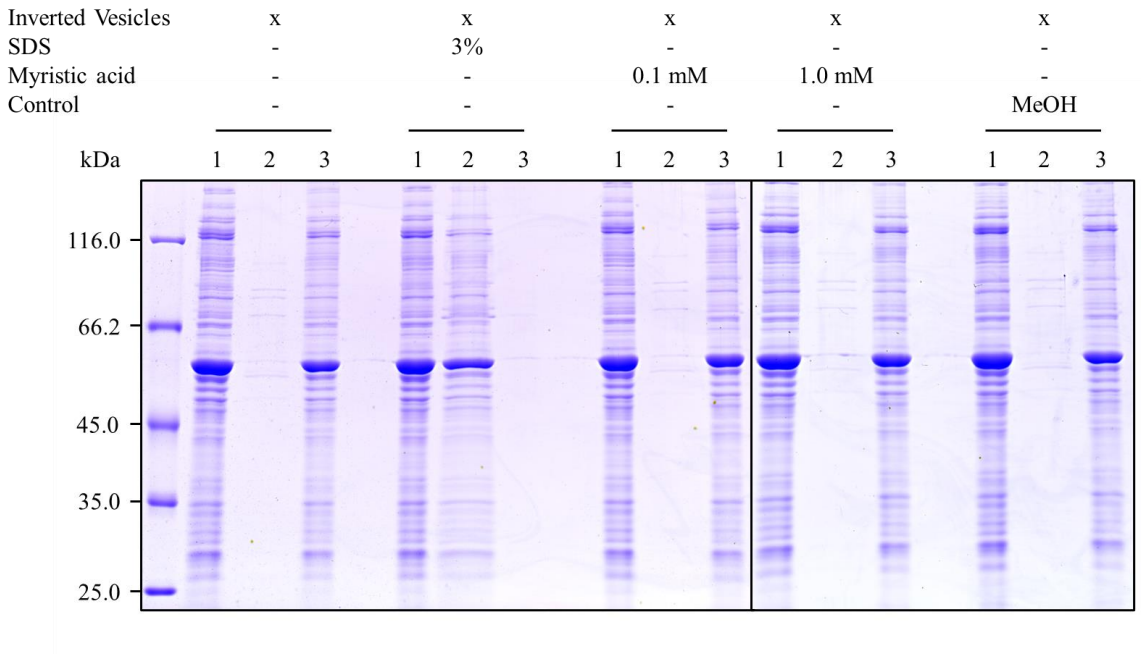

Figure 5. Stability of inverted membrane vesicles with overexpressed BmrA. Inverted vesicles were exposed to either SDS (3% (*w/v*), myristic acid (0.1 mM or 1.0 mM dissolved in methanol) or methanol (0.5% (*v/v*). Intact membranes were found in the pellet, whereas solubilized membrane proteins were found in the supernatant (solely when SDS was added). 1: BmrA and membrane proteins in inverted vesicles not influenced by any substances. 2: Supernatant after ultracentrifugation containing solubilized BmrA (and other membrane proteins). 3: Pellet after ultracentrifugation comprising of inverted vesicles with overexpressed BmrA. This experiment was performed three times with three different inverted membrane vesicle preparations, which all showed the same results.

3. Discussion

In the present study, we identified myristic acid as a potential inhibitor of the BmrA ATPase and transport activity. This saturated C14 fatty acid (Figure 1a) is widely distributed in plant and animal fat and can naturally be found in high concentrations in coconut oil as well as in butter fat. Furthermore, myristic acid is utilized in the food industry as multifunctional food additive and flavor excipient [27]. In *Bacillus subtilis*, around 3.6% of all lipids are myristic acid [28]. Yet, myristic acid inhibits the BmrA activity exclusively as a free acid, but not when part of phospholipids (Figure 1c, black). Thus, while 3–4% of all lipids in *Bacillus subtilis* are myristic acid, most of these will be part of di- or even triacylglycerols and thus the concentration of the inhibiting species, i.e., the free acid, will be low.

As we have shown here, myristic acid does neither inhibit the BmrA activity indirectly, via destabilizing membranes and extracting the protein from membranes (Figure 5), nor via detergent-induced denaturation of the protein (Figure 2). Thus, myristic acid appears to directly

inhibit the BmrA ATPase and transport activities (Figures 1c and 3b), albeit the inhibitory mechanism appears to be complex.

It is well known that, e.g., the detergent Triton X-100 stimulates the ATPase activity of the ABC transporter P-glycoprotein [29], and based on this and other observations, it has been concluded that detergents can serve as P-glycoprotein substrates [30]. In many cases, addition of substrate even increases the ATPase activity of ABC transporters, which was, however, not observed here. ABC transporter substrates have rather diverse structures [11], and also fatty acids are transported by ABC transporters [31]. This has been shown for some ABC transporters, such as MsbA or LmrA [32,33]. When the lipid A ABC transporter MsbA was heterologously expressed in *L. lactis* cells, it has been observed that myristic acid might be transported due to no change in the determined IC_{50} value [33]. Yet, based on the results presented here (Figure 4), myristic acid appears not to simply compete with Hoechst 33342 for the substrate binding site and transport.

But why is the determined IC_{50} value so much higher when the ATPase activity was monitored than when the transport activity was monitored? Although we cannot ultimately answer this question, these two measurements can only be compared to some extent. While we have a well-defined protein and detergent concentration when the isolated protein was analyzed, this was not the case in the inverted vesicles. Furthermore, in inverted vesicles we might have other components that interact with myristic acid. Yet, this would probably reduce, and not increase, the inhibitory activity of myristic acid. In bacterial membranes, most membrane lipids are not part of bulk lipids, but are (more or less tightly) bound to membrane proteins (reviewed [34]). Thus, the concentration of myristic acid added to the lipid phase is probably much higher at any given total myristic acid concentration, compared to the situation in micelles. In the latter, the myristic acid will incorporate into free micelles as well as into BmrA-containing micelles to form mixed micelles. Thus, myristic acid is likely highly diluted in the micellar system, which results in a rather high IC_{50} value for the determined ATPase activity. Finally, it is also possible that myristic acid induces a conformational change or decoupling of the NBD and TMD in the lipid environment, as e.g., observed with the mutant BmrA E474R [35].

4. Materials and Methods

4.1. Screening for BmrA Inhibitors using Fungal Extracts and Isolation of Myristic Acid from IBWF 030-11

448 fungal extracts dissolved in DMSO were tested in 384 well plate format in accordance to assay methodology described in 4.6 at a concentration of 0.5 mg/mL in initial screens. NADH decrease was monitored with a multilabel reader (Perkin Elmer Envision 2104). Among the active extracts was one isolated from the mycelium of strain IBWF 030-11 (*Clavicipitaceae*). This strain is deposited in the strain collection at the *Institut für Biotechnologie und Wirkstoff-Forschung* (IBWF), Mainz. The active principle was identified by subfractionation of the initial extract and retesting whereby the activity was tracked to a natural product which was unknown to the IBWF compound library. To isolate the active principle for structure elucidation and natural product characterization, strain IBWF 030-11 was regrown and cultivated in a 20 L fermenter in YMG medium (YMG: 4 g yeast extract, 10 g malt extract, 10 g glucose, pH was adjusted to 5.5 before autoclaving). For inoculation, a well-grown flask culture in the same medium was used. The mycelium was separated from the culture by filtration 16 days after inoculation, freeze-dried (dry weight 122 g) and subsequently extracted with MeOH to yield 24 g crude extract. Flash chromatography on silica gel 60 (0.04–0.063 mm; Macherey-Nagel) yielded a subfraction (750 mg) which was applied to a second silica gel fractionation to yield intermediate 1 (628 mg). Preparative HPLC (PrepHT Zorbax Eclipse XDB-Phenyl, 5 µm, 21 × 250 mm, Agilent Technologies, MeCN: 0.1% TFA in H2O gradient from 50% MeCN to 70%MeCN in 20 min, 21 mL/min) of intermediate 1 yielded 5 mg of the active substance (myristic acid (RT 11.5 min)). The purity of the active substance was checked with mass spectrometry.

4.2. NMR Analysis

Myristic acid was identified by ^{1}H, ^{13}C, COSY, HSQC, and HMBC NMR using a Bruker Avance III 600 MHz spectrometer, equipped with an inverse Helium-cooled cryoprobe. All shifts are given relative to TMS, using the residual $CHCl_3$ shift as reference (7.26 ppm) [36].

^{1}H NMR (600 MHz, $CDCl_3$) δ = 2.36 (t, J = 7.5 Hz, 2H, H-2), 1.63 (pseudo quin, J = 7.5 Hz, 2H, H-3), 1.44–1.19 (m, 20H, H-4 to H-13), 0.88 (dist. t, J = 6.9 Hz, 3H, H-14) ppm. ^{13}C NMR (151 MHz, $CDCl_3$) δ = 176.6* (C-1, by HMBC), 33.4 (C-2), 31.9 (C-12), 29.8–29.0 (C-4 to C-11), 24.7 (C-3), 22.7 (C-13), 14.2 (C-14) ppm. Shifts are in accordance with literature [37].

4.3. Cloning

The *Bacillus subtilis bmrA* gene was amplified via PCR from genomic *B. subtilis* (strain 168) DNA using the following primers:

Forward: 5′ GCTACCTCTAGAATGCCAACCAAGAAACAAAAATCTAAAAG 3′ and reverse: 5′ GCTATTCTCGAGCCCGGCTTTGTTTTCTAAG 3′.

The PCR product was cloned into the plasmid pET303-CT/His (Invitrogen, Carlsbad, CA, USA), whereby the 3′ end was extended by a sequence coding for a short linker and a His6-tag.

4.4. Expression

The pET303-CT/His-BmrA plasmid was transformed in competent BL21(DE3) pLysE *E. coli* cells, and cells were subsequently plated on LB agar containing 100 µg/mL ampicillin. A single colony was used to inoculate an overnight culture, which was used the next morning to inoculate a 2 L culture, containing 100 µg/mL ampicillin and 30 µg/mL chloramphenicol. The cells were cultivated at 37 °C with constant agitation (150 rpm). When the culture reached an OD_{600} of ~0.8, protein expression was induced via addition of isopropyl-β-D-thiogalacto-pyranoside (IPTG) to a final concentration of 0.5 mM. Cells were harvested after 3–4 h via centrifugation (3050× g, 10 min at 4 °C). The cell pellets then were stored at −20 °C.

4.5. Purification

The cell pellets were resuspended in 50 mM phosphate buffer (pH 8.0), 300 mM NaCl, 10% glycerol (*v/v*) and lysed using a microfluidizer (LM20, Microfluidics, Westwood, CA, USA, 18000 PSi). After centrifuging at 12,075× g (10 min at 4 °C), the supernatant was centrifuged again at 165,000× g for 1 h at 4 °C to isolate membranes. The membranes were solubilized in solubilization buffer (50 mM phosphate buffer (pH 8.0), 300 mM NaCl, 10% glycerol (*v/v*) with 1% n-dodecyl-β-D-maltoside (DDM) (*w/v*)) to extract the membrane-incorporated proteins. After 1 h of incubation, insolubilized protein was removed by centrifugation (165,000 x g, 20 min) and the equilibrated Protino® Ni-NTA agarose (2 mL resin/L of *E. coli* culture; Macherey-Nagel GmbH & Co. KG, Düren, Germany) was mixed with the solubilized proteins and incubated for 1 h. After washing the Ni-NTA agarose with 20 mL washing buffer (50 mM phosphate buffer (pH 8.0), 300 mM NaCl, 10% glycerol (*v/v*) with 0.1% DDM (*w/v*) and 40 mM imidazole), the protein was eluted with 5 mL elution buffer (50 mM phosphate buffer (pH 8.0), 300 mM NaCl, 10% glycerol (*v/v*) with 0.1% DDM (*w/v*) and 400 mM imidazole). To exchange the buffer to the required assay buffer (containing 5 mM DDM), a

PD-10 desalting column (Macherey-Nagel GmbH & Co. KG, Düren, Germany) was utilized. The concentration of the purified membrane protein BmrA was determined photometrically by measuring the absorbance at 280 nm and the calculated extinction coefficient ε = 38850 M^{-1} cm^{-1}.

4.6. ATPase Activity of Purified BmrA

The ATPase activity of 0.2 µM protein BmrA was measured in DDM micelles at 25 °C in 50 mM Hepes-KOH (pH 8.0 and 5 mM DDM) with 3.5 mM ATP, 10 mM $MgCl_2$, 0.28 mM NADH, 2 mM phosphoenolpyruvate, by adding 2 µL of pyruvate kinase (600–1000 U/mL)/lactate dehydrogenase (900–1400 U/mL) mix to the 200 µL test volume. Absorption changes were measured at a wavelength of 340 nm and a slit width of 4 nm using a Lambda 35 UV/Vis spectrophotometer (PerkinElmer, Inc., Waltham, MA, USA). Here the usage of NADH was monitored. The NADH decrease was measured for 180 sec and converted into the BmrA activity in min^{-1}.

$$ATPase\ activity = -\frac{\Delta A_{340}}{\Delta t} \cdot \frac{1}{l \cdot \varepsilon_{NADH}} \cdot MW_{BmrA} \cdot \frac{1}{c_{BmrA}} \quad (1)$$

Equation (1) comprises of the slope ($\frac{\Delta A_{340}}{\Delta t}$) of the NADH decrease, the optical pathlength (l in cm), the extinction coefficient of NADH (ε_{NADH} = 6220 $M^{-1}cm^{-1}$) as well as of the calculated molecular weight of BmrA (65584.27 g/mol) and the used BmrA concentration (c_{BmrA} in g/L). The ATPase activity without substance was set as 100% and the data points measured at different myristic acid and DMPC concentrations were normalized to this level with respect to the error propagation.

For the experiments (except for the screening and NMR), commercially available myristic acid (Sigma-Aldrich, Merck KGaA, Darmstadt, Germany, M3128) with a high purity (≥99%) was used. Myristic acid (dissolved in methanol) or 1,2-dimyristoyl-sn-glycero-3-phosphocholin (DMPC; solved in chloroform) was pipetted at the specified amounts into the reaction tubes. Subsequently, the solvent was removed by a constant stream of nitrogen, and these reaction tubes were further stored for at least 30 min under vacuum. The dried fatty acid was dissolved in sample buffer (50 mM Hepes-KOH, pH 8.0, 5 mM DDM) and the solution was vortexed and further incubated for at least 1 h under constant agitation (500 rpm). Thereafter, the protein was added, and the solution incubated for another 10 min at 25 °C. After adding the other compounds to the solution, the decrease in absorbance was immediately monitored.

4.7. Hoechst 33342 Transport Measured Using BmrA-Containing Inverted E. coli Membrane Vesicles

Inverted *E. coli* membrane vesicles were prepared as described in Steinfels et al., 2002 [38], except that a microfluidizer was used at 18000 Psi instead of a French press.

The membrane protein concentration was determined with a BCA assay (PierceTM BCA protein assay kit, Thermo Fisher Scientific, Rockford, IL, USA), following the vendor´s instructions. In all, 50 µg of inverted membrane vesicles were dissolved in a final volume of 200 µL of 50 mM Hepes-KOH (pH 8.0), 2 mM $MgCl_2$, 8.5 mM NaCl, 4 mM phosphoenolpyruvate and 20 µg/mL pyruvate kinase. Myristic acid (dissolved in methanol) was added to the reaction mixture at various concentrations (3 µM, 7 µM, 10 µM, 20 µM, 30 µM, 40 µM, 50 µM, 75 µM, 100 µM, 200 µM, 300 µM, 400 µM, 500 µM, 750 µM, 1000 µM) and following incubation for more than 10 min. The maximal concentration of methanol in this reaction mixture was 0.5% (*v/v*). Fluorescence emission was measured at 457 nm using a FluoroMax-4 fluorometer (Horiba Instruments Inc., Edison, NY, USA) upon excitation at 355 nm, with excitation and emission slit widths of 2 nm and 3 nm, respectively. After monitoring the fluorescence for approximately 50 s, the measurement was stopped. Then, 2 µM 2′-[4-ethoxyphenyl]-5-[4-methyl-1-piperazinyl]-2,5′-bis-1H-benzimidazole (Hoechst 33342) was added and the fluorescence was measured again for approximately 50 s. Then, ATP was added to a final concentration of 2 mM and the fluorescence was further monitored for ~500 s. Data points were collected every 0.5 s. The slope of the measured fluorescence intensity (after addition of ATP) was determined by fitting a linear regression line with a large coefficient of determination. Then the absolute value of the slope of the sample containing inverted membrane vesicles with overexpressed BmrA (50 µg) plus methanol (0.5% (*v/v*)) was set as "100% transport activity" and the data points measured at different myristic acid concentrations were normalized to this considering error propagation. All presented data are based on three independent inverted vesicle preparations, and the mean with corresponding SEM is shown.

For the competition assay, inverted membrane vesicles containing 50 µg protein were incubated with 0.2 mM myristic acid for at least 10 min at 25 °C. The fluorescence signal was measured as described (exception: slit width of 3 nm). When the measurement was started, the fluorescence was monitored for 50 s. Varying concentrations of Hoechst 33342 were added (0.03 µM, 0.06 µM, 0.12 µM, 0.24 µM, 0.3 µM, 0.4 µM, 0.5 µM, 0.6 µM, 1.0 µM, 1.2 µM) and the measurement and data evaluation continued as described before.

4.8. Destabilization of BmrA in DDM Micelles

Purified BmrA (2 µM) in 50 mM phosphate buffer (pH 8.0), 300 mM NaCl, 10% glycerol (*v/v*), 5 mM DDM was mixed with increasing amounts of sodium dodecyl sulfate (SDS; concentrations: 0 mM, 0.21 mM, 0.43 mM, 0.68 mM, 0.95 mM, 1.25 mM) or myristic acid (concentrations: 0 mM, 0.1 mM, 0.2 mM, 0.3 mM, 0.4 mM, 0.5 mM, 0.75 mM, 1.0 mM). The samples were incubated at room temperature for 1 h. Fluorescence spectra were recorded (from 290–450 nm) using a FluoroMax-4 fluorometer with 280 nm excitation and a slit width of 3 nm. The average emission wavelength (<λ>), which represents changes in shape and position of the spectrum, was used to characterize the entire measured tryptophan fluorescence emission spectrum. The <λ> was calculated as described in the following Equation (2):

$$< \lambda >= \frac{(\Sigma_i \lambda_i \cdot I_i)}{\Sigma_i I_i} \quad (2)$$

Here λ is the wavelength in nm and I is the fluorescence intensity.

4.9. Stability of BmrA in Inverted Vesicles

Inverted vesicles (250 µg/mL) were incubated with either 0.1 mM or 1.0 mM myristic acid for 1 h at room temperature at constant agitation. As a control, 0.5% (*v/v*) methanol was added to inverted vesicles. As a second control, vesicles were incubated with 3% SDS (*w/v*). After incubation, the samples were centrifuged at 140,000× g for 1 h at 25 °C. Samples were taken before incubation with the substances and after centrifugation (from the supernatant as well as the pellet). A total of 10 µL of each sample was analyzed on a 10% SDS PAGE gel.

5. Conclusions and Implications

At first, inhibition of an ABC transporter activity by a naturally occurring fatty acid appears to be unexpected, albeit the physiological concentration of myristic acid in *Bacillus subtilis* membranes is probably not sufficiently high to compromise the BmrA transport activity. However, it might even be beneficial to inhibit a basal ATPase activity, by which ATP might be wasted in cells, *in vivo* using naturally occurring membrane incorporated substances, such as myristic acid.

The initial idea of this project was to identify potential modulators of the BmrA activity. Based on the presented results myristic acid might qualify as a drug excipient, as co-application with ABC transporter substrates might reduce the risk of drug export out of a cell. Furthermore, as mentioned in the discussion, myristic acid is used as a multifunctional food additive and flavor

excipient [27]. Thus, this food additive has the potential to interfere with (human) ABC transporters, an aspect which, to the best of our knowledge, has never been discussed thus far and which we will explore in future experiments.

Author Contributions: Conceptualization, K.O., A.S. and D.S.; methodology, K.O., J.C.L. and H.Ö.; validation, K.O., J.C.L., H.Ö. and A.S.; formal analysis, K.O., A.S. and D.S.; investigation, K.O., J.C.L. and H.Ö.; resources, E.T. and D.S.; writing—original draft preparation, K.O. and D.S.; writing—review and editing, K.O. and D.S.; visualization, K.O. and D.S.; supervision, A.S., E.T. and D.S.; project administration, E.T. and D.S.; funding acquisition, E.T. and D.S. All authors have read and agreed to the published version of the manuscript.

Funding: This work was supported by the Naturwissenschaftlich-Medizinisches Forschungszentrum (NMFZ) Mainz and by DynaMem (State of Rhineland-Palatinate).

Institutional Review Board Statement: Not applicable.

Informed Consent Statement: Not applicable.

Data Availability Statement: The data presented in this study are available on request from the corresponding author.

Acknowledgments: We thank G. Unden for providing the *B. subtilis* strain 168 and N. Hellmann for discussion and proof reading.

Conflicts of Interest: The authors declare no conflict of interest.

References

1. Wilkens, S. Structure and Mechanism of ABC Transporters. *F1000Prime Rep.* **2015**, *7*, 1–9, doi:10.12703/P7-14.
2. Hediger, M.A.; Romero, M.F.; Peng, J.-B.; Rolfs, A.; Takanaga, H.; Bruford, E.A. The ABCs of Solute Carriers: Physiological, Pathological and Therapeutic Implications of Human Membrane Transport Proteins. *Pflugers Arch. Eur. J. Physiol.* **2004**, *447*, 465–468, doi:10.1007/s00424-003-1192-y.
3. Higgins, C.F. ABC Transporters: From Microorganisms to Man. *Annu. Rev. Cell Biol.* **1992**, *8*, 67–113, doi:10.1146/annurev.cb.08.110192.000435.

4. Hanekop, N.; Zaitseva, J.; Jenewein, S.; Holland, I.B.; Schmitt, L. Molecular Insights into the Mechanism of ATP-Hydrolysis by the NBD of the ABC-Transporter HlyB. *FEBS Lett.* **2006**, *580*, 1036–1041, doi:10.1016/j.febslet.2005.11.012.

5. Holland, I.B.; Blight, M.A. ABC-ATPases, Adaptable Energy Generators Fuelling Transmembrane Movement of a Variety of Molecules in Organisms from Bacteria to Humans. *J. Mol. Biol.* **1999**, *293*, 381–399, doi:10.1006/jmbi.1999.2993.

6. Dalmas, O.; Do Cao, M.-A.; Lugo, M.R.; Sharom, F.J.; Di Pietro, A.; Jault, J.-M. Time-Resolved Fluorescence Resonance Energy Transfer Shows That the Bacterial Multidrug ABC Half-Transporter BmrA Functions as a Homodimer. *Biochemistry* **2005**, *44*, 4312–4321, doi:10.1021/bi0482809.

7. Falasca, M.; Linton, K.J. Investigational ABC Transporter Inhibitors. *Expert Opin. Investig. Drugs* **2012**, *21*, 657–666, doi:10.1517/13543784.2012.679339.

8. Smith, P.C.; Karpowich, N.; Millen, L.; Moody, J.E.; Rosen, J.; Thomas, P.J.; Hunt, J.F. ATP Binding to the Motor Domain from an ABC Transporter Drives Formation of a Nucleotide Sandwich Dimer. *Mol. Cell* **2002**, *10*, 139–149, doi:10.1016/S1097-2765(02)00576-2.

9. Neyfakh, A.A.; Bidnenko, V.E.; Chen, L.B. Efflux-Mediated Multidrug Resistance in *Bacillus Subtilis*: Similarities and Dissimilarities with the Mammalian System. *Proc. Natl. Acad. Sci. USA* **1991**, *88*, 4781–4785, doi:10.1073/pnas.88.11.4781.

10. Krügel, H.; Licht, A.; Biedermann, G.; Petzold, A.; Lassak, J.; Hupfer, Y.; Schlott, B.; Hertweck, C.; Platzer, M.; Brantl, S.; et al. Cervimycin C Resistance in *Bacillus Subtilis* Is Due to a Promoter Up-Mutation and Increased MRNA Stability of the Constitutive ABC-Transporter Gene BmrA. *FEMS Microbiol. Lett.* **2010**, *313*, 155–163, doi:10.1111/j.1574-6968.2010.02143.x.

11. Steinfels, E.; Orelle, C.; Fantino, J.-R.; Dalmas, O.; Rigaud, J.-L.; Denizot, F.; Di Pietro, A.; Jault, J.-M. Characterization of YvcC (BmrA), a Multidrug ABC Transporter Constitutively Expressed in *Bacillus Subtilis*. *Biochemistry* **2004**, *43*, 7491–7502, doi:10.1021/bi0362018.

12. Chami, M.; Steinfels, E.; Orelle, C.; Jault, J.-M.; Di Pietro, A.; Rigaud, J.-L.; Marco, S. Three-Dimensional Structure by Cryo-Electron Microscopy of YvcC, an Homodimeric ATP-Binding Cassette Transporter from *Bacillus Subtilis*. *J. Mol. Biol.* **2002**, *315*, 1075–1085, doi:10.1006/jmbi.2001.5309.

13. Lacabanne, D.; Lends, A.; Danis, C.; Kunert, B.; Fogeron, M.L.; Jirasko, V.; Chuilon, C.; Lecoq, L.; Orelle, C.; Chaptal, V.; et al. Gradient Reconstitution of Membrane Proteins for Solid-State NMR Studies. *J. Biomol. NMR* **2017**, *69*, 81–91, doi:10.1007/s10858-017-0135-4.

14. Hunter, A.D. ACD/ChemSketch 1.0 (Freeware); ACD/ChemSketch 2.0 and Its Tautomers, Dictionary, and 3D Plug-Ins; ACD/HNMR 2.0; ACD/CNMR 2.0. *J. Chem. Educ.* **1997**, *74*, 905–906, doi:10.1021/ed074p905.

15. Ravaud, S.; Do Cao, M.A.; Jidenko, M.; Ebel, C.; Le Maire, M.; Jault, J.M.; Di Pietro, A.; Haser, R.; Aghajari, N. The ABC Transporter BmrA from *Bacillus Subtilis* Is a Functional Dimer When in a Detergent-Solubilized State. *Biochem. J.* **2006**, *395*, 345–353, doi:10.1042/BJ20051719.

16. Orelle, C.; Gubellini, F.; Durand, A.; Marco, S.; Lévy, D.; Gros, P.; Di Pietro, A.; Jault, J.-M. Conformational Change Induced by ATP Binding in the Multidrug ATP-Binding Cassette Transporter BmrA. *Biochemistry* **2008**, *47*, 2404–2412, doi:10.1021/bi702303s.

17. Sharom, F.J. Characterization and Functional Reconstitution of the Multidrug Transporter. *J. Bioenerg. Biomembr.* **1995**, *27*, 15–22, doi:10.1007/BF02110326.

18. Ambudkar, S.V.; Lelong, I.H.; Zhang, J.; Cardarelli, C.O.; Gottesman, M.M.; Pastan, I. Partial Purification and Reconstitution of the Human Multidrug-Resistance Pump: Characterization of the Drug-Stimulatable ATP Hydrolysis. *Proc. Natl. Acad. Sci. USA* **1992**, *89*, 8472–8476, doi:10.1073/pnas.89.18.8472.

19. de Athayde Moncorvo Collado, A.; Corbalán, N.; Homolya, L.; Morero, R.; Minahk, C. Resveratrol Modulates ATPase Activity of Liposome-Reconstituted ABCG1. *FEBS Lett.* **2013**, *587*, 2359–2363, doi:10.1016/j.febslet.2013.06.001.

20. Fameau, A.-L.; Ventureira, J.; Novales, B.; Douliez, J.-P. Foaming and Emulsifying Properties of Fatty Acids Neutralized by Tetrabutylammonium Hydroxide. *Colloids Surfaces A Physicochem. Eng. Asp.* **2012**, *403*, 87–95, doi:10.1016/j.colsurfa.2012.03.059.

21. Veerappan, A.; Cymer, F.; Klein, N.; Schneider, D. The Tetrameric α-Helical Membrane Protein GlpF Unfolds via a Dimeric Folding Intermediate. *Biochemistry* **2011**, *50*, 10223–10230, doi:10.1021/bi201266m.

22. Anbazhagan, V.; Cymer, F.; Schneider, D. Unfolding a Transmembrane Helix Dimer: A FRET Study in Mixed Micelles. *Arch. Biochem. Biophys.* **2010**, *495*, 159–164, doi:10.1016/j.abb.2010.01.006.

23. Sehgal, P.; Mogensen, J.E.; Otzen, D.E. Using Micellar Mole Fractions to Assess Membrane Protein Stability in Mixed Micelles. *Biochim. Biophys. Acta-Biomembr.* **2005**, *1716*, 59–68, doi:10.1016/j.bbamem.2005.08.006.

24. Hellmann, N.; Schneider, D. A Complex Unfolding Pathway of α-Helical Membrane Proteins in SDS-Containing Micelles. *Biophys. J.* **2021**, *120*, 3857–3859, doi:10.1016/j.bpj.2021.08.002.

25. Otzen, D.E.; Nedergaard Pedersen, J.; Kumar Somavarapu, A.; Clement, A.; Ji, M.; Hartvig Petersen, E.; Skov Pedersen, J.; Urban, S.; Schafer, N.P. Cys-Labeling Kinetics of Membrane Protein GlpG: A Role for Specific SDS Binding and Micelle Changes? *Biophys. J.* **2021**, *120*, 4115–4128, doi:10.1016/J.BPJ.2021.08.001.

26. Shapiro, A.B.; Ling, V. Reconstitution of Drug Transport by Purified P-Glycoprotein. *J. Biol. Chem.* **1995**, *270*, 16167–16175, doi:10.1074/jbc.270.27.16167.

27. Burdock, G.A.; Carabin, I.G. Safety Assessment of Myristic Acid as a Food Ingredient. *Food Chem. Toxicol.* **2007**, *45*, 517–529, doi:10.1016/j.fct.2006.10.009.

28. Bishop, D.G.; Rutberg, L.; Samuelsson, B. The Chemical Composition of the Cytoplasmic Membrane of *Bacillus Subtilis*. *Eur. J Biochem* **1967**, *2*, 448–453.

29. Doige, C.A.; Yu, X.; Sharom, F.J. The Effects of Lipids and Detergents on ATPase-Active P-Glycoprotein. *Biochim. Biophys. Acta* **1993**, *1146*, 65–72, doi:10.1016/0005-2736(93)90339-2.

30. Sharom, F.J. The P-Glycoprotein Efflux Pump: How Does It Transport Drugs? *J. Membr. Biol.* **1997**, *160*, 161–175, doi:10.1007/s002329900305.

31. Neumann, J.; Rose-Sperling, D.; Hellmich, U.A. Diverse Relations between ABC Transporters and Lipids: An Overview. *Biochim. Biophys. Acta-Biomembr.* **2017**, *1859*, 605–618, doi:10.1016/j.bbamem.2016.09.023.

32. Reuter, G.; Janvilisri, T.; Venter, H.; Shahi, S.; Balakrishnan, L.; van Veen, H.W. The ATP Binding Cassette Multidrug Transporter LmrA and Lipid Transporter MsbA Have Overlapping Substrate Specificities. *J. Biol. Chem.* **2003**, *278*, 35193–35198, doi:10.1074/jbc.M306226200.

33. Woebking, B.; Reuter, G.; Shilling, R.A.; Velamakanni, S.; Shahi, S.; Venter, H.; Balakrishnan, L.; van Veen, H.W. Drug-Lipid A Interactions on the. *J. Bacteriol.* **2005**, *187*, 6363–6369, doi:10.1128/JB.187.18.6363-6369.2005.

34. Lee, A.. Lipid–Protein Interactions in Biological Membranes: A Structural Perspective. *Biochim. Biophys. Acta-Biomembr.* **2003**, *1612*, 1–40, doi:10.1016/S0005-2736(03)00056-7.

35. Lacabanne, D.; Orelle, C.; Lecoq, L.; Kunert, B.; Chuilon, C.; Wiegand, T.; Ravaud, S.; Jault, J.M.; Meier, B.H.; Böckmann, A. Flexible-to-Rigid Transition Is Central for Substrate Transport in the ABC Transporter BmrA from *Bacillus Subtilis*. *Commun. Biol.* **2019**, *2*, 1–9, doi:10.1038/s42003-019-0390-x.

36. Gottlieb, H.E.; Kotlyar, V.; Nudelman, A. NRM Chemicals Shifts of Common Laboratory Solvents as Traces Imputities. *J. Org. Chem.* **1997**, *62*, 7512–7515, doi:10.1021/JO971176V.

37. Murray, A.T.; Matton, P.; Fairhurst, N.W.G.; John, M.P.; Carbery, D.R. Biomimetic Flavin-Catalyzed Aldehyde Oxidation. *Org. Lett.* **2012**, *14*, 3656–3659, doi:10.1021/ol301496m.

38. Steinfels, E.; Orelle, C.; Dalmas, O.; Penin, F.; Miroux, B.; Di Pietro, A.; Jault, J.-M. Highly Efficient Over-Production in *E. Coli* of YvcC, a Multidrug-like ATP-Binding Cassette Transporter from *Bacillus Subtilis*. *Biochim. Biophys. Acta-Biomembr.* **2002**, *1565*, 1–5, doi:10.1016/S0005-2736(02)00515-1.

11.4 Additional material

Table 16: SDS concentration and SDS mole fractions used in the different titration samples.

c_{SDS} [mM]	χ_{SDS}
0.00	0.00
0.21	0.04
0.43	0.08
0.68	0.12
0.95	0.16
1.25	0.20
1.58	0.24
1.94	0.28
2.35	0.32
2.81	0.36
3.33	0.40
3.93	0.44
4.62	0.48
5.42	0.52
6.36	0.56
7.50	0.60
8.89	0.64
10.63	0.68
12.86	0.72
15.83	0.76
20.00	0.80
26.25	0.84
36.67	0.88
57.50	0.92
95.00	0.95

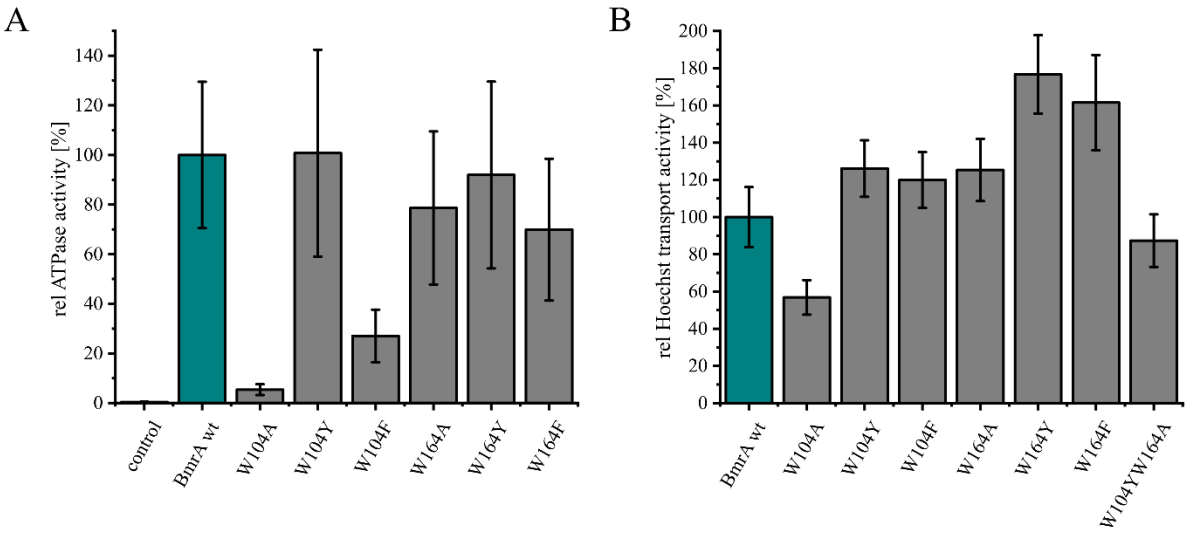

Figure 27: ATPase and Hoechst transport activity of BmrA wt and single Trp variants. The two Trp residues (W104 and W164) in the TMD part of BmrA were replaced by Ala, Tyr or Phe. These single Trp variants of BmrA were tested for the ATPase (A) and Hoechst transport activity (B). The two Trp residues (W104 and W164) of the BmrA-TMD were replaced by Tyr and Ala, thus a single Trp variant of BmrA was generated with the residual Trp in the BmrA-NBD. The double mutated BmrA variant $BmrA_{W104YW164A}$ was still Hoechst transport active. The Hoechst transport activity of $BmrA_{W104YW164A}$ was determined by [redacted] (Bachelor student). Data show each two independent purifications (A) or two inverted vesicle preparations (B) ($n \geq 5$, ± SEM).

Danksagung

Curriculum vitae